Control Methods for Improving Mobility for Persons with Lower Limb Paralysis

By

Andrew Ekelem

Dissertation

Submitted to the Faculty of the

Graduate School of Vanderbilt University

in partial fulfillment of the requirements

for the degree of

DOCTOR OF PHILOSOPHY

in

Mechanical Engineering

September 30, 2018

Nashville, Tennessee

Approved:

Michael Goldfarb, Ph.D.

Eric Barth, Ph.D.

Gerasimos Bastas, Ph.D., M.D

Karl Zelik, Ph.D.

Kevin Galloway, Ph.D.

William Emfinger, Ph.D.

For Karen and Edgar Brichta, who showed me how to walk the walk.

ACKNOWLEDGEMENT

The technological advancements at the Center of Intelligent Mechatronics (CIM) and Center for Rehabilitation Engineering and Assistive Technology (CREATE) have provided comfort over the years following my spinal cord injury and the first-hand experience of the dated rehabilitation process. Paralysis caused by spinal cord injury is a complex condition that has long been considered incurable beyond the earliest academic recording of neurology in the Edwin Surgical Papyrus circa 2700 B.C. The experience of creating new features for rehabilitative robotics then sharing them with subjects who brave the unknown with me as I monitored the controllers has been a treasure. I am filled with gratification from those moments of successfully implementing a new function and seeing the pilot's face fill with enjoyment and hope that the paradigm of neurorehabilitation can shift.

It has been my pleasure and fortune to learn from the top-notch rehabilitation robotics cadre at Vanderbilt University. Michael Goldfarb, Ph.D. has led the centers with comprehensive understanding of user's needs; complimented by his scrupulous expertise in engineering, the resulting inventions are often poised for commercial translation provided they meet the stringent assessment and evaluation process. Michael has set a prime example of leadership by always keeping his cool and his door open for any situation despite the mountain of responsibilities he juggles. His leadership and eye for talented engineers have paved the way for the ongoing developments that have already set the new standard of rehabilitation as the Indego Exoskeleton transitioned from the lab to a commercial medical device within my tenure at Vanderbilt University. Working under his guidance has been a pleasure and honor.

To my senior CIM peers, I would like to thank you for paving the way and the all the effort towards the passage of knowledge. Ryan Farris and Hugo Quintaro's incredible developments on the hardware of the Indego exoskeleton certainly motivated my decision to attend Vanderbilt as it is unquestionably an efficient and marvelous design. Kevin Ha welcomed me to the lab with invaluable mentorship in functional electrical stimulation and controller workflow, not to mention the warm welcome to Nashville with the best house parties in Olin Hall history. Spencer Murray was a pleasure to work with and I appreciate the continued efforts with Parker to improve rehabilitation of paralysis. Ben Gasser, the living encyclopedia and resident expert in hardware repair, construction and design has saved countless hours with the wealth of knowledge he has amassed and willingness to provide consultation. Huge thanks to Don Truex, the secret weapon in the closet, the mastermind behind all circuits and electronics that have made the robots tic.

To the newer members of CREATE, I am excited for your great potential and passion for rehabilitation robotics. The caliber of engineering never ceases to amaze me, and it has been a pleasure working together.

I would like to thank the committee, the experts, therapist and entire community surrounding the treatment of paralysis who have helped with the projects presented in this document. Dr. Gerasimos “Makis” Bastas supported the scientific rigor and gave direction to the intended impacts with his insights to physiatry. Chrissy Durrough of Pi Beta Phi and the Shepherd Center therapists have provided the projects’ demand for expertise in physical therapy and neurorehabilitation needed to develop suitable features for clinal application. I am grateful for William Emfinger of Max Mobility a.k.a. Permobil who has generously mentored my computer science skills and provided the SmartDrive for the clonus study. Tamsyn Street has made networking a joy and exciting, I am truly grateful to warm welcome with the stimulating community at Odstock Medical.

The research and development are the focus of this document, but I would also like the thank the Wondr’y staff, my Innovation Realization team, and Emory Solkin for helping with the commercialization plan to get the technology to as many people it can benefit. I am very proud and appreciative of my apprentice engineers: Nora Ait Boucherbil, Ali Alrabeh, Abdulraham Alotaibi, and Ziming Lou who have supported my vision and volunteered to help develop the technology, together we have more than a dream but a company to chase it, Levmo!

Lastly, I thank my family of hustlers who work incessantly and make graduate school look like a vacation. My parents have always been my role models. My sisters who have elected to study medicine and have kept me good company in times of stress and in times of celebration. Finally, I thank my best friend, Amber, who reminds me to take breaks from behind the computer with her big puppy dog eyes.

TABLE OF CONTENTS

Page

LIST OF TABLES

Page

LIST OF FIGURES

Page

CHAPTER 1: INTRODUCTION

Paralysis or paresis induced by upper motor neuron damage often leaves the lower limbs dysfunctional for basic activities such as walking and climbing stairs. Nearly five and one half million people in the United States, or approximately one in fifty, have some degree of paralysis [4]. The sustained duration and high level of impairment attributed to paralysis motivates research and development for technologies that alleviate the associated deficiencies.

The Indego exoskeleton (Parker-Hannifin, OH) and Chimera muscle stimulator are mechatronic devices developed for the reanimation of paretic limbs. Indego employs electric motors to actuate an orthosis for the restoration of controlled legged mobility, while the Chimera interfaces with the nervous system through transcutaneous electrical stimulation to administer functional electrical stimulation (FES). Described herein are rehabilitative intervention methods that: 1) enable paraplegics to ascend and descend stairs with a lower limb exoskeleton; 2) enhance exoskeleton assisted walking with supplemental FES to overcome moderate to severe spasticity; and 3) suppress clonus using FES during seated mobility. Chapter 2 describes the hardware developed for and/or employed in this research.

Chapter 3 describes the development and assessment of a controller for the Indego that enables paraplegics to ascend and descend stairs. The stair controller expands on a previous implementation of predefined trajectory tracking with an emulated passive state that enables gravity to extend the leg until it meets the next stair tread, then a trajectory is calculated in real-time to perform the intended task of stair ascent independent of step height. The ascent and descent controllers were evaluated by three paraplegic users who traversed numerous size stairs safely within two hours of tuning and training. The resulting controller enabled stair climbing with light exertion despite complete paraplegia.

Subjects with moderate to severe spasticity are typically ineligible for exoskeleton assisted gait due to pathological muscle activation that opposes exoskeleton mediated motion. A novel supplemental stimulation controller was implemented with the Indego exoskeleton and integrated Chimera stimulator in an effort to expand the inclusion criteria of exoskeletons to individuals with severe spasticity whereby FES enhances the synergy between muscles and motors. Chapter 4 explores the effects of spasticity and FES on robot mediated gait for paraplegics and describes the hybrid system's controller that enabled two paraplegic individuals with moderate to severe spasticity to achieve substantially improved gait kinematics.

Mobility impairment of paraplegia can also entail clonus, a self-exciting reflex that can manifest as involuntary shaking of the ankle, a common pathology experienced during wheelchair propulsion. Chapter 5 expands the frontiers of clonus research with the first reported evaluation methods wheelchair clonus

and the efficacy of a novel FES intervention to treat pathological clonus during wheelchair propulsion over rough terrain. The clonus intervention was shown to robustly suppress clonus. The treatment may provide a noninvasive and economical alternative to invasive and commonplace pharmacological interventions.

The remainder of the introduction serves to provide background information pertaining to the nervous system, neurological impairment and the state of the technologies used to restore deficiencies that arise from comorbidities of paralysis.

1.1 The Brain and Injury

The nervous system is an intricate network of neurons that enables life on Earth to intimately, consciously, and even logically interact with the ever-changing environments and thrive in otherwise less than ideal conditions. The human nervous system has an estimated 100 billion neurons, each capable of up to 15,000 connections to other neurons creating the complex network that makes thoughts, memories, movement, and intelligence possible [5], [6]. The development of these neuronal networks is largely done prior to birth where macrostructures of the brain are established, however neural plasticity and neural stem cells enable ongoing development and adaptation throughout life [7], [8]. Injury to the nervous system often causes devastating deprivations of function and may be caused by foundational developmental deformations on a cellular level such as neurogenetic disorder, or on a macro scale such as traumatic injury to brain structures.

1.1.1 The Central Nervous System

The human neuroanatomy consists of a complex network specialized cells, called neurons (see Fig. 1-1), that communicate via *action potentials*, or the propagation of depolarization across a cell membrane. Action potentials mobilize along the cell membranes by way of voltage regulated protein channels that open when an adjacent depolarization occurs, letting ions diffuse across the cell membrane. These electrical impulses are capable of propagating long distances (on the order of meters) and provide means for neurons to interact with one another through special intercellular junctions called *synapses*.

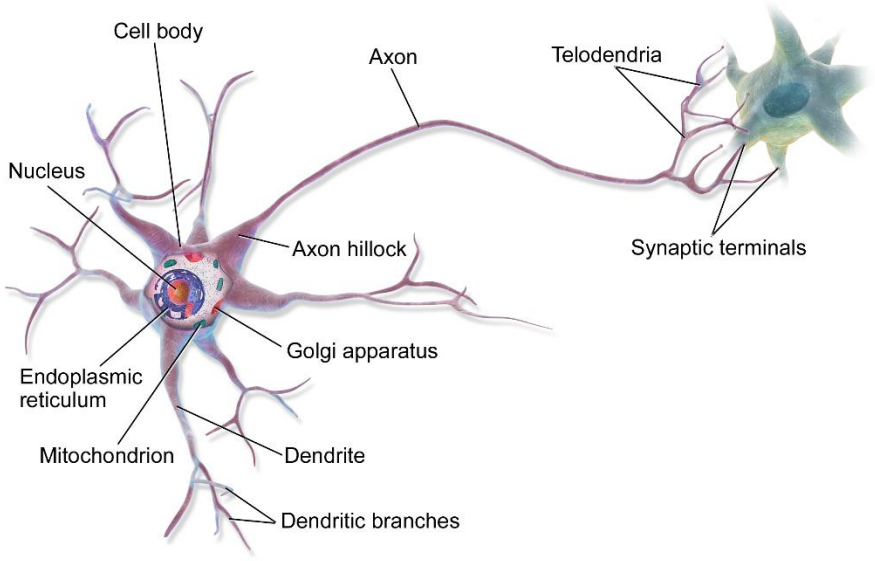

Figure 1-1: Neuron cell structure (source: Wikimedia Commons)

Postsynaptic membranes, *dendrites*, often have a high concentration of receptor proteins that can modulate or depolarize the membranes electrical characteristics in response to chemicals secreted by the presynaptic membrane. The chemicals that enable communication through synapse are called *neurotransmitters*. Most often neurotransmitters are released from axons and diffuse across the synapse (20-40 nm) to react with the receptor proteins located on the dendrites ([9], pg.182). Pharmacological agents and foreign chemicals that enter the nervous system are often capable of modulating the receptor characteristics through weak chemical bonds. Chemicals are often categorized as depressants or stimulants whether they induce an excitatory or inhibitory effect on the central nervous system.

Neurons also interact with other organs including hormonal glands, muscles, skin, etc. to intelligently maintain homeostasis and enable animals to interact with the environment. Muscles are of primary importance for enabling people to move. Neurons that interact with muscles are referred to as motor neurons (or motoneurons) because they convey information for coordinating movements. Motor neurons belong to the efferent group of neurons that project information from the central nervous system to the peripheral organs.

The primary motor cortex, or precentral gyrus houses the cell bodies of the upper motor neurons (UMN) which are responsible for voluntary movements. These upper motor neurons are made up of special pyramidal cells called Betz cells, whose dendritic branches gather information from the sensory-motor cortex to coordinate voluntary movement. Damage directly to the precentral gyrus or neighboring structures is commonly associated with cerebral vascular accidents (CVA, stroke) or traumatic brain injury (TBI). These supraspinal injuries often present as hemiplegia were a single side of the body presents symptoms of paralysis. Both TBI and CVA may cause motor deficiency through damage to associated

cognitive centers that indirectly deprives the upper motor neurons of normal activation. In as much, CVA and TBI often have some capacity to restore functional motor control to an appropriate level to maintain activities of daily living (ADL) [10]. Structural integrity of the descending motor pathways, assessed with diffusion tensor imaging or comparable techniques, can be used to predict recovery potential [11]. Training and the plasticity of the larger cerebral cortex provides means of recruitment of the intact upper motor neurons to restore function [12]. Conversely, damage directly compromising the Betz cells or other motor systems with descending motor pathways (e.g., vestibular) may cause an irreparable motor deficiency [11].

1.1.2 The Spinal Cord

Axons of Betz cells collect in nerve bundles called corticospinal tracts that traverse the brain from the precentral gyrus and are split into two primary tracts: ventral and lateral corticospinal tracts. The *ventral corticospinal tract* is responsible for neck and back (axial) muscles that coordinate voluntary postural movements. The *lateral corticospinal tract* descending from the pyramidal gyrus cross to the contralateral side of the brainstem at the pyramidal decussation and descend through the anterior lateral white matter of the spinal cord to synapse with lower motor neurons (LMN) responsible for interaction with muscles.

Other descending pathways from the midbrain and brain stem subconsciously mediate reflexes and balance components of motion. The additional descending pathways include the reticulospinal, vestibulospinal, tectospinal and rubrospinal tracts, see the spinal cord cross-section shown in Fig. 1-2. The *tectospinal tract* receives input from the visual and auditory systems and cause the upper limbs and head to react to loud noises, bright lights, and sudden movements. Essentially this is the network that makes it fun to spook people and watch them jump. The *reticulospinal tracts* is responsible for modulating the flexor reflexes. Cortical inputs utilize this pathway to make reflexes more sensitive, such as when one is worried about to touching a hot pot; alternatively, the reflexes can be inhibited, such as when one is holding the hot pot and does not want to drop it, rather rush to place it down. The *rubrospinal tracts* is an alternative pathway for voluntary flexor and extensor muscles, however, this tract plays a minor role in humans and great apes, and is thought to speed learned patterned motions such as running. The *vestibulospinal tract* conveys information from the inner ear (the vestibular system) to control head and limb movements for posture and balance. Together these pathways make up the subconscious descending motor tracts that traverse the white matter of the spinal cord.[13]

The spinal cord also conveys afferent signals from sensory fibers of the peripheral nervous system (PNS). Afferent neurons reside in the dorsal root ganglions and use specialized dendrites, often with specialized sensors for pain, touch, proprioception, etc. to convey information about the body and its interactions with the environment. Ascending pathways include the spinocerebellar tracts, gracile and

cuneate fasciculus, and the spinothalamic tract; each tract coveys particular sensations enabling the brain to make informed decisions, when these pathways are intact.

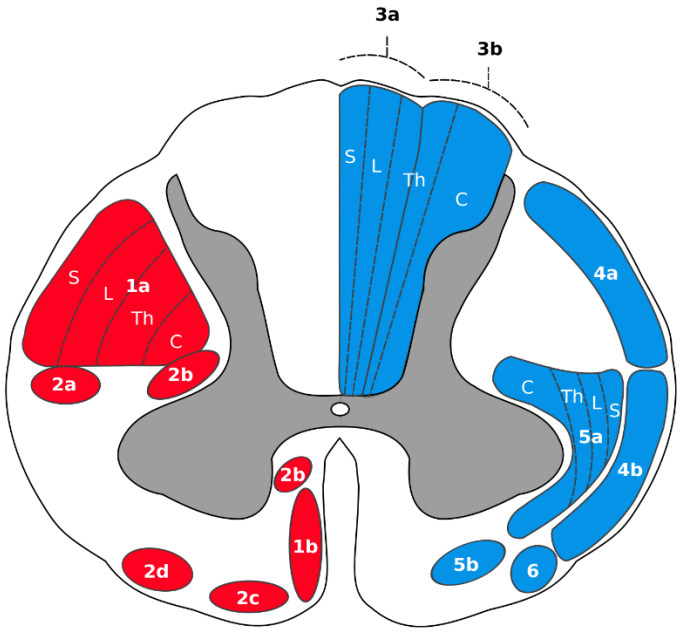

Motor and decending (efferent) pathways (left, red)	Sensory and ascending (afferent) pathways (right, blue)
1. Pyramidal Tracts	**3. Dorsal Column Medial Lemniscus System**
1a. Lateral corticospinal tract	3a. Gracile fasciculus
1b. Anterior corticospinal tract	3b. Cuneate fasciculus
2. Extrapyramidal Tracts	**4. Spinocerebellar Tracts**
2a. Rubrospinal tract	4a. Posterior spinocerebellar tract
2b. Reticulospinal tract	4b. Anterior spinocerebellar tract
2c. Vestibulospinal tract	**5. Anterolateral System**
2d. Olivospinal tract	5a. Lateral spinothalamic tract
	5b. Anterior spinothalamic tract
Somatotopy Abbreviations:	
S: Sacral, **L: Lumbar**	6. Spino-olivary fibers
Th: Thoracic, **C: Cervical**	

Figure 1-2: A cross-section of the spinal cord shows the ascending (blue) and descending (red) tracts that make up the white matter of the spinal cord. (source: Wikimedia Commons licensed under CC)

The millions of axonal fibers that ascend and descend the spinal cord link the brain to the lower motor neurons of the ventral horns and sensory afferent neurons of the dorsal horn. The myelinated axons of these tracts make up the white matter of the spinal cord. Injury to the spinal cord results in deprivation of the affected networks, often leaving limbs and organs caudal the injury dysfunctional.

1.1.3 The Peripheral Nervous System

Axons of the spinal segments branch out of the anterior and dorsal horns of the spinal cord into peripheral nerves. The nerves split throughout the musculature and sensate tissues transmitting both afferent and efferent signals. Lower motoneurons directly interface with muscles through specialized synapses, called *neuromuscular junctions*, which enable action potentials stemming from the central nervous system to depolarize muscle membranes and induce contractions in the muscle tissue. Tension created by the muscle activation often acts through tendons that connect skeletal muscles to bones resulting in joint torque. Typical motor neuron pools have upwards of 300 motor neurons for contracting a single muscle; recruitment follows the *Henneman size principle* such that these neurons are coordinated from smallest to largest as the commanded force increases [14], [15]. Coordinated movement is monitored by the cortex and spinal networks, using feedback from proprioceptors and exteroceptors, to activate and inhibit motor neurons.

Proprioception is largely attributed to *muscle spindle fibers*, a specialized muscle unit innervated by afferent fibers and gamma motoneurons and lies parallel with other force producing muscle fibers as opposed to the typical alpha motoneurons. Primary muscle spindles are wrapped in type Ia afferents that sense the rate of change in length of muscles, and type Ib afferents called Golgi tendon organs that sense tension. Secondary muscle spindles interface with type II afferents that sense muscle length. Each of these muscle spindles are innervated by gamma motoneurons for tuning the tension of the sense organs during muscle contractions.

Peripheral nerve damage is often repairable with surgical grafting techniques, as axons inherently sprout following damage and Wallerian degeneration [16]. The growing axons are capable of re-establishing synapses provided the remaining Schwann cells provide mechanisms for guiding the axon growth [17]. Peripheral neuron regeneration contrasts the limited capacity of central neurons to regenerate due to both intrinsic and extracellular factors [18]. Although, similarly for both central and peripheral neurons, damage to the cell bodies of the spinal neurons is irreparable by natural means. Severe damage to the lower motoneurons causes atrophy of the entire *motor unit* (the neuron and all its innervating muscle fibers). If the motoneuron undergoes apoptosis or extensive degeneration, the *endplate*, where the muscle's neurotransmitter receptors are concentrated, first upregulates the receptor concentration, then degrades if a connection is not established, leaving the muscle incapable of excitation thereafter ([9], pg. 1099).

1.1.4 Spinal Reflexes

It has been long understood that animal nervous systems rely on reflexes; Rene Descartes describes them as a result of "[e]xternal objects, which by their presence alone, act upon the sense organs of this machine [the body], and by this means force it to move in several different ways…and cause without

thought the movements which are made in their presence [19] (circa 1632)." Ivan Pavlov then furthered understanding of the development and conditioning of reflexes in the 20th century and describes "[t]he essential feature of the highest activity of the central nervous system, with which we are concerned and which in the higher animals most probably belongs entirely to the hemispheres [cortex], consists not in the fact that innumerable *signaling stimuli* do initiate reflex reactions in the animal, but in the fact that under different conditions these same stimuli may initiate quite different reflex reactions; and conversely the same reaction may be initiated by different stimuli [20]." The removal of many of the *innumerable* input signaling stimuli results in a variety of symptoms that are interdependent, globally modulated, adaptable and eventually summated to interact with the lower motoneurons to activate skeletal muscles. The core symptomatic pathological spasms that result from SCI include tone (e.g., postural reflexes), nocuous (e.g., withdrawal reflex), and phasic (e.g., Babinski, clonus).

James Sherrington classified reflexive inputs as proprioceptive and exteroceptive inputs circa 1910 [21]. Proprioception include the muscle spindle afferents and Golgi tendon organs that relay joint position information to the spinal cord. Action potentials of these organs relay information of tension, velocity and position of the joints, enabling spinal circuitry to control complex motions. Exteroceptors are skin receptors that respond to pressure enabling further modulation of subconscious motion (e.g. walking on non-uniform surfaces). Supraspinal inputs modulate reflex activity; abnormal reflex activity contributes to diagnostics of neurological impairment. Below are a few of the major reflexive and central physiologies that contribute to the neuronal circuits of the spinal cord.

Stretch (myotatic) reflex is a monosynaptic reflex that causes contraction in response to the stretch within the muscle. The stretch reflex functions to reduce cognitive demand by encoding muscle activity in response to changes in length and velocity. The phasic component of the stretch reflex involves primary muscle spindles innervated by dynamic gamma motor neurons that sense rapid stretching of muscles. Furthermore, the phasic stretch reflex is self-regulating, the reflex modulates the muscle spindle tension to maintain quality signals of afferent neuron organs during movement. There is also a tonal stretch reflex resulting from the secondary muscle spindles; the muscle length is proportional to the action potential firing rate of the afferent static gamma motor neurons. Static gamma motor neurons are responsible for the maintenance of posture and slow movements.

The phasic component of stretch reflex is responsible for clonus spasticity in the neurogenic spinal cord, while the tonal stretch reflex is the primary contributor to tonal spasticity (e.g., extensor tone) after neurological impairment.

Golgi tendon (inverse myotatic) reflex functions to preserve the tendon integrity during excessive tension by inhibiting the agonist muscle group and activating the antagonist muscle group [22].

Babinski reflex is normal in infants, this reflex is typically absent after voluntary control is established, and replaced with a plantar reflex. The reflex is observed when drawing a blunt instrument along the sole of the foot. The sign of the Babinski reflex is the large toe moving towards the top of the foot.

Flexor Withdrawal Reflex is a polysynaptic nociceptive reflex initiated by nociceptive receptors (pain receptors typically in the skin) to preserve tissue integrity from the stimuli. This typically results in a concerted flexion motion of the limb, a result of excitation of ipsilateral flexors and inhibition of ipsilateral extensors.

Central pattern generators (CPGs) have a rhythm generating neuronal network that coordinates joint extensor and flexor muscles. The excitatory state of a CPG is typically modulated by the supraspinal corticospinal and reticulospinal tracts. A typical central pattern generator is structured for cyclical motions like gait, swimming; an exemplary block diagram of the pattern generators role in locomotion can be seen in Fig. 1-3.

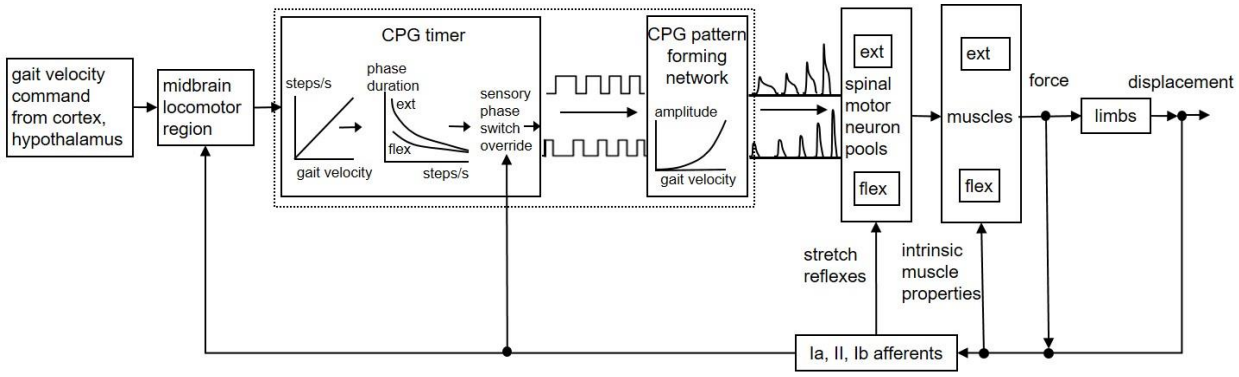

Figure 1-3: "Schematic of the locomotor central pattern generator in the mammalian nervous system" by Neuromechanics is licensed under CC BY-SA 4.0

Even completely decerebrated animals can exhibit primitive gait restoration under certain conditions. Recent efforts of exciting the CPGs through pharmacological and/or electrical (TENS, Russian) of the spinal cord stimulation (TSCS) have resulted in rhythmic stepping activation patterns of SCI individuals [23]–[25]. After SCI axonal sprouting enables plasticity of the CPGs can aid in restoring functional recovery by adapting to the incomplete supraspinal control or reinforce involuntary pathological behavior [18], [26], [27].

Impairment of the interlaced spinal networks comprised of afferents, interneurons, supraspinal inputs and efferent neurons establish the basis of spasticity and other comorbidities of injury to the central nervous system. Just as spinal reflexes and pattern generators are the underlying mechanisms for locomotor function, consideration of these physiological networks is essential to restoring maximal function after injury. Neurological impairment can appear diverse and unique due to the complex and aggregated nature of the central nervous system.

1.2 Spinal Cord Injury

Focusing on SCI is an attempt to narrow the scope of the technologies described here. Many symptoms of SCI are common to a variety of other causes of paralysis, however spinal cord injury typically leaves persons with para- or tetraplegia, where both legs are paretic. In the United States, there are an estimated 54 cases of SCI per million each year, or approximately 17,000; the prevalence ranges between 243,000 to 347,000 persons. Average age of injury is increasing, currently at 42 years old, with males comprising 80% of new cases. Vehicular and fall accidents are the leading causes of SCI. Average acute care is 11 days followed by 35 days of rehabilitation, however severe cases can range much longer. Less than 1% of SCI persons have had a complete neurological recovery by hospital discharge. Of the remaining majority, 45% incomplete tetraplegia, 21.3% incomplete paraplegia, 20% complete paraplegia, and 13.3% complete tetraplegia, where incomplete refers to retainment of either sensation or motor control below the level of injury [28]. SCI often leads to serious disability that adversely affects employment opportunities while increasing cost of living through medical related expenses. Improved rehabilitation techniques that promote preventative health and restore function are the motivation of the research and development of rehabilitation robotics.

The level and extent of a SCI is often reported on the American Spinal Injury Association (ASIA) scale which reports the neurological level of the impairment and a letter score A-D, see Table 1.1. The neurological level refers to the most caudal spinal segment with normal function. Sensation is evaluated by pin prick and light touch at each dermatome, or area of skin innervated by a single spinal root; the evaluator scores each dermatome from 0-2 or not testable. The motor evaluation is graded at ten muscle groups ranging from 0-5 (total paralysis – normal active movement). [29]

Table 1-1: ASIA Scale

Score	Description
A	Complete. No sensory or motor function is preserved in the sacral segments S4-S5.
B	Incomplete. Sensory but not motor function is preserved below the neurological level and includes the sacral segments S4-S5.
C	Incomplete. Motor function is preserved below the neurological level, and more than half of key muscles below the neurological level have a muscle grade less than 3 (Grades 0-2).
D	Incomplete. Motor function is preserved below the neurological level, and at least half of key muscles below the neurological level have a muscle grade greater than or equal to 3
E	Normal. Sensory and motor function are normal.

The ASIA impairment scale communicates level of impairment of motor and sensory deprivation, however it does evaluate spasticity or neuropathic pain which are other common comorbidities of SCI.

1.2.1 Spasticity

After impairment of the upper motor neurons, the distal neuromusculature may have unsupervised activity termed *spasticity*. Spasticity is a common comorbidity resulting from SCI, where approximately 68-75% of individuals with SCI experience spasticity and 20-40% have problematic spasticity that restricts activities of daily living [30]. Spasticity can manifest as uncontrolled muscle activity, influenced by disinhibited reflex pathways and central pattern generators resulting from upper motor neuron damage. In contrast, lower motor neuron damage is typically characterized by flaccidity and eventually muscle atrophy. SCI may result in the deprivation of a wide range of components involved in the comprehensive spinal networks that control the activity of lower motor neurons. The variety of manifestations of spasticity require a slew of evaluation techniques.

Spasticity has been categorized as intrinsic tonic, intrinsic phasic, or extrinsic nocuous [30], [31]. *Tonic spasticity* may manifest as either flexor or extensor rigidity and is largely dependent on joint position. *Phasic spasticity,* chiefly caused by the hyperactive stretch reflex circuits after central neurologic impairment of the corticospinal inhibitory pathways, causes muscle activity proportional to joint angular velocity. *Extrinsic nocuous spasms* are evoked by external stimuli that trigger cutaneous afferents (i.e., the withdrawal reflex). Nocuous spasms often appear spontaneous for persons with sensory deficit however there is typically underlying tissue damage (e.g., pebble in the shoe, decubitus ulcer). The various components of spasticity require that each symptom have an independent evaluation, for which there are numerous clinical tests. Some common spasticity evaluation procedures include:

The *Ashworth or Modified Ashworth Scale (MAS*) involves a trained assessor rapidly advancing a joint through its range of motion and evaluating the stiffness of the joint on a scale from zero to four [2], [32].

Spinal Cord Assessment Tool for Spastic reflexes (SCATS) is used to assess a subject's spasticity in three subfields: clonus, flexor spasms, and extensor spasms [3], [33].

The Drop Test is used to examine a subject's ankle clonus by raising the subject's leg above a platform (approximately 5 cm) and dropping it such that the heel is hanging off the edge of a platform to dorsiflex the ankle while the subject is sitting. The Drop Test may excite clonus and elicit an oscillatory response. Both number of oscillations and duration of the sustained clonus are valid points of measuring the response to the Drop Test [34].

Electrophysiology has inherent limitations as far as electrode placement and equipment measurement resolution but provides definitive measurements for muscle activation and reflex activity. The Hoffman reflex is a monosynaptic reflex that results in an action potential as a result of stimulation to the tibial nerve; stimulation of the tibial nerve simultaneous activates motoneurons. The H wave is the action potential measure resulting from the reflex while the M wave is that of the direct muscle stimulation. Together the H/M ratio describes the excitability of the Hoffman reflex informing experimental or pathological influences [35].

These clinical measures are used to evaluate reflex health and inform the diagnosis of a neurological impairment or treatment thereof. Treating spasticity is not straight forward as there are beneficial outcomes of spasticity induced muscle activity, such as: reduced muscle atrophy, improved blood circulation and withdrawal from harmful stimuli. Hence, spasticity reduces predisposition to other comorbidities that commonly result from frequent wheelchair use [30], [36]. Therefore, spasticity must be managed to achieve a balance between useful and detrimental effects by progressing from physical rehabilitation, pharmacological intervention, injection, intrathecal baclofen, and surgery [30]. Discussions between healthcare professionals and patients are necessary to achieve an optimal management level that maximizes quality of life (QOL).

1.2.2 Neurorehabilitation

Physical rehabilitation for neurological impairments varies vastly depending on the pathological conditions that present themselves. Active movement exercises (subject voluntarily commands motion) are typical for cases of motor incomplete paralysis where subjects are capable of strengthening the recruitment of voluntary activation. Passive movement exercises, such as range of motion exercises (e.g., stretching) are commonplace for managing spasticity, and fundamental in therapy for call cases of paralysis. Other practices are encouraged for preventative measures, such as pressure relief and daily load bearing exercises. Rather than explore the broad range of specialized therapies that have been developed, this section will focus on functional electrical stimulation and exoskeletons.

Functional Electrical Stimulation

Functional electrical stimulation (FES) has been prescribed for paraplegics to restore motor activity to paretic lower limbs since the 1960s. It is estimated 5.4 million people suffer from paralysis in the United States [4], and far more people suffer from muscle atrophy or other injuries that can be treated with an electrical stimulation system. Merits of electrical stimulation to treat paralysis and combat predisposition to numerous comorbidities are well established in the literature: improving locomotion performance and recovery [10], [37]–[41], maintaining bone health[42]–[45], combating muscle atrophy [39], [46]–[48], deep vascular thrombosis [49], and decubitus ulcers [50]–[52] (A.K.A. “pressure ulcers” or ”bedsores”), and many more [53]–[57]. FES can treat numerous predispositions to comorbidities that otherwise can be extremely debilitating; for example, pressure ulcers lead to 60,000 deaths annually and cost anywhere from $9.1-11.6 billion per year in the United States according to the Agency for Healthcare Research and Quality. Meanwhile studies have shown electrical stimulation both prevents and accelerates healing of decubitus ulcers, and maintains general tissue health by increasing blood flow and oxygenation through the paretic limb [58], [59]. Artificial activation of muscles and nerves is typically not as efficient as natural recruitment of muscles, but it is effective in preserving tissue health in addition to achieving some intended functional outcomes.

Artificial electrical stimulation can induce action potentials in neurons by depolarizing the neuronal membrane that is gated by protein-based voltage-dependent ion channels. Typical nerves targeted for transcutaneous electrical stimulation contain hundreds to thousands of axons from motor neurons and sensory dendrites. Stimulation activation of these fibers depends largely on two variables: the diameter of the neuron fiber and the field strength of the stimulation current. Because larger fibers have reduced intracellular resistance they draw more current and reach threshold prior to smaller neurons. Hence, motor neurons can be activated prior to sensory neurons, see Fig. 1-4. This is opposite the natural pattern of motor neuron recruitment that targets smaller neurons first, the Hennemen size principle.

The field of the induced current is dependent on the artificial stimulation, and controlled by the system (stimulator parameters, electrodes, and electrode position). The electronic field strength decays in proportion to the square of the distance to the electrodes, so neurons closest to the surface of the skin are recruited before similar fibers farther from the electrodes. The electric field is controlled by the system, either by varying the amplitude of the pulse or the pulse-width to proportionally activate the number of motor units. Typical pulse-widths are on the order of 100-500 μs. Pulse amplitudes are either current controlled or voltage controlled depending on the stimulator hardware architecture. Stimulators typically use a transformer to control current or store a high-voltage potential on a capacitor and administer the charge via an H-bridge. Typical non-invasive gel electrode applications utilize pulse amplitudes of 10-120 mA, or 0-120 V.

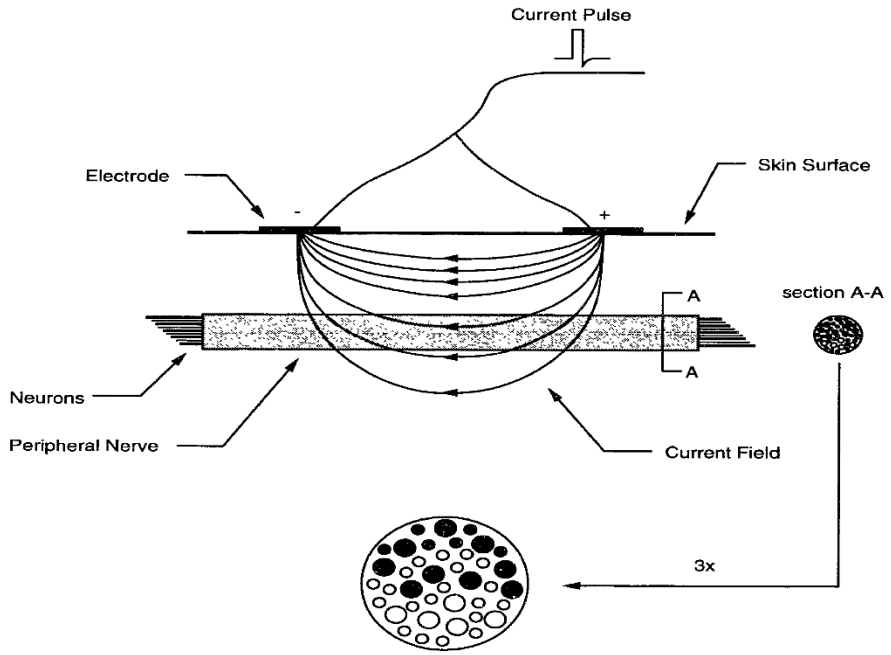

Figure 1-4: Illustration of the factors that affect neuron recruitment during functional electrical stimulation: cross sectional area, strength of induced electric field and distance from electrodes. Reproduced from Goldfarb 1994 [60].

Liberson's foot drop stimulator was the first FES device designed to treat foot drop, a common symptom of paresis, most commonly caused by stroke. Liberson's device relied on a heel-switch to detect *heel-off*, indicating the initiation of swing, then applying transcutaneous electrical stimulation of the common peroneal nerve to activate the flexor withdrawal reflex, improving toe clearance during swing [61]. In the 1990's accelerometer sensors enabled foot drop stimulators to use the acceleration of the tibia to indicate swing initiation to trigger stimulation [62].

Current devices that treat foot drop include the L300 (Bioness), Walkaide (Innovative Neurotronics) and Odstock (Salisbury, UK) with out of pocket price range of $4500-5900 [63], [64]. These devices are only reimbursable in the United States under code E0770 for SCI, leaving them inaccessible for majority of the customers who could benefit from the FES orthosis over the standard ankle foot orthosis in the long run [38], [65]. It is difficult to rationalize the current products price point; however, it is possible they used value-based pricing with the nearest comparable product being custom molded ankle-foot-orthoses that have substantial labor cost involved. Recent publications of a randomized clinical trial found equivalence in performance when comparing ankle foot orthosis to FES foot-drop orthosis; however, a long term follow-up found patients had greater satisfaction with an FES orthosis [38], [65].

FES is commonly used to combat muscle atrophy in paraplegic and tetraplegic subjects; but also has proven instrumental in restoring critical bodily functions such as bowel, bladder and respiratory systems [66]. As the intended function varies in importance, FES systems vary in invasiveness, from

transcutaneous to implanted. Typical commercially available non-invasive devices each enable a single function. Common functions for paraplegia are stationary cycling, assistive walking and intermittent stimulation for pressure ulcer prevention or muscle strengthening.

The Parastep system is a gait restoration device for paraplegia that uses a push-button interface for an FES system whereby stimulation of the flexor withdrawal is responsible for swing and stimulation of extensors provide stance stability [67]. The Parastep is the only gait training FES system reimbursable under HCPCS Code # E0764. Parastep is sold by a nonprofit; therapists are often unaware of the Parastep device despite the proven merits of FES for the SCI community [68]. Cost for the Parastep FES system is $12000 (6 channels), 80% of which is covered by Medicare [69]. Besides cost, the FES system for complete paralysis was deemed too fatiguing for community ambulation [70]. Orthoses are well suited for offloading effort towards weight bearing and balance during FES assisted ambulation. Systems that offer orthotic support and FES are called *hybrid-* orthoses.

Exoskeletons

Many orthoses have been available to provide individuals with SCI some degree of legged mobility. Orthoses can be categorized as *passive* or *active.* Active orthoses provide power to assist movement, whereas passive orthoses rely on the user to input the energy necessary for movement. Of passive orthoses, the knee-ankle-foot orthosis (KAFO) is the most basic. A KAFO operates by fixing the ankle position and having a lock mechanism at the knee, such that the knee can be locked in full extension. Likewise, the hip guided orthosis (HGO) stabilizes the hip, preventing abduction or adduction. Reciprocating gait orthoses (RGOs) employ a reciprocal coupling mechanism at the hip, which permits the user to induce extension in one hip by means of weight shifting, inducing flexion in the contralateral hip. For these passive devices all motion is initiated by the user's upper body with aid of a walker or forearm crutches for stability.

Powered exoskeletons have been developed by several researchers to improve the functionality of orthoses and reduce the physical exertion of the user, with the aim of enabling community ambulation. The state-of-the-art motors, batteries and integrated circuits have enabled powered robotic orthosis, coined *exoskeletons or exos*, for the rehabilitation setting. The Rewalk (Rewalk Robotics, Isreal) was the first exoskeleton to be approved for sale in the US by the Food and Drug Administration (FDA). Exos typically strap around the legs and waist and use electric motors to actuate the hip and knee joints as to restore mobility to stand-up and walk over ground. A recent review of various exoskeletons is reported in [71], [72]. These systems have been shown to reduce energy expenditure during assisted walking, relative to passive orthoses [73]. Further, powered exoskeletons are capable of adapting to the presence of obstacles or varied terrain such as stairs and slopes.

The portability of exoskeletons enables over ground gait which can be contrasted to body weight support systems that offload the weight of the lower limbs with a harness and requires a robot or multiple therapists to assist as needed in the progression of gait (often on a treadmill). Exoskeleton technology restores the capability of locomotor control while preserving loading of the limbs.

Similarly to FES, the price points of exoskeletons are out of reach for most customers to use at home, with the cheapest at $50k[74]; furthered by non-natural controls, substantial weight, and top speed ⅓ that of needed for community ambulation, it is not likely this technology will be reimbursed by insurances until greater evidence of efficacy or health merits are presented. Recent reviews identify the following limitations of exoskeletons:

"One of the largest hurdles to be overcome in exoskeleton research is the user interface and control. More intuitive and flexible user interfaces are needed to increase the success of robotic exoskeletons."[75]

"Future research should: 1) develop criteria for optimal selection and training of patients most likely to benefit from this technology, 2) design multimodal gait intention detection systems that engage and empower the user, 3) develop real-time monitoring and diagnostic capabilities, and 4) adopt comprehensive metrics for assessing safety, benefits, and usability."[71]

The structural stability of exoskeletons enables upright rehabilitation for even the most severely affected subjects. Hybrid FES-exoskeletons systems are mutually beneficial whereby exoskeletons add support for safety and endurance while the FES amplifies the physiological benefits of an upright posture and synergy between motors and muscles. Although the Food and Drug Administration (FDA) has not approved any hybrid robotic exoskeleton, the Indego exoskeleton team has an integrated FES system in development and Ekso Bionics' EksoGT has recently partnered with Hasomed's Rehastim2 [76] to deliver a hybrid FES system that is CE marked and available in the US for research.

1.3 Summary of Contributions

The devices and methods developed herein aim to enable paraplegics to climb stairs, overcome significant spasticity with functional electrical stimulation (FES) during exoskeleton gait training, and quell clonus with FES. The research described here incorporates two devices for exploring new modalities of rehabilitation for paraplegics: the Indego exoskeleton and the Chimera stimulation device. The Indego is previously developed hardware, while the Chimera device was developed for this research. Both these devices can communicate via a controller area network (CAN) that allows them to be controlled simultaneously or individually, with a high-level controller in Simulink (Mathworks). More detail on the hardware is given in Chapter 2.

1.3.1 Stair Climbing

The stair section describes a control approach for a lower limb exoskeleton intended to enable stair ascent and descent of variable geometry staircases for individuals with paraplegia resulting from SCI. This work expands on the demonstration of stair climbing for a single subject and single stair geometry. Assessment of novel the controller was implemented in a lower limb exoskeleton and tested in experimental trials on three subjects with motor-complete spinal cord injury on numerous staircases of varying geometry. Results from the assessment indicate a high-degree of movement consistency within each subject; a high-degree of consistency in average ascent and descent rates between subjects; the ability to accommodate variable step heights without changing controller parameters; and a corresponding low degree of physical effort required during the stair ascent and descent activity.

1.3.2 Exoskeleton Gait Training and Spasticity

Robotic exoskeletons have recently emerged to facilitate legged mobility in people with motor complete SCI, however, involuntary muscle activity attributed to spasticity can prevent such individuals from using an exoskeleton. Specifically, although most exoskeleton technologies can accommodate low to moderate spasticity, the presence of moderate to severe spasticity can significantly impair gait kinematics when using an exoskeleton. This study investigates the use of common peroneal stimulation in conjunction with exoskeleton gait assistance to potentially enable individuals with moderate to severe spasticity to use exoskeletons more effectively. The stimulation was timed with the exoskeleton swing phase and is intended to mitigate extensor spasticity through recruitment of the flexion withdrawal reflex. To examine the potential efficacy of this approach, two SCI subjects with severe extensor spasticity (i.e., modified Ashworth ratings of three to four) walked in an exoskeleton with and without supplemental stimulation. These experiments indicated that common peroneal stimulation on average increased peak hip flexion during the swing phase of walking by 15.8 deg (151%) and peak knee flexion by 14.3 deg (58.8%). Additionally, use of the stimulation decreased the swing phase RMS motor current by 249 mA (15.3%) at the hip motors and 581 mA (29.8%) at the knee motors. This preliminary data indicates that such supplemental stimulation may be used to improve the quality of movement provided by exoskeletons for persons with severe extensor spasticity in the lower limb.

1.3.3 Wheelchair Propulsion and Spasticity

The phasic component of spasticity can manifest as clonus, or a self-activating stretch reflex arc that may have a central component [77], [78]. Clonus of the ankle can manifest during wheelchair propulsion, when terrain causes afferent activation either through proprioceptors or exteroceptors. Typical ankle clonus is initiated with a stretch to the calf muscles that activates muscle spindle fibers which contributes to the stretch reflex, a monosynaptic reflex whereby a stretch to a muscle induces self-

activation. Self-activation of the stretched extensors then raises the heel, only to relax, enabling gravity to the heel back down, causing the calf to stretch, thus repeating the reflex. Clonus occurs at 3-8 Hz, continuously shaking the leg and the user until the cycle is physically disrupted, often requiring the use of arms to manipulate the shaking leg(s), thereby interfering with propelling the wheelchair. Furthermore, shaking may cause feet to fall off the footplate, exposing them to injury.

The explored method for treating clonus employs a bandpass filtered accelerometer signal used to classify clonus activity and appropriately stimulate the afferent nerves of the ankle to disturb the reflexive cycle. The performance was advanced further by detecting inertial activity indicative of traversing rough terrain and applying a preventative stimulation to the afferents to preempt clonus activity. The methods were evaluated in a real-world setting where subjects traversed rough terrain and the controller adapted to reduce clonus. Experiments were conducted on four subjects with SCI; overall results of eleven trials show the devices reduce wheelchair spasticity by 86% (median).

CHAPTER 2: HARDWARE

The Indego and Chimera are mechatronic devices developed for the reanimation of paretic limbs. Each provide different means of actuation that can independently or complementarily restore legged mobility after spinal cord injury (SCI). Indego implements electronic motors, while the Chimera interfaces with the nervous system through transcutaneous electrical stimulation. Control of the devices is typically done with low-level actuator controllers and a high-level hierarchical finite state machine (HFSM) controller.

HSFM enable complex systems to be represented in simple charts where states and sub-states define the discrete characteristics of the system [79]. HFSM conventions enable rapid prototyping of novel functions for the devices through visualization of the controller in Simulink/Stateflow (Mathworks). The HFSM integrates system data (i.e., sensors, timers) to make informed state transitions that determine the behavior of the actuators. Once validated, HFSMs charts are easily translated to computer code (e.g., C) and flashed into the firmware of the devices. The developments described here are largely composition and additions to prior developments. One of the greatest challenges for adoption and implementation by new developers is the familiarization with the system organization and naming conventions of the many parameters. Compilers often reveal fatal system errors before implementation and validation.

The development of novel functions in software requires reliable hardware for implementation. Stateflow enabled real-time validation of HFSM enabling rapid turnaround from concept, to software prototypes and implementation. Here the Indego and Chimera systems are described in detail to give context for the implementation of controllers described in the following chapters.

2.1 Indego Exoskeleton

The Indego exoskeleton is a medical device that restores motion to the lower limbs for people with paralysis or paresis. The exoskeleton straps around the lower limbs and waist of the user to actuate the hip and knee joints using feedback from kinematic measurements, see Fig. 2-1. The Indego was developed at Vanderbilt University and has since been commercialized by Parker-Hannifin Corp. (Cleveland, Oh).

Hardware, Firmware and Network

The Indego exoskeleton hardware platform incorporates four motors for powered movement of bilateral hip and knee joints in the sagittal plane, in addition to built-in ankle-foot-orthoses (AFOs) at both ankle joints to provide ankle stability and transfer the weight of the exoskeleton to the ground. Onboard electronic sensors include encoders at each joint that provide the respective joint angles and angular

velocities, and a six-axis inertial measurement units (IMU) in each thigh link, which provide the left and right thigh angles with respect to the vertical. The total mass of the exoskeleton including the battery is approximately 12 kg (26 lbs); the device can be dissembled into five segments: two shanks, two thighs, and the hip for portability and fitting (each segment has three sizes).

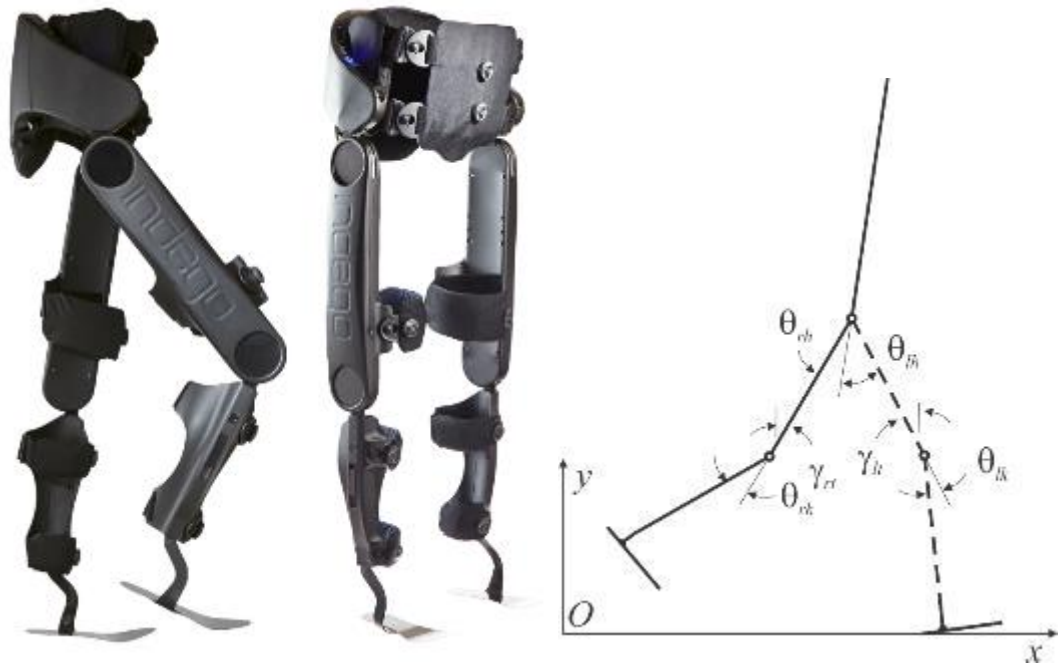

Figure 2-1: Indego Exoskeleton (Photograph courtesy of Parker) and kinematic measurements

During the works presented here, the exoskeleton hardware evolved from research prototypes that were prone to malfunction, to a reliable medical device approved by the Food Drug Administration (FDA). The firmware remained largely the same throughout the transition and enabled a near seamless transition of controller implementation from the various revisions of the hardware. The firmware is written in C and flashed to the PIC microcontrollers (Microchip, Chandler, AZ). There are two microcontrollers in each leg of the Indego that communicate with each other via a serial peripheral interface (SPI). One microcontroller, the PIC32 is tasked with the processing the state machine controllers, parsing sensors and networking. The other microcontroller, the dsPIC, manages the brushless motor drivers that consist of six hall effect sensors and six half-bridges for driving two brushless DC motors (*EC 90* – Maxon Motor, Switzerland). The Indego commercial hardware has an additional microcontroller in the hip segment that manages the start-up and shut-off processes that are mediated by momentary push-buttons on the front of the device. The three segments with embedded electronics have connectors such that when assembled power and a controller area network (CAN) unify the segments.

The experimental high-level control software was implemented in MATLAB Simulink/Stateflow through a CAN serial cable which was plugged into a CAN port in the exoskeleton. Typical development using the exoskeleton utilized real-time controls via CAN to Simulink. CAN relayed data from the robot to

the HFSM controller in Simulink's Stateflow. Typical data rates were 200 Hz although controllers that integrated EMG systems were typically 1000 Hz. This design environment enabled efficient iteration of controllers and convenient visualization of sensor data, output commands, and outputted actuation. The design process progressed from testing controllers with the motors unplugged, then plugged while hanging, then active with an able-body (non-SCI) subject, then finally evaluated on SCI pilots.

Prior Efforts and Contributions

Prior to the works described herein, numerous talented engineers had laid a wealthy foundation of technological developments; the Indego has demonstrated walking, sitting, standing, stair climbing and hybrid-FES assisted [73], [80]–[82]. Here the capabilities, limitations and contributions are discussed for the Indego exoskeleton.

Inertial ques detected by the robot enable autonomous control by the paraplegic to locomote the exoskeleton. For example, the Indego sit-to-stand protocol enables users to safely trigger the standing state were the motors extend abruptly by requiring the user to lift both legs with the robot donned. Lifting is detected by the inertial sensor and the change in robot joints angle measurement. Once given indication of intent, the robot then progresses to a pre-standing state where the motors vibrate when the hip flexes; the robot is ready to. Once a que in the thigh inertial sensors is detected, the user has initiated the standing process and the controller advances to the standing state where the exoskeleton rapidly extends the legs [80]. Fault detection monitors the success of the standing state, whereby if the thighs remain more horizontal than normal the robot will return to the sitting state.

The Indego standing controller was adapted to the Chimera stimulator device (described below), whereby the user triple-taps the device to indicate intent to stand and the controller progresses to pre-stand, then waits for the user to initiate standing, or times out and returns to sitting. This contribution demonstrated parallels between the neural prosthetic and exoskeleton control methodology for human robot interactions involved in limb reanimation.

Kinematic measurements (orientation and joint parameters) gate many of the Indego's HFSM state transitions. For example, users must advance the center of pressure (lean forward) to indicate intention to take a step in the Indego [80]. Leaning is a natural process of gait, so this method improves intuitive control over other methods, such as pushbuttons; however, the users typically relies on the stability aid and upper limbs to achieve the needed weight advancement. A case study described in Appendix B describes an electromyography (EMG) interface that has demonstrated a motor complete paraplegic reliably varying commanded step effort. Although implemented with the Chimera, the interface could potentially enable exoskeleton and hybrid implementation of intuitive gait for paraplegics.

The prior SCI controller of the Indego implements motor control by following predefined joint angle trajectories. Although this method is advantageous for enhancing repeatability and reliability, it is also

limited in the rigidity of the trajectory control and does not permit controlled step size variability. The works described in Chapter 3 aim to expand the flexibility of a stair-ascent controller with a state that is free of a predefined position trajectory and enables variable step sizes to be accommodated. The novel stair controller also requires a state that calculates trajectories upon state entry to transition smoothly from non-controlled position to a trajectory. This contribution builds on the prior work for a stair ascent and descent controller that was demonstrated on a single stair geometry on a single subject [81].

Hybrid FES exoskeletons are experimental only, i.e. currently there are no FDA approved systems for the rehabilitation modality. Efforts have demonstrated that FES can supplement the exoskeleton motors for stance and extension [82]. Stimulation hardware was developed to be compatible with the Vanderbilt Exoskeleton (Indego research prototype) and integrated via CAN cable. The works here, specifically in Chapter 4 expand the hybrid capabilities with the Chimera and additionally by demonstration of peroneal stimulation to enhancing the kinematic performance, while reducing effort demanded from the Indego motors during gait with persons who have moderate to severe spasticity due to SCI.

The Indego hardware has enabled rapid development of novel functions to restore mobility to paralyzed legs and has demonstrated hybrid exoskeleton-FES capabiilities to enhance the therapeutic effects for the many beneficiaries. The CAN cable and Simulink provides a flexible work environment portable enough for over-ground or up-stairs research and development. Although the Vanderbilt Exoskeleton had breaks, burns, electrocutions, etc., the Indego research prototypes have proven robust, dependable, and capable exoskeletons.

2.2 Chimera Stimulation Board

The Chimera stimulation board was developed with the intention of providing FES to enhance gait for incomplete spinal cord injuries (iSCI). Specifically, an undergraduate C5-6 ASIA C (ASIA section 1.2) needed additional assistance with hip flexion that current off-the-shelf rehabilitation devices could not provide; during outpatient therapy this individual would use a WalkAide (Ness, CA), a wearable single-channel transcutaneous foot-drop stimulator device. The WalkAide coordinates common peroneal nerve stimulation with shank rotation indicative of swing initiation. The timed stimulation of the common peroneal nerve activates dorsiflexion that assist the user with toe clearance during swing. The nocuous withdrawal reflex (section 1.1.4) can be triggered if the stimulation amplitude is great enough, and results in a concerted flexion of the hip, knee and ankle. Hesitation for his method arises as it is uncomfortable for persons with preserved sensation. Rather than increasing the stimulation amplitude, a therapist used a manual switch trigger to coordinate the peroneal stimulation with supplemental stimulation of the hip flexor muscles using a second device. Hence, the undergraduate proposed the research project to build a custom device that could infer inertial ques and coordinate two channels of electrical stimulation per leg.

This proposed project then combined with Ekelem's research aspirations to explore an electromyography-based swing intent detection method.

The name Chimera comes from a mythological creature that has the body of a goat, a tail of snake, and a fire-breathing head of a lion. The name is fitting because majority of the components, code, and circuit schematics were sourced from previous developments at the Center for Intelligent Mechatronics. The inertial measurement unit (Invensense - MPU6020) was sourced from the Vanderbilt Powered Leg; the differential amplifier (TI ADS1298) was sourced from the Vanderbilt Upper Limb Prosthetic; and the electrical stimulation and Bluetooth Low Energy (BLE) were sourced from the Vanderbilt Lower Limb Exoskeleton. The design objective may have been implemented using the multiple available PCBs and a serial communication protocol, however, the bulk of hardware and conglomerate of source files would have made such a method too cumbersome for the proposed wearable device. Hence, the key advantage of designing a custom embedded system for the Chimera was to have a compact form factor with a lot of functionality, providing a basis for numerous controller prototypes. Furthermore, sourcing example code and PCB layout techniques from proven hardware is an ideal introduction for a novice at mechatronics.

2.2.1 Hardware Development

Development began in Altium PCB designer with layout of selected of components, which are primarily surface mount technology (SMT) integrated circuits (IC). These components enable millions of transistors to operate specific functions millions of cycles per second with very low energy consumption and cost. The PIC32 microcontroller is the processing unit for the device that runs the custom firmware for interacting with the peripheral hardware. The PIC32MX575F512H-80I/PT was chosen for available repository of firmware and peripheral component layouts. Identifying available pins on the PIC32 and assigning them to new functions was a significant challenge in integrating the numerous embedded peripherals. The resulting system enables EMG capable of sensing microvolts while the stimulator can amplify the 7.4 V battery to 180 V; such breadth in electrical characteristics necessitated layout consideration for managing analog noise and electrical separation of the differential amplifier for electromyography (EMG) and a powered muscle stimulator. Strategic PCB layout and bypass capacitors were employed to stabilize the ground plane and minimize interference between the various peripheral subsystems.

The resulting Chimera system enables EMG (6-channels), inertial sensing (6-axis), analog inputs (2 for force sensing resistor, or pushbutton), controller area network (CAN), Bluetooth low energy (BLE), and electrical stimulation (6-channels), see Fig 2-2.

Figure 2-2: Chimera PCB and Package

Stimulator Architecture

The Chimera uses an audio transformer to amplify the 7.4v supply to the high voltage stimulation waveform needed for FES. Transformers are an electrical component that transfers energy from one coil (i.e, the primary coil) to at least one other coil (i.e., secondary coil). The transformer uses the principles of inductance described by Faraday's law which describes the proportionality between the rate of change of magnetic flux ($\frac{d\phi_B}{dt}$), number of coil turns (N) and an electromotive force (ε), see Equation 2.1.

$$\varepsilon = -N\frac{d\phi_B}{dt} \tag{2.1}$$

Ideal transformers conserve energy to yield an input to output voltage ratio that is equivalent to the turns ratio, and inverse the current ratio, as in Equation 2.2.

$$\frac{V_P}{V_S} = \frac{I_S}{I_P} = \frac{N_P}{N_S} = n = \text{turn ratio} \tag{2.2}$$

The subscripts "*P"* in Equation 2.2 denote the primary coil and "*S"* denote the secondary coil. Hence, by controlling the current through one of the coils you control the current on the output coil, and the two electrical systems are electrically isolated. An electrical representation of the stimulation circuit is shown in Fig. 2-3.

The first step to design the circuit was select the desired output current,120 mA was chosen. Next, we found a rechargeable battery with excellent capacity at 7.4 V, in a traditional "9-volt" PP3 size (720mAH

– HiTECH 9V). To select a transformer, consideration to the maximum power is essential for preventing the coils from overheating and leading to a shorted coil. For each FES channel the power is equal to:

$$\mathrm{F} * \mathrm{PW} * \mathrm{I_P} * \mathrm{V_P} = \mathrm{F} * \mathrm{PW} * \frac{\mathrm{I_S}}{\mathrm{n}} * \mathrm{V_P} = \mathrm{P_{peak}} \quad (2.3)$$

where *F* is the stimulation frequency, *PW* is the pulse-width, I_S is the secondary (the stimulation) current, and P_{peak} is the peak power. An example of typical peak stimulation power would be a pulse-width of 200 *us* at 50 Hz, and the peak primary-side current (120 mA divided by the turns ratio) and the supply the maximum energy. The selected transformer is a PICO 76460 (PICO Electronics, NY) configured for a turns ratio of 1:22.4 and maximum power 0.6 W, which can be purchased for $56.54 at the time of writing. Using the turns ratio selected, the peak power of operation for a single channel is calculated as 0.194 W. Therefore, three channels can safely operate at full stimulation. For simultaneous operation of four to six channels it is advised to run the stimulators at 25 Hz rather than 50 Hz.

A few factors limit the number of channels a single transformer can provide stimulation waveforms for: the stimulation duty cycle (i.e., 1% in the above example), and the primary side current controller. The current control employed uses pulse-width modulated (PWM) digital output that is lowpass filtered (f_c=55 Hz) to establish a reference voltage. The reference voltage can selectively be amplified to open the low-side bipolar junction transistor such that the amplification is proportional to the difference between the reference voltage and the voltage sensed at the sense resistor. Note, detailed schematics are included in Appendix C. The 55 Hz lowpass filter limits the rate at which channels reference voltage can be generated independent from the preceding channel. The rise/fall time of the lowpass filter is 6.6 ms, suggesting the current controller can change current amplitude approximately 150 times per second, or control three separate channels independently at 50 Hz, six channels at 25 Hz, or ten channels at 15 Hz.

The secondary side uses one optical double pole double throw switches (Omoron G3VM-202J) per stimulation channel to create a demultiplexer from the transformer. Outputs of the optical switches are connected to the headers for the electrode leads. At most, a single channel switch is open at any given time, ensuring the current is controlled rather than split between two or more channels.

Safety Concerns

Harm from FES can cause injury, cardiac interference, electrocution, and skin irritation. Risk are mitigated by proper use and hardware design. Care is needed for persons with epilepsy, heart conditions or who use a pacemaker. Electricity across the pacemaker can cause a malfunction leading to cardiac arrest. Stimulation of the lower limbs is far enough from the heart, so long as the electrodes are secured and placed appropriately, the electrical stimulation safe. Electrode selection, amplitude settings and proper electrode adhesion are critical variables for mitigating harmful current densities that can burn the skin when using current controlled stimulator. Other misuse concerns are function dependent. For

example, if stance is dependent on FES, a fall prevention mechanism, such as a walker, spotter, harness, exoskeleton, etc., will mitigate risk.

There are numerous safety considerations implemented in design of the hardware. Isolation is one consideration to protect the input or draw of excessive electricity between the user and device. Even if the circuit is battery powered and has no 110v AC connection, there must be protection against the possibility of Earthing the patient through the stimulator. Functional isolation is enough to make a circuit work. Safety isolation is much more robust, typically able to withstand a few thousand volts and longer insulation distances, to protect the patient against potential hazards. International safety standards such as IEC 60601-1 (medical electronics) and IEC 60601-2-10 (stimulators) set out the minimum insulation thickness, dielectric strength, gaps (creepage and clearance) to provide a means of patient protection. The optical switches used provide a dielectric strength of 1500 V_{RMS}, however the dielectric strength between the transformer coils is only rated to 200 V_{RMS}, hence the Chimera is functionally isolated, but not to the safety isolation standards of IEC 60601-2-10 that requires at least two means of patient protection [83]. A custom transformer with triple dielectric layers may resolve this, albeit may increase the weight, cost and size of the transformer. Rather the device was used with caution to not operate near high-voltage hazards that would put users at risk of Earthing electrocution.

Another potential hazard is implementing an imbalanced charge to the patient that can ensue electrolysis of the tissue. The implementation of a bipolar waveform that uses the current-sense feedback to ensure adequate current is achieved each pulse is the method employed to enforce current-balancing. This is evaluated through observation with an oscilloscope using either a current probe (capable of reading the current passing through an electrode lead), an isolated voltage probe, or the difference between two grounded voltage probes, as the lead to the electrodes are electrically “floating” or isolated from the oscilloscope’s reference. Additionally, skin irritation or discoloration is a symptom of imbalance charge, although this has yet to be observed from using the Chimera.

One last safety concern is direct current leakage. This is less of a concern for transformer (current controlled) stimulators and more of a concern for boost converter stimulators that store a high-voltage charge on a capacitor and use an H-bridge to selectively apply stimulation pulses. The reverse impedance of the H-bridge MOSFETs is not infinite and MOSFETs are not identical, therefore there is a leakage current that can accumulate electrolysis of the tissue. In this case blocking capacitors can be employed to reduce leakage current. Blocking capacitors have not been employed in the Chimera because DC is not an issue with transformers, as the induced EMF occurs in proportion to the time derivative of magnetic flux.

While standards are in place to prevent tissue damage and electrocution, electrical stimulation is generally harmless; transcutaneous FES is a low-risk option for reanimating paralyzed limbs.

2.2.2 Firmware

Firmware for the Chimera is implemented on a PIC32 and incorporates functions from other projects to provide functionality through a novel HFSM controller. The high-level user-defined *mode* state determines the function that the Chimera device will perform. Currently the Chimera has the following modes: prototype (rely on Simulink CAN inputs), push-button walking, intuitive EMG walking, inertial swing assist walking, clonus treatment, intermittent stimulation, and cycling. Each mode has a sub-HFSM to coordinate FES based on sensor data and user-defined FES parameters. The control loop operates at 500 Hz; the HFSM, sensors, and communications all occur at this rate unless independently triggered by an interrupt, such as for the BLE and FES controller. An excerpt of the code can be found in Appendix C.

Communication Protocols

Controller Area Network (CAN)

CAN permits the high-level controller to be prototyped in Matlab Simulink/Stateflow, in addition to enabling simultaneous control of multiple Chimeras and/or Indego through a network cable. One advantage of CAN over serial communication is the CAN bus isolates the system from the device; hence, the various robots and laptop computer do not need to share a common ground reference to operate. CAN requires two signals, a *high* and *low,* resulting in two wires connecting multiple devices in series. Typical CAN cables were constructed twisted pair (multi-stranded copper had better durability than solid wire); for long wires, four wires enable multiple devices to be daisy-chained. Ends of cables were reinforced with shrink wrap and epoxy for stress relief at connector-heading junctions. Long cables were typically desired for an assistant to hold the laptop and follow the subject with the experimental device.

BLE and Android Development

Bluetooth Low Energy (BLE) has become a common wireless protocol with mobile devices (e.g., smartphones). The BlueGecko112 (Silicon Labs) microcontroller provides means for the Chimera to connect to other BLE enabled devices and communicates with the PIC32 via a serial peripheral interface (SPI) protocol. An Android application, *ChimeraBLE*, was developed in Android Studio to enable the user to input parameters such as parameters that define mode, FES settings, and controller operation characteristics. The application enabled wireless interfacing with the device, unlocking the expansive potential of the Chimera hardware for portable use.

2.2.3 Devices Conclusion

The flexible CAN hardware enabled rapid prototyping and data acquisition for the numerous exploratory studies for treating lower limb paralysis. The Indego and Chimera hardware enabled first-order

demonstrations of novel functions and in the process proved robust to significant malfunction. Combining the Chimera with the Indego compounded the functionality. This data intensive operation required a cut-back on CAN signals as it initially overloaded the CAN buses. After streamlining the controller the hybrid FES exoskeleton system was used for the exoskeleton spasticity study (Chapter 4). The flexibility of CAN is exemplified when the simple construction of a new cable enabled simultaneous control of multiple Chimera boards, such as in the clonus study described in Chapter 5 that uses three Chimeras simultaneously for over-ground demonstrations. CAN and Simulink have provided an expansive environment for creativity that has proven invaluable during the iterative process of research and development of rehabilitation robotics.

Despite performing without adverse events, the Chimera prototype is insufficient for meeting the strictest of medical device safety standards. Furthermore, the limited bandwidth of BLE and the cumbersome cable routing of CAN has motivated the development of a modular discrete wireless stimulation device for future commercialization of the novel control methods. The multi-faceted, sensor packed Chimera stimulation board is a powerful research device that has demonstrated numerous prototypes with commercial potential, see the anti-clonus application (Chapter 5), and two SCI FES assisted gait case-studies (Appendices A and B). The Chimera met and exceeded the design objectives with densely packed functionality and expansive networking modalities.

The Indego exoskeleton is capable medical device. Despite the commercial success, Parker has been very supportive of the research and development of novel functions, such as the stair controller described in Chapter 3. The FDA-approved hardware proved more durable than the research prototypes, while the electronic hardware and firmware remained largely unchanged. The hardware and firmware architecture described for Indego and adopted by the Chimera is an intelligent design platform that promotes innovation and will continue to fuel major impact in the rehabilitation industry.

CHAPTER 3: MANUSCRIPT 1 - VARIABLE GEOMETRY STAIR ASCENT AND DESCENT CONTROLLER FOR A POWERED LOWER LIMB EXOSKELETON

By Andrew Ekelem, Gerasimos Bastas, Christina Durrough, and Michael Goldfarb

Published in the ASME Journal of Medical Devices, July 3, 2018.

DOI: 10.1115/1.4040699

3.1 Abstract

The prior SCI stair controller of the Indego (Vanderbilt Exoskeleton) implements motor control by following predefined joint angle trajectories. The prior work established hardware capabilities meets the kinetic demands of stair climbing and the initial controller demonstrated capabilities [84]. Further development was essential to develop the controller to be suitable for a range of users, safe, and robust to various step sizes. The research presented here began with an exploratory study that achieved repeatable ascent and descent of a single stair geometry with a single subject [85]. The rigidity of the trajectory control and does not permit controlled step size variability. The works described here describes methods that expand the flexibility of a stair-ascent controller with a state that is free of a predefined position trajectory and enables variable step sizes to be accommodated. The novel stair controller also requires a state that calculates trajectories upon state entry to transition smoothly from non-controlled position to a trajectory. This contribution builds on the prior work for a stair ascent and descent and evaluates the novel controller on three subjects who quickly learned the controls and surmounted a variety of stair geometries. The following manuscript is published.

3.2 Introduction

One of the potential impairments resulting from SCI is the loss of legged mobility. Recently, powered lower limb orthoses, or lower limb exoskeletons, capable of providing legged mobility to individuals with lower limb paralysis have started to emerge (see, for example, the recent review [86]). These devices incorporate motors at various joints, typically a combination of hip, knee, or ankle joints, to provide assisted movement of the lower limbs during walking, and in most cases, require that the user use a stability aid (e.g., a rolling walker or forearm crutches) to maintain balance. Since these are (nearly) uniformly robotic devices, they require a control method that enables an SCI user to autonomously control the basic movements associated with legged mobility (i.e., sitting, standing, and walking). Specifically, a controller should: 1) allow a user to command various movements, ideally without extraneous instrumentation; 2)

provide movement that is safe and well-coordinated with the user's upper body movement; and 3) provide movement that is adaptable to varying environment geometry. A recent paper provides a thorough review of various control methodologies for lower limb exoskeletons in general, and for individuals with complete SCI in particular [72]. Among the control approaches described for individuals with complete SCI are the methods described in [73], [80], [87], [88], all of which use some form of trajectory control, governed by either impedance or computed-torque control methods.

The intent of lower limb exoskeletons for individuals with SCI is to enable individuals with lower limb paralysis the ability to independently sit, stand, walk, and transition between these activities. In addition to potentially alleviating some of the secondary health effects caused by paralysis, the legged mobility enabled by these devices promises to enhance accessibility in the home and community, particularly by enabling access to spaces that are not amenable to wheelchairs. In order to deliver their full promise in this regard, such devices need to provide the ability to ascend and descend stairs, which are one of the primary impediments to wheelchair accessibility.

Despite the importance of stair ascent and descent functionality, very few publications exist that describe control methodologies that enable exoskeleton stair ascent and descent for individuals with lower limb paralysis, or that characterize the mobility associated with such functionality. The authors note that two commercially-available lower limb exoskeletons, ReWalk (Argo Medical Technologies) and Rex (Rex Bionics), have both demonstrated stair ascent and descent functionality, although no technical information has been published in the medical, engineering, or scientific literature regarding either control methodology or functionality in this regard. According to two recent reviews of lower limb exoskeleton control methodologies [72], [89], only one (conference) paper [81] describes and validates a control methodology that enables exoskeletal-based stair ascent and descent for individuals with complete lower limb paralysis. That paper, which is a precursor to this one, describes a control methodology for a powered hip and knee exoskeleton intended to provide stair ascent and descent functionality to individuals with paraplegia, and presents representative of stair ascent and descent data for a single subject traversing a single stair geometry. The work presented here is an extension of that work that enables an improved ability to accommodate variable stair geometry without reconfiguring the controller, and also better leverages the combined efforts of the hip and knee joints during the stance phase of stair ascent. This paper further presents experimental data corresponding to stair ascent and descent of three SCI subjects with motor-complete injuries, and specifically assesses their ability to traverse three staircases of differing stair geometries. A preliminary version of this work was presented in [90], which presented some preliminary results on a single subject.

The work presented here specifically describes a stair ascent and descent controller to enable variable-geometry stair ascent and descent with a lower limb exoskeleton, and experimentally characterizes the functionality of the exoskeleton in doing so on three subjects with motor-complete

paraplegia. The experimental characterization includes measurement of exoskeleton joint angles, torques, and power, and comparison of those measurements to similar measures from healthy subjects.

3.3 Controller

This stair ascent and descent controller described here was developed on a single subject (poster/paper EMBC 2015), and then evaluated on three SCI individuals (submitted ASME 2017). Development initially began on the Vanderbilt exoskeleton (prototype hardware), then transferred to the Indego (commercial hardware) when it became available. The evaluation of three subjects was performed with the Indego. The hardware, consisting of four brushless motors, joint encoders and inertial position sensors, and control electronics did not change significantly, enabling the development of the stairs controller to span from the research prototype to the commercial version of the device (courtesy of Parker). Controller methods for the device were developed in Simulink (Mathworks). Walking, sit-to-stand, and stand-to-sit controllers were established controllers.

The method for the controller is to give the user control of the exoskeleton via inertial ques, which the user can manipulate with the use of balance aid, such as crutches and or a hand rail. Via the inertial information the exoskeleton can consistently make predictable transitions from state to state. Furthermore, haptic feedback in the form of vibration gives the user indication of particular impending state transitions. The work presented here aims to define a robust controller that is intuitive to new users, tunable for various skill levels, and accommodates a range of stair geometries.

3.3.1 Joint-level Controllers

The control architecture consists of a set of joint-level controllers that govern the behavior of each actuated joint, and a high-level finite state machine that provides commands to the joint-level controllers based on movement queues from the user and other configuration-based measures. Each joint-level controller consists of a full-state-feedback servo (FSFS) controller, which incorporates the following local control law:

$$\tau_i = k_i(\theta_{eqi} - \theta_i) + b_i\dot{\theta}_i \tag{3.1}$$

where τ_i, θ_i, and $\dot{\theta}_i$ are the joint torque, angle, and angular velocity, respectively, of the i^{th} joint, and where the joint behavior is determined by the vector of control parameters θ_{eqi}, k_i, and b_i, which are the commanded joint equilibrium angle, commanded stiffness, and commanded damping, respectively. This type of control structure emulates a position controller when used with relatively high values of k_i and b_i

, and emulates controllable passive impedances of k_i and/or b_i when used with an invariant joint equilibrium angle (and assuming the joints are sufficiently backdrivable). The column vector of controller parameters that determines the behavior of each joint can therefore be defined as:

$$\lambda_i = \begin{bmatrix} \theta_{eqi} & k_i & b_i \end{bmatrix}^T \tag{3.2}$$

For the exoskeleton considered here, with four actuated DOFs, the behavior of the entire exoskeleton will be determined completely by the matrix consisting of the collected controller parameter vectors:

$$\Lambda = \begin{bmatrix} \lambda_{rh} & \lambda_{lh} & \lambda_{rk} & \lambda_{lk} \end{bmatrix} \tag{3.3}$$

where the subscripts of each column vector correspond to the right hip, left hip, right knee, and left knee joints, respectively. Given this localized control structure, the role of the supervisory controller is to define the matrix (3) in response to user input, such that the exoskeleton will perform the desired stair ascent and descent function as intended.

3.3.2 Ascent Supervisory Controller

Ascent mode is entered and exited from the standing (1) position; the state machine and state transition conditions are shown in Fig. 3-1 below. When forward thigh lean, detected by the IMUs is sustained for a predetermined amount of time, the user indicates intention to step up a step. The step up (2) state consist of the right leg advancing through a predetermined trajectory. This predetermined trajectory was calculated with inverse kinematics, such that the right leg is an inverted double pendulum, and the ankle raises to a maximum height (a vertical path), which is limited by the maximum knee flexion (105°). Then the hip continues to flex to position the foot over the step. During the drop (3) state, a virtual link between the thigh and the knee ankle was developed such that as the thigh drops due to gravity, the knee extends proportionally to maintain a near vertical orientation. This virtual link required one joint torque to be commanded by current as opposed to an equilibrium position and PD controller, to avoid error in one joint culminating error in the other, which caused a jerk at foot contact when PD was used at both joints. The controller then checks (4) for foot contact as indicated by the right thigh angular velocity approach to zero. There is also a lean check that enables the user to stop if desired but was found users were comfortable with a minimal check time of 0.1s. The final state is the lift state (6), where, upon entry, a trajectory is calculated such that the current position is driven to the standing position such that the right leg lifts the user while the left leg steps to avoid the step and possible lip.

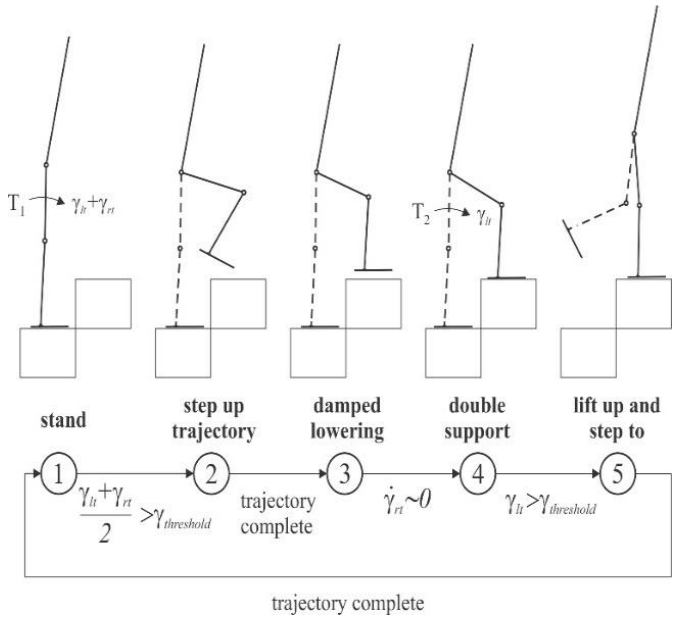

Figure 3-1: Ascent Supervisory Controller

3.3.3 Descent Supervisory Controller

The stair descent controller consists of four states, as illustrated in Fig. 3-2. The basic description of operation is as follows. The descent of each stair starts in State 1, which is a standing state, in which the exoskeleton provides standing support at both hips and knees. In order to initiate the stair descent movement, the user must shift his or her posture forward, presumably using the handrail and/or stability aid(s), such that the average thigh angle with respect to the vertical exceeds a predetermined threshold for a predetermined period of time (e.g., one second). Doing so will move the state machine into State 2, which is the step-out state, in which the right leg, and more specifically the right hip and knee joint angles, will follow a predetermined trajectory to extend the right foot out over the next stair tread, while the left leg maintains postural support. After the predetermined (time-based) trajectory has completed, the state machine enters State 3, in which the left (stance leg) hip and knee joints undergo a predetermined flexion trajectory, which produces stance knee yielding (i.e., lowering), which enables the body center of mass and right foot to settle smoothly to the next lower stair tread. The flexion trajectory is sufficient for the maximum stair height, and thus provides accommodation of variable step height, since continuing knee flexion following foot strike serves only to transfer load to the forward foot and unload and lift the rearward foot. Once the timed flexion trajectory is complete and the user shifts his or her posture over the right stance leg, as indicated by the right thigh angle with respect to vertical surpasses a second predetermined threshold, the controller will transition into State 4, in which the flexed left leg will follow a predetermined

trajectory to return the exoskeleton to the standing position of State 1 (although positioned one step below the preceding cycle). Each successive stair is descended via a similar process.

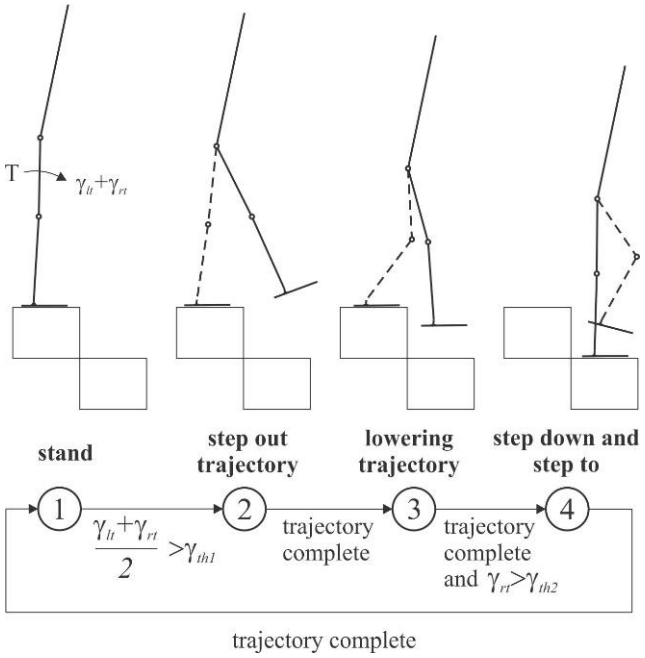

Figure 3-2: Stair descent supervisory controller

3.4 Assessment Method

In order to provide an assessment of the efficacy of the controller with respect to enabling variable-geometry stair ascent and descent, the exoskeleton controller was experimentally assessed on three subjects with motor-complete spinal cord injuries ranging from levels T10 to L1, who used the exoskeleton to ascend and descend three staircases of differing geometry ranging from 3-6.5” tread height, shown in Fig. 3-3.

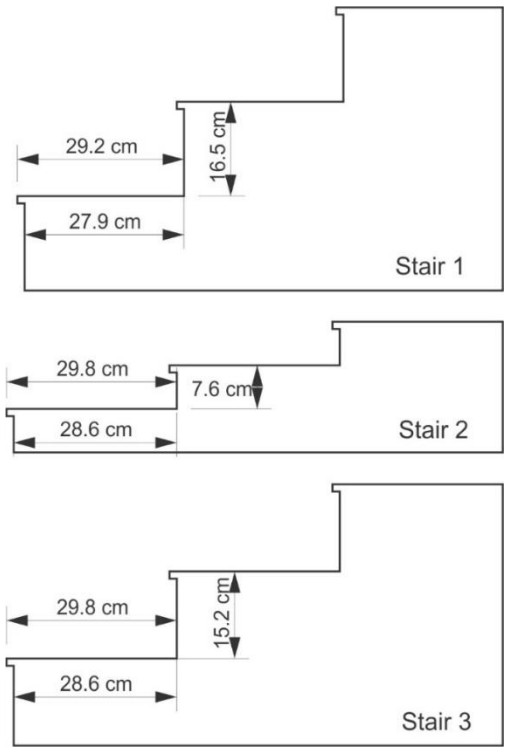

Figure 3-3: Stair geometries used in controller assessment

3.5 Results

3.5.1 Stair Ascent Results

Kinematic data of the left and right hip and knee joint angles corresponding to a total of 153 total strides from all subjects are shown in Fig. 3-4. The left and right hip and knee joint angles correspond to a total of 153 total strides from all subjects, including 90 stair ascent strides on Stair 1 (i.e., 22 strides from S1, 35 from S2, and 33 from S3), shown in black, and 63 stair ascent strides on Stair 2 (i.e., 21 strides from each subject), shown in red. Note that this stride data is synchronized at two points (which correspond to the first and second user-supplied lean thresholds), rather than one point (i.e., heel strike), as is more typical in analyzing stride data. This is due to the fact that the ascent "stride" is comprised of two consecutive movements, each independently triggered by the user, rather than a single continuous movement. As such, the data shown in Fig. 7 is synchronized at zero percent stride cycle, which corresponds to the user meeting the first forward lean threshold (i.e., entry into State 2), and also at 45% stride cycle, which corresponds to the user meeting the second forward lean threshold (i.e., entry into State 5). Note that the vertical lines on the plot separate states, and that zero percent corresponds to entry into State 2 (and exit from State 1). Specifically, the start of the stride cycle begins upon entering the

step-up state (State 2) where the right leg undergoes flexion such that the right foot is raised above the next stair tread, as indicated in the rise of the measured right joint angles.

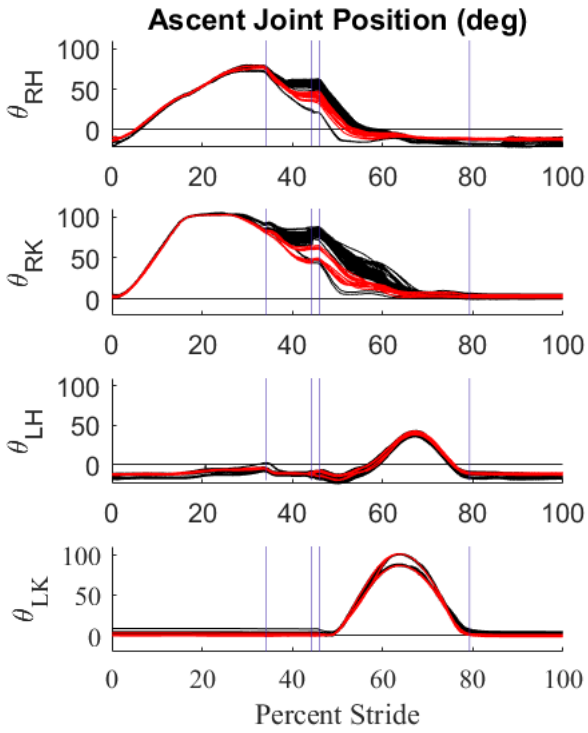

Figure 3-4: Joint angle trajectories corresponding to stair ascent for 90 steps from three subjects on Stair 1 (black), and 63 steps on Stair 3 (red). The trajectories start from state 2 and the vertical lines mark the state transitions.

The motor current and kinematic data were processed to determine the joint torques and powers during the strides; kinetic data were normalized by body-mass and plotted in Fig. 3-5 and 3-6. Figure 3-5 shows the mean body-mass-normalized joint torques for stair ascent for the three subjects for Stair 1, which includes a total of 90 strides (i.e., 22 strides for subject S1, 35 for S2, and 33 for S3), along with plus and minus one standard deviation about the mean. Figure 3-6 shows the corresponding mean body-mass-normalized joint power, along with plus and minus one standard deviation about the mean.

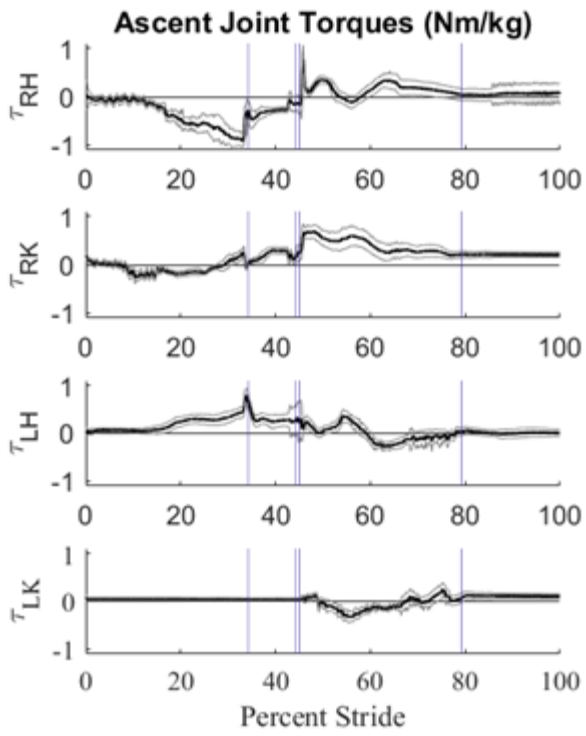

Figure 3-5: Average ascent joint torques are shown for three subjects over 90 steps on Stair 1. Dashed lines are plus and minus one standard deviation. The plots begin in State 2 and vertical lines mark state transitions

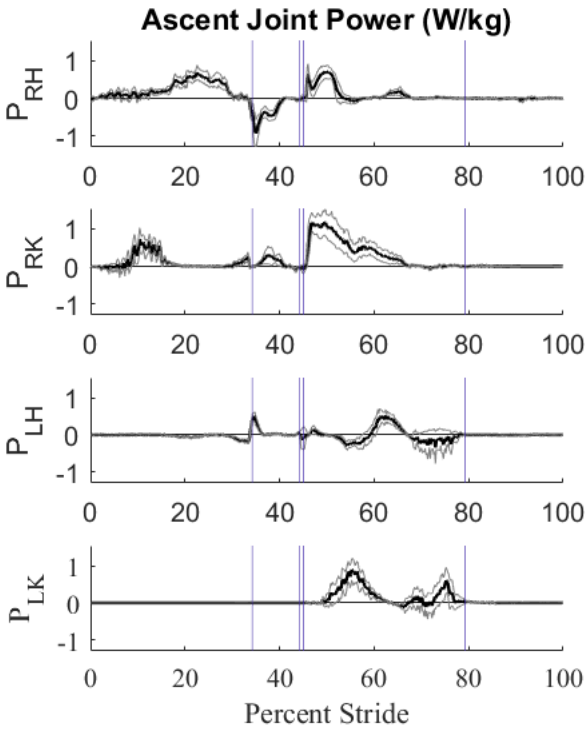

Figure 3-6: Average ascent joint powers are shown for three subjects over 90 steps on Stair 1. Dashed lines are plus and minus one standard deviation. The plots begin in State 2 and vertical lines mark state transitions

3.5.2 Stair Descent Results

Figure 3-7 shows the left and right hip and knee joint angles corresponding to 152 total strides, which are 89 strides (22 strides for subject S1, 34 for S2, 33 for S3) on Stair 1, shown in black, and 63 strides (21 each) on Stair 2, shown in red. Like the ascent stride, the descent stride has two user dependent state transitions, and therefore is parsed (i.e., synchronized) twice per stride, at zero percent stride and at 54% stride, which corresponds to the user-provided lean triggers (i.e., entry into State 2 and entry into State 4). Specifically, the stride begins with the predetermined step-out trajectory (State 2) where the right leg undergoes hip flexion, and the right knee flexes and extends, such that the right foot is above the next stair tread and the user is supported by the left leg in a stance configuration. After the step out is complete, the controller enters the damped lowering trajectory (State 3) where the left joints flex to accommodate the maximum step height, while the right hip extends to a stance position, which enables the user to transfer weight from the left leg to the right leg on the next step. The controller exits State 3 when the trajectory is complete and the right thigh angle with respect to vertical surpasses a threshold for a predetermined period of time. Once exited, the step-to trajectory (State 4) is executed to return to the

stance configuration. When the predefined trajectory is complete, the user remains in stance (State 1) until voluntarily exited.

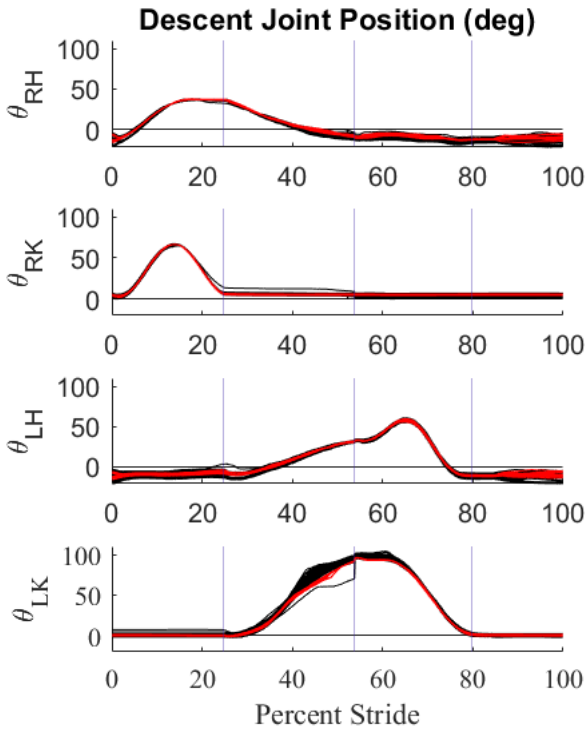

Figure 3-7: Joint angle trajectories corresponding to stair descent for 89 steps from three subjects on Stair 1 (black), and 63 steps on Stair 3 (red). The trajectories start from state 2 and the vertical lines mark the state transitions.

The motor current and kinematic data were processed to determine the joint torques and powers during the strides; kinetic data were normalized by body-mass and plotted in Fig. 3-8 and 3-9. Figure 3-8 shows the mean body-mass-normalized joint torques for stair ascent for the three subjects for Stair 1, which includes a total of 89 strides (i.e., 22 strides for subject S1, 34 for S2, and 33 for S3), along with plus and minus one standard deviation about the mean. Figure 4.9 shows the corresponding mean body-mass-normalized joint power, along with plus and minus one standard deviation about the mean.

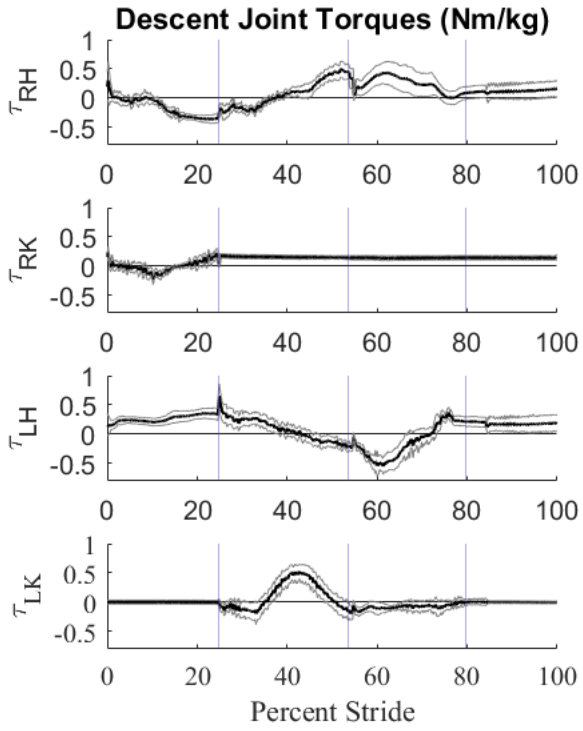

Figure 3-8: Average descent joint torques are shown for three subjects over 90 steps on Stair 1. Dashed lines are plus and minus one standard deviation. The plots begin in State 2 and vertical lines mark state transitions. Positive torques correspond to extensive moments

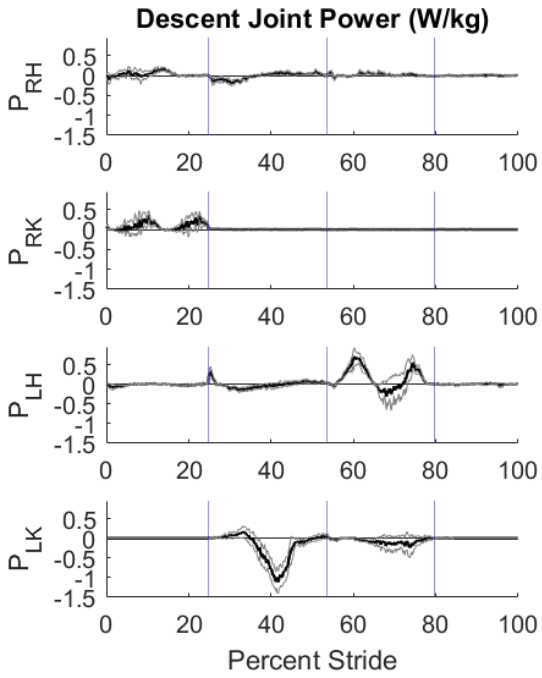

Figure 3-9: Average descent joint powers are shown for three subjects over 89 steps on Stair 1. Dashed lines are plus and minus one standard deviation. The plots begin in State 2 and vertical lines mark state transitions

3.5.3 Other Results

Step time (i.e., the time required to ascend or descend a single stair) is a determined by the trajectory speed and the user's ability to trigger the step sequence. Figure 3-10 shows the average step time (i.e., the time required to ascend or descend a single stair) for each subject for three consecutive ascents and descents of the staircase depicted in Fig. 5(a), along with the average across all subjects, along with plus and minus one standard deviation for each. The average ascent time per step across users was 7.8±0.64s, while the average descent time per step across users was 9.2±1.1s.

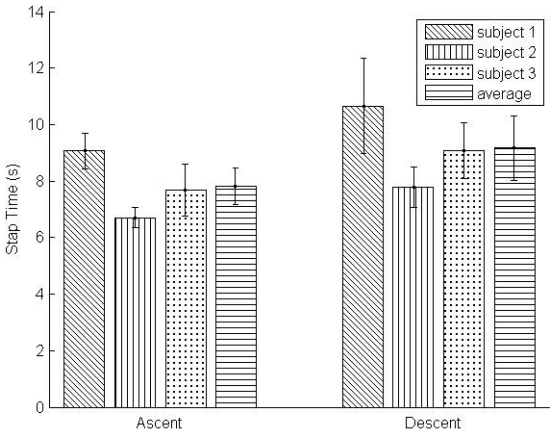

Figure 3-10: Average time per step of each user for 36 steps, and the average of the group with plus/minus one standard deviation bars.

Variable step height accommodation is observed in ascent State 3 as the controller only progresses to the following state after tread contact is detected. Figure 3-11 shows the hip and knee joint angles of the right leg at the exit of the damped lowering state of ascent (i.e., State 3, when the exoskeleton senses foot contact with the next stair tread). For taller steps the damped lowering is exited in a more flexed position (i.e., greater angles) than the shorter steps. The percent difference of joint angles is 32% at the hip and 30% at the knee when comparing Stair 2 to Stair 3, for which the percent difference in step height is 66%. Stair 1 is omitted from this evaluation because of the similarity in height to Stair 3, with a percent difference in step height of 8%. Note that the similar differences in joint angles are not observed in stair descent because the lowering state has a predetermined trajectory component that flexes the leg to a maximum desired flexion, thereby achieving contact on the stance leg regardless of variation in step height.

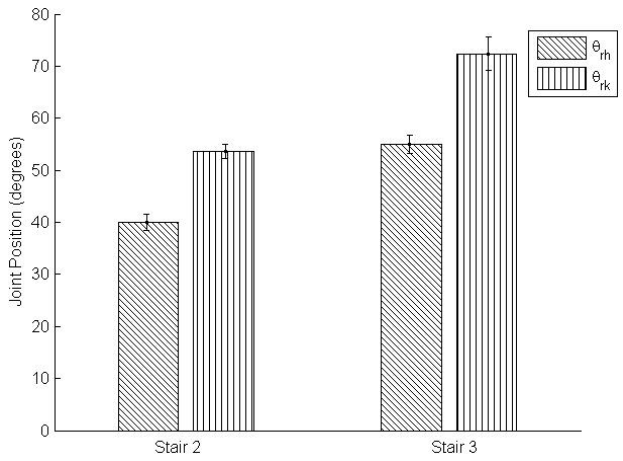

Figure 3-11: Average angle measurements and plus/minus one standard deviation bars for the right hip (RH) and right knee (RK) at the transition point from the state 3 of ascent where stair tread contact is made for stair 2 and stair 3, corresponding to step heights of 7.62 cm and 15.24 cm respectively.

Finally, the average Borg perceived exertion rating for ascent and descent were both 9.7±1.5, where a rating of 9 corresponds to “very light” exertion, and a rating of 11 corresponds to “light” exertion. The reported perceived exertion indicates that the robot is supplying and dissipating energy to significantly reduce the effort required by the wearer. The energy generated and dissipated by the exoskeleton motors is found by integrating the power data shown in Figs. 3-6 and 3-9. Positive power occurs when the exoskeleton adds energy to the system, such as lifting the total mass during State 3 of ascent or increasing a joints velocity. Negative power occurs when the exoskeleton dissipates energy from the system (e.g. lowering the total mass, reducing joint velocity). The energy generated or dissipated by the exoskeleton during ascent and descent was normalized by the potential energy of one step, i.e., by the amount of energy required to ideally raise or lower the combined human and exoskeleton mass through the height of one step under gravity. As such, the energy delivered or dissipated is described as a “normalized energy,” where the energy is normalized by the change in system potential energy associated with ascent or descent of a single stair (i.e., by the center-of-mass work). Integration of motor power for stair descent across all stairs and subjects indicates a mean normalized energy per step dissipated by the exoskeleton during stair descent of 57±6% (of the center-of-mass work). Integration of motor power for stair ascent across all stairs and subjects indicates a mean normalized energy per step provided by the exoskeleton during stair ascent of 140 ± 14% (of the center-of-mass work). Note that in both cases, the power and energy is measured at the motors, not at the joints; as such, inefficiencies in the drive trains will result in increased energy dissipation at the joints during stair descent relative to that reported, and decreased energy contribution during stair ascent. Further, it is important to recognize the distinction between center-of-mass work and joint-level work. The former accounts strictly for center-of-mass motion relative to gravity, while the latter entails components of movement that are associated with changing body configuration

and horizontal progression, in addition to components of movement associated with center-of-mass relative to gravity. Therefore, although the energy dissipated or generated by the motors provides some indication of energy contributions relative to center-of-mass work, motor contributions should be interpreted with appropriate limitations. In order to more clearly account of the energetic contribution of the exoskeleton in stair ascent and descent would require force plates in the stair treads that measure vertical forces under the exoskeleton, and a motion capture system that measures vertical center-of-mass motion, which were not available during the studies described here. Nonetheless, the numbers presented here at least indicate that the exoskeleton motors provide substantive energy dissipation and contribution relative to the energy requirements of stair descent and ascent, respectively.

3.6 Discussion

The three subjects were able to capably ascend and descend stairs of heights varying from 7.6 to 16.5 cm, without any stair-specific adjustments in the controller. Further, the same controller parameters were employed for all three subjects, with the exception of the lean thresholds, which were adjusted to suit each subject, although subsequently left to remain invariant between stair geometries. Note that the lean thresholds used in the walking controller (as described in [80]) are also adjusted to suit each subject. Doing so is necessary, since each subject has a unique posture, and the exoskeleton generally fits each subject somewhat differently. Nonetheless, the results suggest the proposed control structure is able to accommodate different subjects with minimal customization (i.e., lean thresholds), and subsequently different stair geometries without controller adjustment. Table 1 provides a comparison between some characteristics of exoskeleton stair ascent and descent on Stair 1 and data from healthy subjects presented in [1] on a comparable stair geometry, which are referenced in the discussion below. It should be noted that the healthy stair ascent and descent data corresponds to a step-over gait, while the exoskeleton provides a step-to gait. Despite this limitation, in the absence of a more appropriate benchmark, the step-over healthy data provides some context with which the exoskeleton ascent and descent performance can be compared. The following discussion considers each row of Table 1 sequentially.

Table 3-1: Exoskeleton and healthy stair ascent and descent characteristics. Healthy data from [1]

	Exoskeleton		*Healthy*	
	Ascent	Descent	Ascent	*Descent*
Step Time (s)	7.8±0.6	9.2±1	1.4±0.1	*1.2±0.1*
Max Hip Flexion (°)	78±1	58±1	70	*45*
Max Knee Flexion (°)	103±1	97±2	95	*90*
Mean Joint Std (°)	1.5	0.8	8	*8*
Peak Hip Moment (Nm/kg)	0.9±0.2	0.7±0.2	0.5	*0.6*
Peak Knee Moment (Nm/kg)	0.9±0.1	0.6±0.1	1.1	*1.3*
Peak Hip Power (W/kg)	0.9±0.2	-0.3±0.1	1	*-0.4*
Peak Knee Power (W/kg)	1.4±0.3	-1.3±0.2	2.5	*-4*

As observed in the first row of the table, ascent and descent with the exoskeleton is considerably slower than healthy gait. Despite this, the consistency of step time is quite similar. Specifically, the standard deviation in ascent and descent for the three subjects using the exoskeleton was 7.6% and 10.8%, respectively, while the corresponding standard deviation for a cohort of healthy subjects was reported to be 7.1% and 8.3%, respectively [1]. As shown in the second and third rows, the maximum hip and knee joint angles during ascent and descent are also quite similar. Specifically, the maximum knee joint flexion is 103 and 97 deg for stair ascent and descent, respectively, with the exoskeleton, and 95 and 90, respectively, for healthy. The maximum hip joint flexion angles are 78 and 58 deg (ascent and descent) for the exoskeleton, and 70 and 45 (ascent and descent) for healthy. The exoskeleton provides larger hip and knee movements than typical of healthy subjects in part to compensate for a lack of ankle dorsiflexion, and also to accommodate variable stair geometry in ascent.

The fourth row of Table 3-1 provides the standard deviation of joint movement, relative to the mean, over a stride, for a single stair geometry. In this case, each joint is considered separately, but the resulting standard deviation between joints averaged together to provide a single measure to characterize consistency of joint motion. As seen in the table, the exoskeleton data indicates an average standard deviation of 1.5 and 0.8 deg, respectively, for the exoskeleton, while [1] reports 8 deg for both. As such, the exoskeleton provides more consistent motion between subjects, relative to healthy data. This may be expected, however, since the exoskeleton employs the same trajectories between subjects, while healthy subjects are not similarly controlled.

The fifth row of Table 3-1 lists the peak hip and knee joint torques (corresponding to Stair 1). Specifically, the mean peak torques at the stance hip and knee during State 5, the step-to motion (i.e., when the exoskeleton lifts the body mass up to the next step) are 0.89±0.2 Nm/kg at the hip and 0.86±0.07 Nm/kg at the knee. These body-mass-normalized peak torques are 176% and 78%, respectively, of the corresponding peak hip and knee joint torque during the same phase of healthy ascent. Averaged between joints, the exoskeleton provides an average peak joint torque of 0.88 Nm/kg, while the corresponding torque for healthy ascent is 0.8 Nm/kg. As such, the averaged system-level torque provided by the exoskeleton is approximately 110% of healthy, indicating that the exoskeleton is providing a similar level of “lifting effort” to that observed in healthy ascent. The corresponding data for descent indicates peak torque of 0.62±0.07Nm/kg at the knee and 0.72±0.18 Nm/kg at the hip during State 3 where the exoskeleton lowers the body mass of the subject. The corresponding torques for healthy subjects are 0.6 and 1.3 Nm/kg, respectively. Considering the joint-averaged “torque effort,” the exoskeleton provides 0.67 Nm/kg while healthy subjects are characterized by 0.9 Nm/kg. As such, the exoskeleton is providing approximately 74% of the healthy effort during descent, while the remaining effort is presumably provided by the upper body (using handrails and/or crutches).

The last two rows of Table 3-1 show peak power (corresponding to Stair 1 and Figs. 9 and 13). The peak power at the stance hip during State 5, the step-to motion (i.e., when the exoskeleton lifts the body mass up to the next step) is 0.88±0.2 W/kg, and at the knee is 1.4±0.3W/kg. By comparison, the corresponding values for healthy ascent are 1.0 and 2.5 W/kg, respectively. Employing a joint-averaged power, the exoskeleton provides 1.14 W/kg, while healthy are characterized by 1.75 W/kg. As such, the exoskeleton provides approximately 63% of the peak power of healthy ascent.

The peak power during descent during State 3 (i.e., the lowering state) is -0.3±0.1 and -1.3±0.2 W/kg for hip and knee, respectively, while the corresponding values for healthy gait are -0.4 and -4.0 W/kg. Averaged across the two joints, the exoskeleton provides -0.8 W/kg peak power dissipation, while healthy provides -2.2 W/kg. Therefore, the exoskeleton provides approximately 36% of peak healthy power dissipation.

3.7 Conclusion

A variable-stair-height exoskeleton controller was presented to enable stair ascent and descent in an exoskeleton employing powered hip and knee joints. The controller was implemented in a lower limb exoskeleton, and its efficacy in providing stair ascent and descent functionality was assessed in trials involving three motor-complete SCI subjects, who performed stair ascent and descent on three stair geometries. All subjects were able to capably ascend and descend all staircases. Data from these trials support the ability of the controller to accommodate staircases of variable geometry, without altering control parameters. Data recorded from these trials further indicate movement that is considerably slower relative to healthy subject stair ascent and descent, but with otherwise similar motion characteristics. Specifically, the exoskeleton provides peak joint torques on average 110% and 74% of the corresponding healthy peak joint torques during ascent and descent respectively, and peak joint powers on average 63% and 36% of healthy data during ascent and descent, respectively, with differences provided by upper-body effort. Finally, despite data indicating effort required of the upper body, ratings of perceived exertion by the users rated the effort required to perform the activity between “very light” and “light.”

CHAPTER 4: MANUSCRIPT 2 - SUPPLEMENTAL STIMULATION IMPROVES SWING PHASE KINEMATICS DURING EXOSKELETON ASSISTED GAIT OF SCI SUBJECTS WITH SEVERE SPASTICITY

By Andrew Ekelem and Michael Goldfarb

Published in Frontiers in Neuroscience, vol. 12, June 2018.

DOI: 10.3389/fnins.2018.00374

4.1 Abstract

A hybrid FES-exoskeleton system comprehensively address SCI by providing structural stability with the exoskeleton and muscle activation with the FES. The Indego and Chimera enabled a hybrid system to be explored when combined with a cable network and unifying controller. Up to this study, most exosksleton controllers for SCI had been demonstrated on complete motor paralyzed individuals with mild spasticity. It was apparent through empirical observation that spastic individuals had difficulty making meaningful strides when using the exoskeleton alone. The lack of synergy between the spastic muscles and the exoskeleton motors not only detrimental to the performance but fails the fundamental objective of rehabilitation as the muscles are activating in opposition to the user's intention.

Strong extensor spasticity resists the exoskeleton movements sufficiently to expose dramatic misalignment between the exoskeleton joints and the user's. A lack of synergy between the anatomical and robotic actuators causes excessive deformation of straps and soft tissue when using orthotic or wearable devices. Modeling strap dynamics and inferring device limitations and possible control compensators is the objective of other studies [91]–[93]. Here, pathological muscle activity due to spasticity is treated with FES to improve physiological and robot synergism.

4.2 Introduction

Spasticity is a common comorbidity resulting from spinal cord injury (SCI), where approximately 68-75% of individuals with SCI experience spasticity and 20-40% have problematic spasticity that restricts activities of daily living [30]. Spasticity is commonly defined as involuntary muscle activity initiated by uninhibited reflex circuits, and can be categorized as intrinsic tonic, intrinsic phasic, or extrinsic nocuous [30], [31]. Tonic and phasic spasticity are thought to be caused by the hyperactive stretch reflex circuits after central neurologic impairment of the corticospinal inhibitory pathways. Symptoms of spasticity include a counter torque proportional to the angular velocity about the joint and an increase in muscle tone. Spasticity is ordinarily evaluated through the Modified Ashworth Scale (MAS) which involves a trained

assessor rapidly advancing a joint through its range of motion and evaluating the stiffness of the joint on a scale from zero to four, see Table 1 [2], [32]. Significant tonic and/or phasic spasticity can be problematic for attempts to restore mobility to a paretic or paralyzed limb.

Spasticity may be managed to achieve a balance between useful and detrimental effects by progressing from physical rehabilitation, pharmacological intervention, injection, intrathecal baclofen, and surgery [30]. Useful effects of spasticity induced muscle activity include: reduced muscle atrophy and improved blood circulation, which can reduce predispositions to other comorbidities that commonly result from frequent wheelchair use [30], [36]. Therefore, spasticity is typically managed to a level that best balances comfort and quality of life (QOL).

Recently, lower limb exoskeletons have begun to emerge onto the commercial marketplace. Such devices can facilitate legged mobility for individuals with SCI. These devices have the potential to improve the QOL of people with lower limb paralysis by enabling them to walk, generally via actuated knee and hip joints [86]. Exoskeletons have been shown to enable safe over-ground weighted walking and gait training for the mobility impaired, particularly for individuals with SCI [86]. The presence of severe spasticity, however, can severely impair the ability of an exoskeleton to provide a viable walking movement [94]–[96]. Severe extensor spasticity, in particular, can preclude hip and knee flexion during the swing phase of walking, thereby largely nullifying the ability of the exoskeleton to provide effective legged mobility.

Functional electrical stimulation (FES) applies artificial electrical impulses to initiate action potentials in muscle and nerves for a functional response. FES has proven effective in enabling ambulation in the SCI population when used alone, but when used alone can be metabolically taxing, is prone to rapid fatigue, and may lack limb control and stability. A few studies have proposed the use of FES with orthotic devices, generally called hybrid FES systems, which can provide several advantages relative to using FES alone [97]–[100], and one prior study investigated a hybrid FES system that couples FES with a robotic exoskeleton [101]. That study specifically coupled a lower limb exoskeleton with FES of the quadriceps and hamstrings muscle groups of each leg, and demonstrated reduced exoskeleton motor torque and power when used in a hybrid FES manner.

The intent of this research is to investigate the potential of supplementing a lower limb exoskeleton with FES for the purpose of enabling individuals with severe extensor spasticity to effectively walk in a lower limb exoskeleton when those individuals would otherwise have difficulty to do so. Preliminary studies indicate that exoskeleton walking may have beneficial effects with respect to mitigating spasticity [86], [94], [96], and as such, making this technology available for individuals with moderate to severe spasticity may have particular value for this sub-population. In order to do so, the authors propose here to supplement an exoskeleton with stimulation of the common peroneal nerve with the intent of exciting the flexion withdrawal reflex. Common peroneal nerve stimulation has been shown to assist in swing by

initiating a concerted flexion of the hip, knee, and ankle [102]–[104]. Stimulation of the common peroneal nerve activates the flexor withdrawal reflex, which comprises afferent neurons activating motor units responsible for flexion, as well as inhibitory interneurons that inhibit ipsilateral extensors while activating contralateral extensors [21]. As such, the hypothesis behind peroneal stimulation is twofold: first, the reflex is hypothesized to temporarily inhibit the extensor tone resulting from severe extensor spasticity, and second, the reflex is expected to recruit the lower limb flexors, and therefore supplement the exoskeleton motors during swing. In order to evaluate this hypothesis, a lower limb exoskeleton system was configured to incorporate supplemental FES of the common peroneal nerve, and experiments were conducted on two SCI subjects with severe extensor spasticity to evaluate the effect of supplemental peroneal stimulation on exoskeleton-generated swing phase movement.

4.3 Methods

4.3.1 Clinical Status

Two subjects were recruited for these experiments. The subjects had thoracic-level motor-complete SCI (i.e., ASIA A or B) to exclude voluntary motor control of the lower limbs; had right and left leg extensor spasticity rated on the Modified Ashworth Scale (MAS) of three or greater (see, Table 4-1); and were responsive to stimulation of the flexor withdrawal reflex. Subject characteristics relevant to the experiments are given in Table 4-2, and respective MAS scores given in Table 4-3. This study was conducted with the informed consent of each subject and with the approval of the Vanderbilt University Internal Review Board.

Table 4-1: Modified Ashworth Scale description [2]

Modified Ashworth Scale	*Description*
0	No increase in muscle tone
1	Slight increase in muscle tone, manifested by a catch and release or by minimal resistance at the end range of motion when the affected parties moved in flexion or extension
1+	Slight increase in muscle tone, manifested by a catch, followed by minimal resistance throughout the remainder (less than half) of the range of motion
2	More marked increase in muscle tone through most of the range of motion, but the affect part is easily moved
3	Considerable increase in muscle tone, passive movement is difficult
4	Affected part is rigid in flexion or extension

Table 4-2 Subject characteristics

Subject ID	S1	S2
ASIA	T11 B	T4 B
Level	T11	T4-5
DOI	Mar 2010	Dec 2013
Body Mass (kg)	66	88
Height (m)	1.83	1.73

Table 4-3: Modified Ashworth Scale ratings for each subject.

Muscle Group	S1 R/L	S2 R/L
Hip flexors	1+/1	0/1
Hip extensors	2/1	0/0
Knee flexors	2/2	2/2
Knee extensors	3/3	3/3
Hip adductors	3/3	3/3
Hip abductors	0/0	0/0
Ankle dorsiflexors	0/0	0/0
Ankle plantarflexors	3/3	4/3

4.3.2 Stimulator

A custom stimulator was developed on an embedded system, which was controlled in the same MATLAB Simulink/Stateflow environment used to control the exoskeleton, and connected via the same CAN cable. As such, the sensor information and control associated with the exoskeleton and stimulator were fully synchronized. The custom stimulator employed a bipolar stimulation waveform with 200 μs pulse widths at a frequency of 50 hz. The device controls the peak current output with a maximum amplitude of 80 mA. Square sticky-gel 3.8 x 3.8 cm (1.5 x 1.5 in) electrodes were placed over the common peroneal nerve on each leg, see Fig. 4-1. A total of two stimulator channels were used, one for each leg. The stimulation amplitude was set prior to donning the exoskeleton to a level that elicited strong ankle dorsiflexion, but not so high as to raise the heel off the ground while in a seated position.

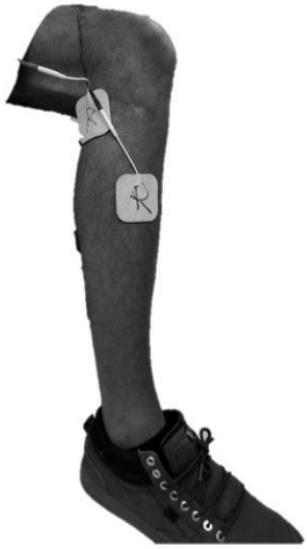

Figure 4-1: Typical electrode placement for stimulation of the common peroneal nerve.

4.3.3 Hybrid Controller

The state machine for the Indego walking controller is shown in Fig. 4-2 with state transition conditions described in Table 4-4. To account for the latency of the stimulation to produce movement, the stimulation was activated during the lean check state, which identifies the user's intent to take a step by maintaining a forward lean (i.e., forward movement of the estimated center of pressure), as measured by inertial sensors in the exoskeleton, for 200 ms. Once swing is initiated, the stimulation remains on for 40% of the swing phase, during which the majority of flexion occurs.

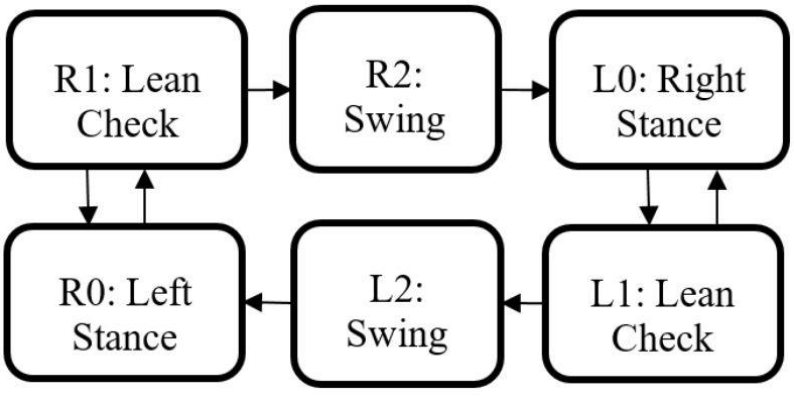

Figure 4-2: Walking state machine with corresponding transition conditions in Table Table 4-4

Table 4-4: State machine transition conditions

Transition	Condition
R0 to R1 or L0 to L1	Rear thigh angle exceeds lean threshold
R1 to R0 or L1 to L0	Rear thigh angle less than lean threshold
R1 to R2 or L1 to L2	State timer exceeds 200 ms
R2 to L0 or L2 to R0	State timer exceeds 1.1 s

Figure 4-3 shows the desired joint trajectories commanded by the exoskeleton controller as the state machine cycles through a right and left step, along with the corresponding timing of the stimulation pulse. When the stimulation is off, the stimulation amplitude is maintained at zero.

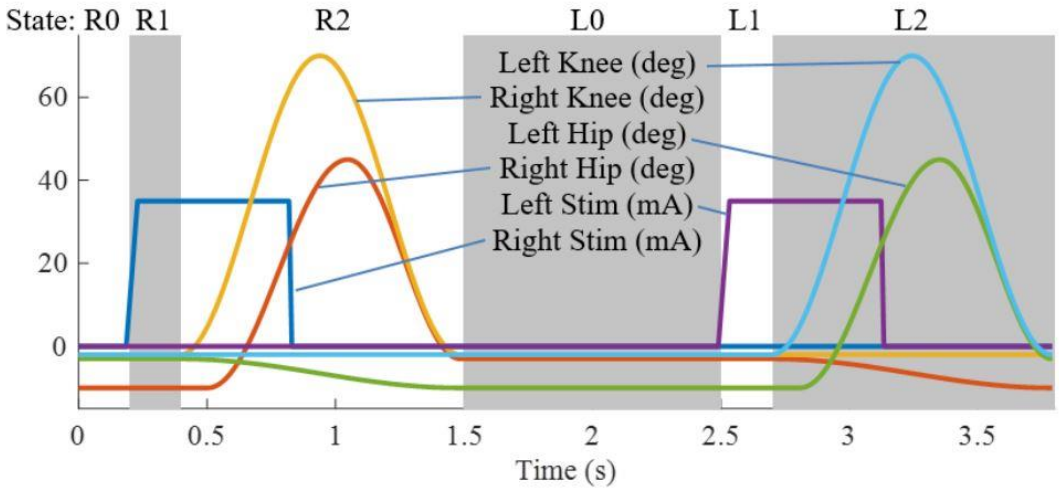

Figure 4-3: Trajectories for the four exoskeleton joints and the stimulation amplitude for the right and left legs as the state machine progresses through two steps.

4.3.4 Experimental Procedure

Participants were fit with the exoskeleton and given practice sessions (< 4 hours per day) walking with FES on and off, until they could comfortably walk and advance the balance aid (i.e., the walker), see Fig. 5.4, for one hour taking breaks as needed. After sufficient training sessions, each subject had a data session where they donned the FES system, Indego, and XSens MVN Awinda system (Xsens Technologies B.V., Netherlands) motion capture system and walked for approximately one hour, taking rest breaks as needed. The Xsens wireless sensor based motion tracking system was used to capture the kinematic data of the lower limbs during each session. This system includes seven sensors, one sensor for each limb segment (feet, shanks, thighs, and hip). The trajectories measured by Xsens Motion tracker were then processed in MATLAB to identify the peak flexion angle of each joint for each step. For these experiments,

the stimulation was programmed to alternate on and off every 10 steps to assess the relative value of stimulation on exoskeleton motion. Gait data was recorded during the data session, totaling 232 steps for S1, and 260 steps for S2. MAS were evaluation prior to donning the equipment and after doffing the equipment.

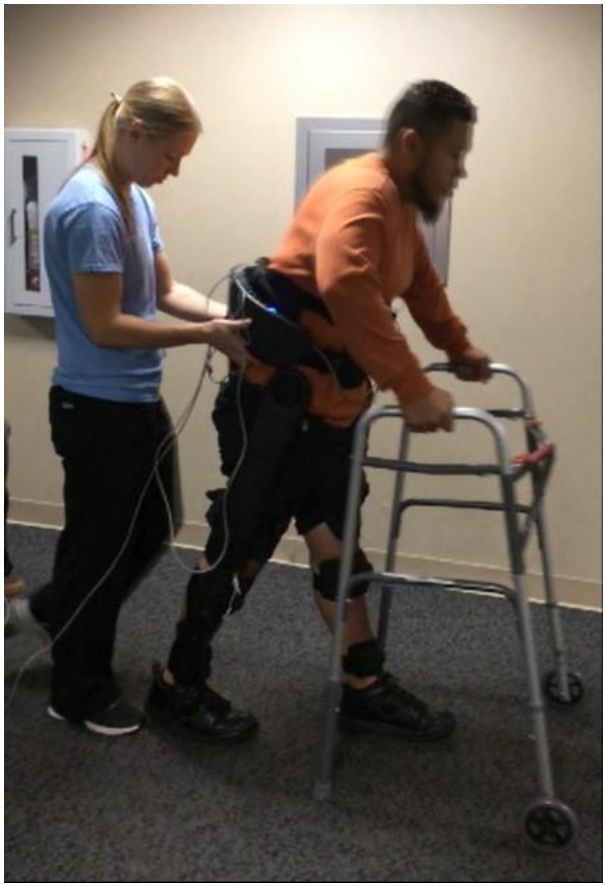

Figure 4-4: Subject walking with the exoskeleton and stimulator, using a walker for balance. The physical therapist monitors the gait as a precaution in accordance with the Vanderbilt IRB. The subject has consented to the use of this photograph.

4.4 Results

Common peroneal stimulation increased the step length for both subjects, which was reflected in the kinematic data. The hip and knee angles of a representative walking session is plotted in Fig. 4-5. The colored dots/hashes indicate the peaks found with a MATLAB algorithm, and does not include half steps, which are the steps in and out of neutral stance (when both hip equilibrium positions are equivalent). The grey bands indicate periods where FES is off. As seen in the data, the subject was able to achieve significantly greater hip and knee flexion with FES, which is indicative of larger steps and greater toe clearance.

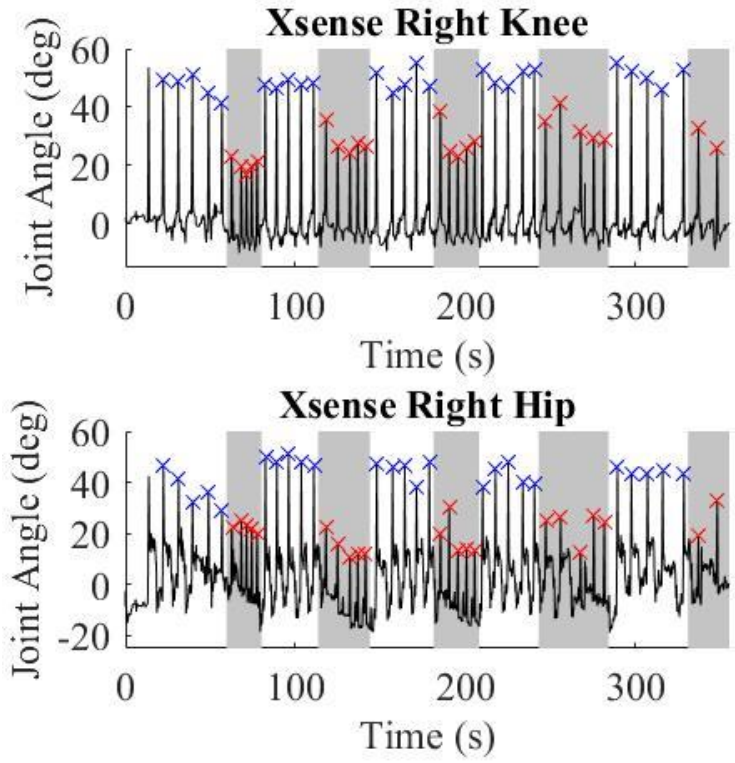

Figure 4-5: Representative joint angles from walking trial with subject S2. The gray bars indicate periods with FES off and the white bars indicate steps taken with FES on. Flexion peaks are identified by hash marks; blue for steps with FES assistance, red for steps without FES assistance.

The peak flexion found for each step was averaged for the hip and knee joints of each subject and plotted in Fig. 4-6, with error bars denoting the standard deviation. Stimulation assistance increased the mean hip peak flexion angles by 15.8 deg (151%) and the mean peak knee angle by 14.3 deg (58.8%). Significance in differences in the means were assessed using paired t-tests for the intra-participant peaks, which indicated that the differences in average knee and hip joint flexion between the FES-on and FES-off cases was significant with greater than a 1% confidence level.

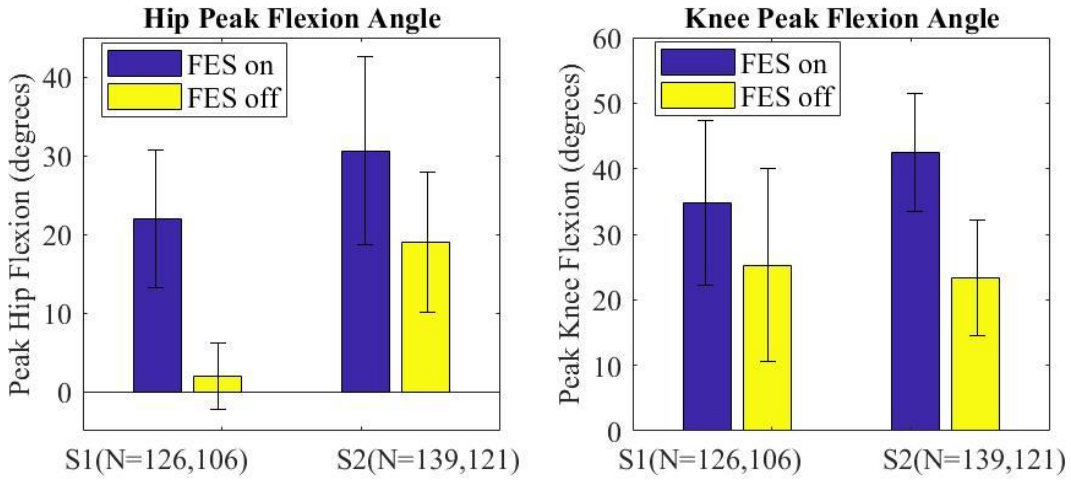

Figure 4-6: Median peak joint angle across all steps for each subject plotted for FES assistance on and FES assistance off. Error bars mark plus and minus half of the interquartile range. Wilcoxon analysis determines FES on and off had significantly different medians for each joint of each subject, $p < 0.01$.

Motor current data from the exoskeleton was logged and analyzed to evaluate the effects of FES assistance on motor torques. The RMS motor current for the swing leg was averaged for all steps for each subject and grouped into FES on and FES off, see Fig. 4-7. Across subjects FES decreased the swing RMS current by 249 mA (15.3%) at the hip motors and 581 mA (29.8%) at the knee motors. Additionally, the intra-participant mean swing RMS currents with FES-on and FES-off were significantly different within 1% confidence level for both subjects.

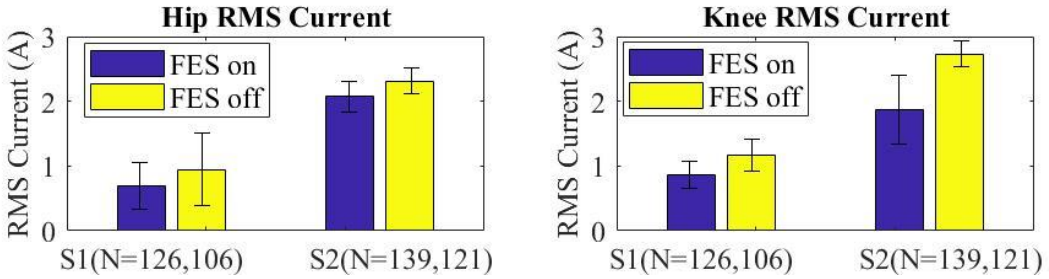

Figure 4-7: Median of the RMS current of the swing leg for all steps plotted for FES assistance on and FES assistance off. Error bars mark plus and minus half of the interquartile range. Wilcoxon analysis determines FES on and off are significantly different for each joint of each subject, $p < 0.01$.

4.5 Discussion

Stimulation the flexion withdrawal reflex improved the flexion kinematics significantly during exoskeleton assisted gait for participants with severe extensor spasticity. Qualitatively, both subjects had difficulty achieving toe clearance while walking with the exoskeleton without stimulation (i.e., toes consistently dragged on the ground). Adding stimulation greatly improved the gait kinematics and enabled these participants to take significantly larger strides.

Additionally, FES has been shown to provide therapeutic value for persons with SCI by activating the dormant neuromuscular tissue of the paralyzed limbs. The improved blood flow furthermore may reduce the likelihood of some comorbidities associated with SCI. For these reasons the addition of flexor withdrawal stimulation may be beneficial to all SCI, including individuals with minimal spasticity.

Although some prior studies indicate a possible reduction in spasticity resulting from the use of exoskeletons, in this research, the MAS scores did not change significantly from before to after the walking session.

A greater number of subjects should be evaluated to make generalized claims regarding the use of supplemental FES for subjects with severe extensor spasticity. Furthermore, the rehabilitation community would benefit from studies that explore the broader impact of exoskeletal walking in the SCI population.

4.6 Conclusion

In two thoracic-level SCI subjects with severe lower limb extensor spasticity, supplemental stimulation of the common peroneal nerve was shown to significantly enhances walking movement generated by the exoskeleton, and to significantly reduce the current demand on the exoskeleton motors. Results of more subjects would strengthen the conclusion of this work. The authors hope that employing supplemental FES as described here will make exoskeletal walking a viable option for individuals with SCI and severe extensor spasticity, who otherwise would not be candidates for viable exoskeleton walking.

CHAPTER 5: CLONUS ATTENUATOR EVALUATION

5.1 Abstract

This chapter describes a FES controller for the treatment of clonus. Clonus is caused by disinhibited self-exciting reflexes from both proprioceptors and exteroceptors, along with mediation from central pattern generators. Pathological clonus is often evoked by perturbations from the terrain during wheelchair propulsion. As such, clonus interrupts wheeled mobility by displacing the limbs once excited. An *anti-clonus model* using FES was presented in 1967; however, data presented is limited to a single subject in a controlled environment [105]. To evaluate the adaptive anti-clonus FES controller presented here, inertial and video data acquired from wheelchair users traversing rough terrain was analyzed. Visual review of clonus and clonus-attributed foot displacement enabled quantitative evaluation of the clonus treatment. The treatment uses inertial sensors to classify clonus activity and terrain perturbations likely to evoke clonus, and intelligently administers electrical stimulation to suppress the spasticity.

5.2 Introduction

Injury to the descending neurons interrupts supraspinal communication with the affected spinal neurological circuits. Void of supraspinal inhibition, spinal networks may exhibit involuntary reflexive muscle activity referred to as spasticity. Spasticity is a symptom of many neurological conditions. Clonus is one manifestation of spasticity that consists of cyclical muscle activation due to hyperactive stretch reflexes. 65-78% of people with SCI have spasticity, 40-60% of which is described to affect activities of daily living (ADL); 50% of whom are prescribed pharmacological intervention [30], [106]–[108].

Wheelchair propulsion is critical to activities of daily living (ADL) for the majority of persons with spinal cord injury (SCI). Shaking caused by ankle clonus often interferes with propelling a wheelchair; the movement can involuntarily remove the feet from the footrest. The resulting dislodged appendage is exposed to injury and often necessitates wheelchair users to stop to reposition. Such effort and discomfort caused by clonus may deter SCI individuals from traversing bumpy terrain, even sidewalks, thereby negatively impacting ADL Other symptoms of spasticity may aid with ADLs and tissue health, however clonus has little benefit and should be managed to eliminate detrimental effects with interventions ranging from physical rehabilitation, pharmacological agents, botulinum toxin injection, intrathecal baclofen, to rhizotomy [30]. As the treatments progress, the associated costs, risks, and effectiveness increase. This work describes an effort to evaluate the efficacy of a noninvasive naturopathic therapy for treating clonus with functional electrical stimulation (FES).

5.2.1 Mechanisms of Clonus

The rhythmic muscle contractions of ankle clonus occur consistently in the range of 3-8 Hz and are typically initiated with a dorsiflexion stretch of the ankle. The contingency on joint position suggests that the stretch reflex is a key contributor to the condition [30], [77]. Additionally, clonus frequency has been shown to correlate with external load and neural pathway length, suggesting the proprioceptive afferent feedback loop is important for the mechanism of clonus [109], [110]. The stretch reflex is a monosynaptic reflex where muscle spindle type Ia afferents (proprioception afferent types: Ia - velocity, Ib – tension, II - length) synapse with motor units. Percutaneous electromyography has confirmed that stretch does correspondingly activate single motor units, and likely needs continuous excitation to sustain clonus [111], [112]. Such continuous excitation may arise from extrinsic perturbations to the joint or intrinsic activity of pattern generators.

In the case of wheelchair propulsion there is no shortage of extrinsic perturbations from vibrations or bumps to elicit afferent activity, however, the diverse degree of excitability among persons with paralysis and the inter- and intra-day variability is likely due to the complex interaction of central mechanisms with the paralyzed muscles. Three elements suggest the involvement of central mechanisms for maintaining clonus: electrophysiological evidence of simultaneous antagonist muscle activation, contralateral muscle activity modulation of clonus, and inputs other than stretch may evoke clonus [78], [113]–[115]. Hence, there are at least two contributing factors to the manifestation of clonus after upper neuron damage: disinhibited reflexes (stretch and vibration) and afferent excitation of central pattern generators.

5.2.2 Therapeutic Interventions

Identifying the outcome measures are critical for prescribing and evaluating an intervention for spasticity. Although numerous tests exist for quantifying various components of spasticity (Ashworth, pendulum, Tardieu, SCATS), other outcomes such as risk, cost, and patient expectation must all be considered when prescribing an intervention [116]. The preliminary treatment is physical intervention.

Physical therapy for managing spasticity includes appropriate positioning, weight bearing and stretching [30], [117], [118]. These lower the excitability of the stretch reflex with effects that may range from ineffective to effects carrying over a day [119]. Therefore, the benefits of physical therapy require frequent repetition.

The market leading pharmacological agent for anti-spasticity is oral Baclofen taken by about half of people with SCI. Baclofen has been established as the most effective treatment for spasticity although its exact mechanisms is still unknown. Literature suggest that Baclofen acts by on interneurons to selectively inhibit reflex activity, enabling voluntary muscle activity to be unaffected [120], [121]. Baclofen is often

covered by insurance, however has been attributed to general side-effects; transient drowsiness is the most common side-effect (63% of Baclofen users) [122]. The total cost per year before insurance is $3,500.

Botulinum toxin (Botox) is another option for those with spasticity and is a treatment where the patient receives a shot injected once a month into the spastic muscle. This focal treatment acts on the axon endings of the neuromuscular junction, preventing acetylcholine neurotransmitter from activating the muscle. Botox costs $300 to $500 per treatment (often not covered by insurance).

The other two options for severe cases of spasticity are surgical procedures: rhizotomy and intrathecal baclofen pump implantation. These are highly invasive and have upfront costs of approximately $16,000 and $19,000 respectively [123]. The high cost of pharmacological interventions necessitates the development of naturopathic interventions for treating paralysis cost effectively.

5.2.3 Electrotherapy for Reducing Clonus

Many efforts have demonstrated some form of electrical stimulation to effectively reduce some aspects of spasticity [23], [124]–[129]. The neural activation from the artificial stimulation modulates the spinal networks, and if properly applied, stimulation has been shown to have short-term and long-term merits for treating spasticity. FES of the peroneal nerve has been attributed to long-term reduction in tone and phasic spasticity for hemiparesis [126], [130]. Recent applications of epidural or transcutaneous spinal cord stimulation (SCS) has also demonstrated promise for treating spasticity and restoring volitional control by inhibiting the hyperexcited reflexes [24], [131]–[135]. Nonetheless, widespread adoption of noninvasive neurostimulation for treating spasticity has not occurred despite growing evidence supporting that the efficacy of such therapeutics is equal to or better than baclofen [136], [137].

While many studies have evaluated transcutaneous electrical nerve stimulation (TENS) and transcutaneous SCS for treating general symptoms of spasticity (hyperactive reflexes), just a single model first described in 1967 has explored using FES to suppress clonus, specifically presented as the “anticlonus model” credited to Milan Dimitrijevic [105], [138], [139, pp. 217–218]. The anti-clonus model treats clonic triceps surea via stimulation of the peroneal nerve for the monosynaptic reflex that results in a slight tonic contraction of the tibialis anterior and reciprocal inhibition of the tricep surea [21]. Dimitrijevic expresses that although efficacy is dependent on frequency of the stimulation pulses, the method is robust to temporal variability of excitability, and has potential beneficial long-term potentiation of clonus suppression. Although Dimitrijevic suggests this model is suitable for a device that uses myoelectrical or electromechanical sensor to detect clonus and the stimulation to suppress clonus, no literature, sale or publication of such a device has been found to validate the efficacy of the anti-clonus model.

The two objectives of this research are to develop a controller to intelligently administer anti-clonus stimulation, then evaluate functional outcomes of the system with wheelchair users who experience clonus when traversing real-world terrain. One evaluation method, *the Benchtop Clonus Study* (described below), repeatedly initiates clonus using triceps surea stimulation while the anti-clonus device suppresses clonus. This method provides a controlled study paradigm for repeatedly initiating clonus in an effort to observe the temporal response to repeated anti-clonus stimulation for a sample of the heterogeneous user population. The second method, *the Over-ground Study,* uses instrumentation to observe wheelchair propulsion over rough terrain, enabling a comparison between traversing the terrain with FES and without FES.

5.3 Methods

5.3.1 Overview

Subjects were recruited to explore the real-world efficacy of the proposed FES intervention for clonus treatment. The experimental protocol began and ended with a spasticity evaluation using the Spinal Cord Assessment Tool for Spinal Reflexes (SCATS) and Drop Test (DT) [34], [140], [140]. Three Chimera boards were donned: one on each of the subject's legs (just below the knees), and one on the subject's wheelchair. Minimum and maximum peroneal stimulation amplitudes were established and input to the state-machine controller to limit stimulation to a comfortable range. The intervention was evaluated on real-world terrain by alternating the controller off then on for each trial while collecting data: video, three accelerometers, real-time wheelchair speed (SmartDrive encoder), and stimulation parameters. The over-ground study was intended to characterize real-world clonus through data collection while the subjects traversed bumpy terrain with and without FES intervention. To supplement the over-ground study, a benchtop evaluation was also performed to examine the temporal nature of FES for activating clonus consistently and suppressing the potential resulting clonus.

5.3.2 Controller

The Chimera stimulation devices of each leg were controlled by a hierarchical finite state machine (HFSM) for administering anti-clonus peroneal stimulation for the ipsilateral leg. State transitions are dependent on timers and the filtered accelerometer signals that construct the *terrain* and *clonus signals*. Both signals are linear functions of the accelerometer signal with the axis aligned with that of the tibia.

To derive the clonus signal, the raw accelerometer signal is bandpass filtered from 3-8 Hz, rectified and enveloped with a low-pass filter (0.5 Hz), see Fig. 5-1. The clonus measure gives an indication of the magnitude of shaking within the bandwidth indicative of clonus.

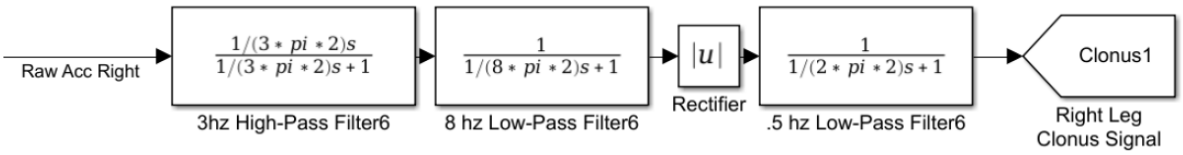

Figure 5-1: Clonus signal processing

The anti-clonus controller for over-ground was developed to not only detect clonus but additionally detect bumpy terrain. To detect rough terrain, the accelerometer signal was high-pass filtered to eliminate the steady state gravity acceleration, rectified and lowpass filtered to create an enveloping signal of acceleration magnitude, see Fig 5-2.

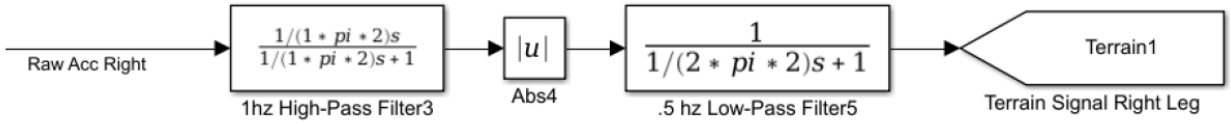

Figure 5-2: Terrain signal processing

The clonus and terrain signal from each leg is then used in the HFSM controller, such that if the terrain or clonus signals exceeds a threshold the controller leaves the resting state for the rough terrain or clonus state, where anti-clonus stimulation is applied. Within the clonus state the stimulation amplitude adapts to limit the duration of clonus to a predetermined time (e.g., 3 seconds for SCATS *mild* clonus [140]). When the clonus signal is reduced below 50% the threshold, indicating clonus is no longer present, the stimulation ramps down to 0 ma and returns to rest state. The four sates of the state machine controller are shown in the Fig. 5-3, with state transitions in Table 5-1.

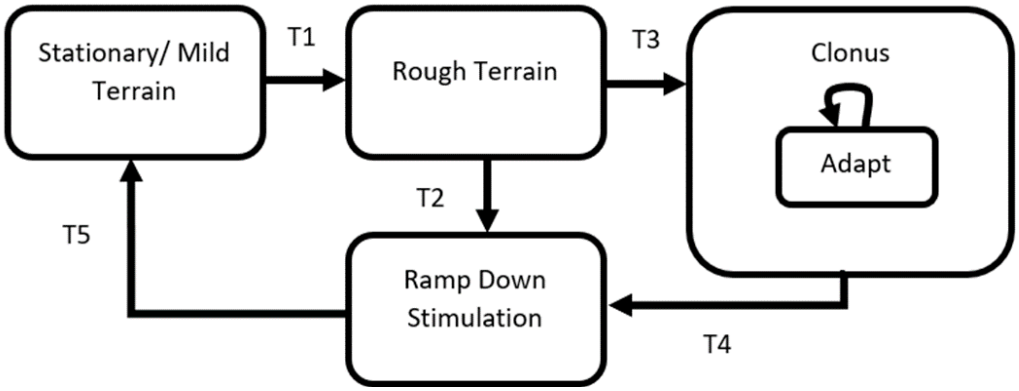

Figure 5-3: The anti-clonus controller hierarchical finite state machine. Refer to Table 5-1 for state transition conditions.

Table 5-1: State transition conditions for the anti-clonus controller

Transition	Condition
T1	Terrain signal > terrain threshold (e.g. ~0.1)
T2	Terrain signal < 0.7*(terrain threshold)
T3	clonus signal > clonus threshold (e.g. ~0.25)
T4	clonus signal < 0.5*(clonus threshold)
T5	Stimulation amplitude is zero

Thresholds for the state transitions were found empirically by traversing a smooth terrain and rough terrain. The threshold for the terrain was set slightly greater than the maximum measured terrain signal of smooth terrain; the clonus threshold was set slightly greater than the maximum clonus signal of the rough terrain (aged asphalt).

One limitation of a threshold detection method is the clonus signal includes interference introduced by the terrain that resembles clonus (3-8 Hz) (e.g., traversing 15 cm cobble stones at 1 m/s). While false positives may erroneously adapt the stimulation amplitudes, this is predicted to have non-substantial negative consequences in practice as the stimulation is limited to non-disruptive amplitudes. Furthermore, terrain of this nature is likely to excite clonus and the stimulation may prevent excitation. A supplemental accelerometer fixed to the wheelchair may be used to detect terrain interference and use differential analysis to distinguish the ground reaction accelerations from clonus detected at the leg accelerometers. A Chimera board was mounted to the wheelchair to explore this limitation further, although, a differential leg-chair signal has yet to be implemented.

The *adapt* sub-state-machine (Fig. 5-3) of the clonus state adapts both the anti-clonus and the preventative stimulation amplitudes. If the clonus state is re-entered within a predefined time (e.g., 6 s) the preventative stimulation is incremented (e.g., 2 mA); alternatively, if an extended period goes by without clonus, the preventative stimulation can be decremented. Rather than decrementing the preventative stimulation upon entry to the clonus state, however, it may be advantageous to decrement the preventative stimulation in the rough terrain state such that the effect occurs immediately. All incrementing, and decrementing is followed by a maximum and minimum saturation as to prevent an ineffective or uncomfortable stimulation amplitude setting.

The anti-clonus stimulation amplitude is set by the FES_Amplitude_Ch1 parameter of Fig. 5-4. This parameter is incremented if clonus lasts in excess of 3 seconds. Saturation at the maximum was implemented. A method for decrementing the anti-clonus stimulation has yet to be implemented.

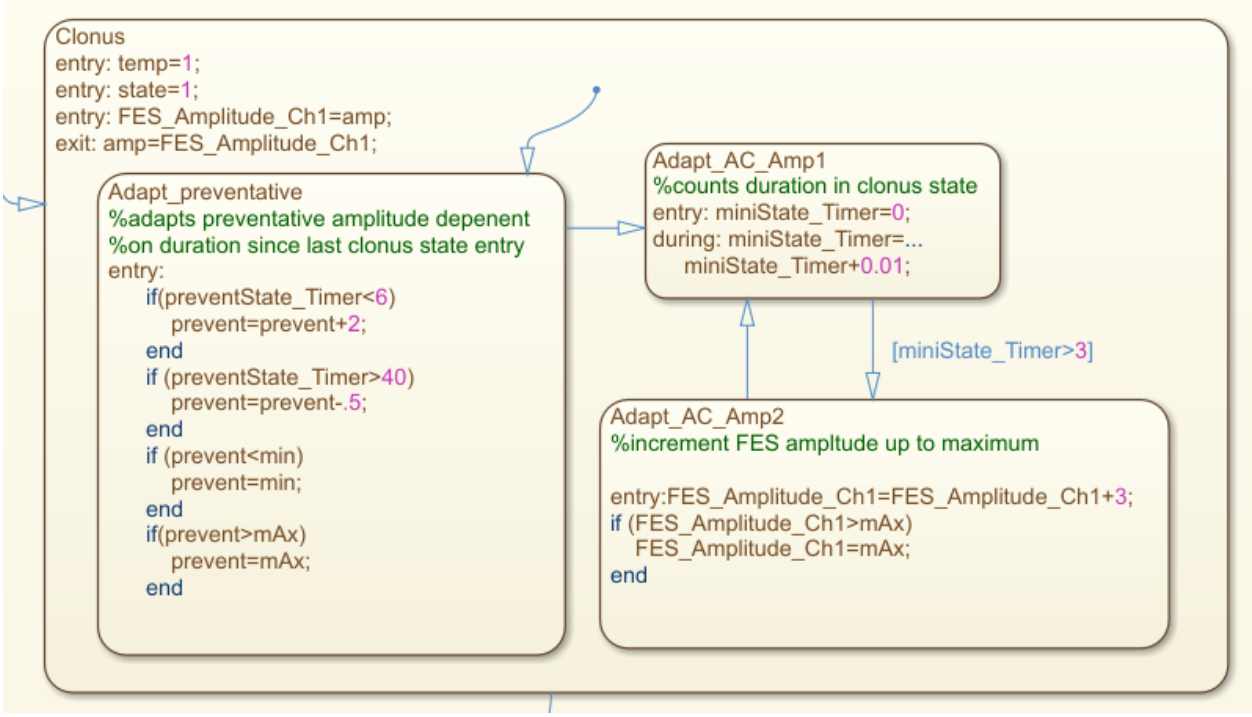

Figure 5-4: Anti-clonus controller *adapt* sub-state machine as implemented in Stateflow.

5.3.1 Over-ground Study

Each trial consisted of two sub-trials where the subject traversed a course for approximately 5 minutes while acquiring inertial and video data. During the first sub-trial, *the control sub-trial*, the stimulator was turned off while the sensors collected data and the controller ran; during the second sub-trial, *the intervention sub-trial*, the stimulator was activated allowing the controller to administer anti-clonus stimulation. The data was then used to evaluate the performance of the anti-clonus intervention in comparison to the control sub-trial.

Three of the Chimera boards where daisy chained via a CAN cable to synchronously communicate with Simulink. One Chimera board was strapped to each lower leg just below the knee. The third board was placed under the seat cushion, on top of the upholstery, or fixed to the bottom of the footrest using cable-ties and foam on the underside of the device, such that the cable-ties affixed the top of the 3D printed case rigidly to the underside of the footrest, see Fig. 5-5.

Figure 5-5: Three Chimera devices mounted on the wheelchair frame for the footrest inertia and on the lower legs for the over-ground clonus study

The Chimera boards sampled the MPU6000 IMU at 200 Hz and transferred the data to Simulink at a sampling rate of 100 Hz. This rate was suitable as to not overload the computer with long data collection sessions, and fast enough to ensure capture of the 5-8 Hz clonus signals, which would need sampling greater than 16 Hz to avoid aliasing. The bandwidth of the system is limited to the Nyquist frequency of 50 Hz at the sampling rate of 100 Hz.

Terrain

A variety of rough terrains were used to excite clonus: aggregate (5/8 pea gravel mixed with concrete), aged asphalt and large gravel (#4 limestone) were explored (Ground A-C, see Fig. 5-6). Each session consisted of multiple trials and possibly multiple terrains; although, each trial consisted of a pair of sub-trials with a control trial with anti-clonus stimulation off followed by an intervention trial with the anti-clonus stimulation turned on. The subjects were instructed to traverse at a self-selected speed. Each trial's sub-trials had the same number of laps of the same course.

Course A – Aggregate Course B – Age Asphalt Course C – Large Gravel

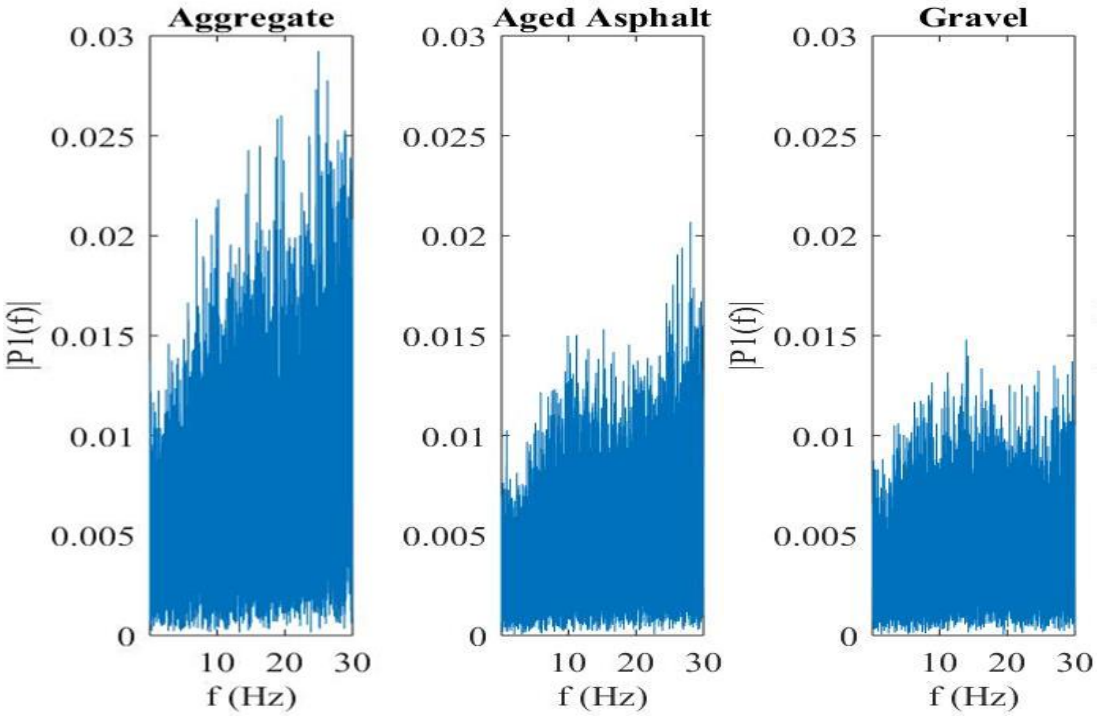

Figure 5-6: Three rough terrains were traversed during the over-ground study. The fast Fourier transform (FFT) of vertical acceleration from the footrest frame inertial sensor is plotted for 3 separate terrains. The FFT characterizes the terrain perturbations. Note, these example FFT are not intended to compare different terrains as they are from different wheelchairs and conditions.

Instrumented SmartDrive

A SmartDrive was programmed and provided by Permobil (Antioch, TN) to stream serial data to monitor velocity. The data includes: speed (mph), cumulative distance traveled, motor speed (mph), cumulative motor propelled distance, roll, yaw, and pitch at transfer rate of 10 Hz. A "Stream Input" block in Simulink enabled the data from the SmartDrive to be sampled at 100 Hz and logged synchronously with the Chimera CAN system. Subjects were given a tutorial on how to use the SmartDrive device for propulsion and allowed to use the device as desired to supplement manual propulsion.

One concern of adding the SmartDrive was the omni-wheel could introduce an interference due to the evenly spaced tangential wheels along the circumference of the drive wheel. To test the SmartDrive induced inertial interference, a test run was taken with a Chimera device fixed to a wheelchair, while the subject traversed a flat ground with and without the SmartDrive. The results indicate SmartDrive adds a power value of ~0.01 vertical acceleration interference to the wheelchair sensor, primarily at 14-17 Hz when moving approximately 2 mph shown in Fig. 5-7. Since the clonus signal of interest is between 3-8 Hz, the SmartDrive's minute interference was determined insignificant to the study of clonus.

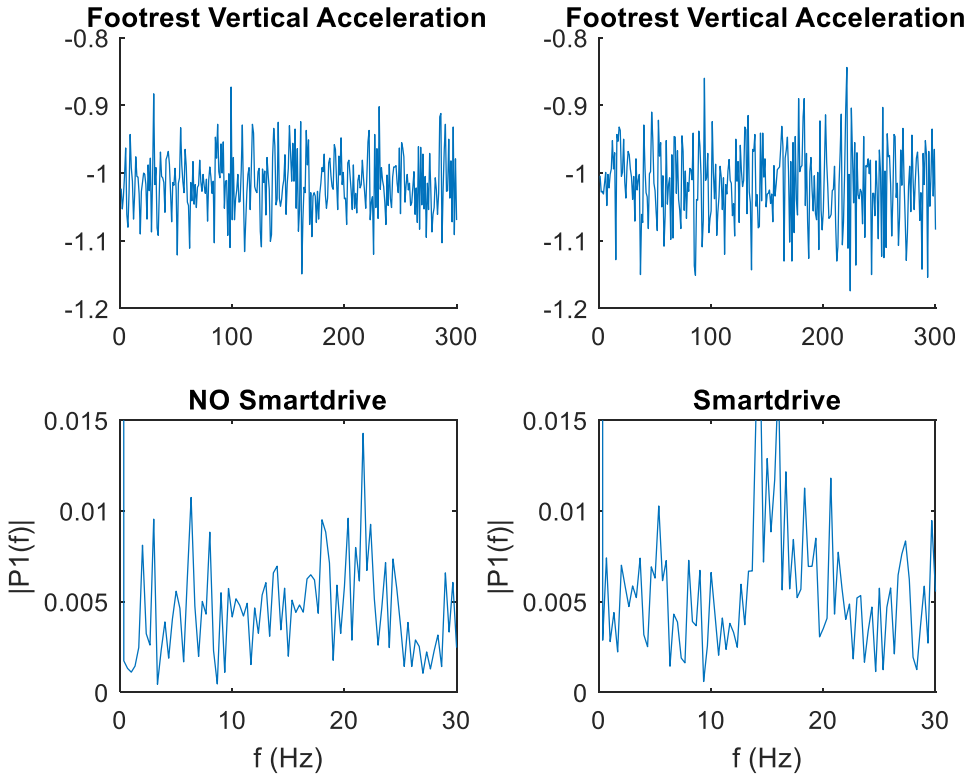

Fig 5-7: Shows traversing a flat ground in a wheelchair with and without a SmartDrive attached to the device.

Other considerations to explore further are the impact of pushing on clonus. Proprioception impacts the central pattern generators, thus the movement associated with pushing may alter clonus. For this experiment the subjects were not instructed to traverse the terrain in any specific manor, however they were given instructions on how to use the SmartDrive for propulsion assistance should they elect to use it.

Wheelchair-mounted Camera

Video footage of the ankles was taken with a camera (Samsung S7, Seoul, SK) mounted to a "selfie stick" that was secured (cable-tied) to the wheelchair frame. Footage of the trials was used quantify the duration of *clonus* and *foot-off* during of each trial. Raters subjectively evaluated the video for clonus, while the foot was on the footrest and separately for foot-off which is defined as the ball of the foot off the footrest and positioned such that that the foot points down abnormally, see Fig. 5-8. The videos were stabilized and watched at x0.5-1 speed in Youtube Creator Studio. A stopwatch was used to evaluate the percentage of each trial video footage with clonus while the foot was on the footrest, and separately evaluated when each foot was misplaced from the footrest. Hence, there are three exclusive conditions for each foot during the trials: normal, clonus, and foot-off. Visual analysis was used to evaluate the ability of the Chimera to prevent clonus and the foot from being displaced from the footrest.

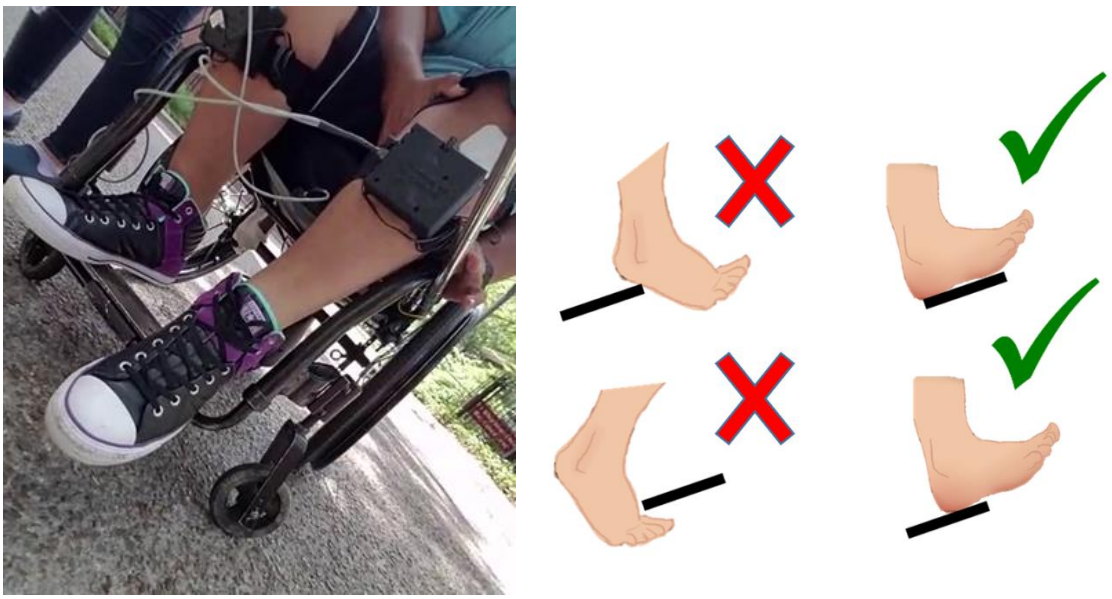

Figure 5-8: Foot-off is shown in the exemplary frame of the video from the wheelchair mounted camera. Foot-off and foot-on conditions illustrated with the foot in relation to the footrest (denoted by the black bar). The red X depicts that the foot is off the footrest, and the green check depicts the foot on the footrest. Foot images adapted from http://www.militarydisabilitymadeeasy.com/images/muscles%20of%20the%20foot/

5.3.2 Benchtop Study

Characterization of the short-term response to anti-clonus controller was performed by repeatedly initiating clonus and quelling it with the anti-clonus controller and device. The state machine controller autonomously initiated clonus by implementing a disturbance stimulus to the plantar flexors for 0.5 s after ten seconds of rest state. The disturbance evoked clonus by raising the ankle off the wheelchair footrest and allowing it to drop with gravity upon relaxation. Anti-clonus stimulation was applied to the common peroneal. This method was performed for a duration of 30 minutes unless no clonus was observed within ten-minutes. This test was conducted after the over-ground protocol and before the final clinical subject evaluation described below. The disturbance stimulation only initiated clonus in two of five of the sessions. Results from this portion of the protocol are still under review. Preliminary results from a pilot study are shown in Appendix D.

5.3.3 Subject Evaluation

Subjects with clonus were recruited through the Pi Beta Phi Rehabilitation Center at Vanderbilt University. The subjects were informed and consented in accordance with the Declaration of Helsinki and the Vanderbilt Internal Review Board. Inclusion criteria indicated that the subject have clonus as a symptom of SCI and not have taken Baclofen or other pharmacological spasticity treatment for eight hours prior to the experiment; general information is shown below in Table 5-2.

Table 5-2: Subject information.

SUBJECT ID	S1	S2	S3	S4
ASIA	T11 B	T4 B	T6 A	C5 B
MASS (KG)	66	88	59	65
HEIGHT (M)	1.83	1.73	1.88	1.53
LEVEL	T11	T4-5	T6	C5-6
DOI	Mar 2010	Dec 2013	Oct 2004	Jul 2008

The maximum and minimum stimulation amplitudes were found before and after over-ground trials by incrementing the stimulation amplitude over the peroneal nerve by 4 mA approximately every two seconds while the subject sat on a padded therapy table with feet flat on the ground (hip, knee, and ankle all at approximately right angles). The evaluation was done prior to the trials to set the boundaries for the controller, and after the trials to evaluate electrophysiological change over the period of the experiment. The *minimum stimulation amplitude* is defined as the minimal stimulation amplitude that elicits a visible muscle twitch or joint motion. The *maximum stimulation amplitude* is defined as the stimulation amplitude that elicits a visible hip flexion (heel off the platform or trunk flexion) or subject-reported discomfort. The controller was set to saturate 2 mA lower than the found maximum.

The Spinal Cord Assessment Tool for Spastic reflexes (SCATS) clonus evaluation and Drop Test (DT) exams were used to assess each subject's sensitivity to external stimuli and the intensity of their clonus reaction. The evaluations were conducted before and after the experimental protocol to inform any change in spasticity that might occur over the course of the experiment. Additionally, the established exams were employed to inform the observation and extent of clonus during the experimental protocol.

SCATS exam consisted of three tests to assess spasticity in three subfields: clonus, flexor spasms, and extensor spasms [3], [33]. This study utilized just the SCATS clonus test protocol to assess clonus. The test was adapted to observe the proprioceptive variability of the assessment by rating clonus in three positions from full extension, then flexed at 90°, and fully flexed; SCATS clonus protocol does not specify position of the leg [3]. It was observed that leg position did affect the outcome measure within each subject, however no pattern was established between subjects. For simplicity the mean score from the three positions and both legs is reported in the results. The SCATS clonus assessment was done by an assessor and scored on a scale of 0-3, see Table 5-3

Table 5-3: Spinal Cord Assessment Tool for Spastic reflexes clonus examination scores adapted from Benz et al 2005 [3].

Rating	Description
0	No Reaction
1	Mild; Lasting: < 3 Seconds
2	Moderate; Lasting: 3-10 Seconds
3	Severe; Lasting: > 10 Seconds

The Drop Test was used to examine a subject's ankle clonus by raising the subject's leg above a platform (approximately 5 cm) and dropping it. The setup requires that the heel is hanging off the edge of a platform to dorsiflex the ankle while the subject is sitting. DT may excite clonus and illicit the oscillatory response. Both number of oscillations and duration of the sustained clonus are valid points of measuring the response to the DT [34]. For this experiment, subjects donned the Chimera system on each leg prior to the DT, and the system recorded the inertial response. Figure 5-9 below shows an exemplary data of a DT (pre- and post- experiment).

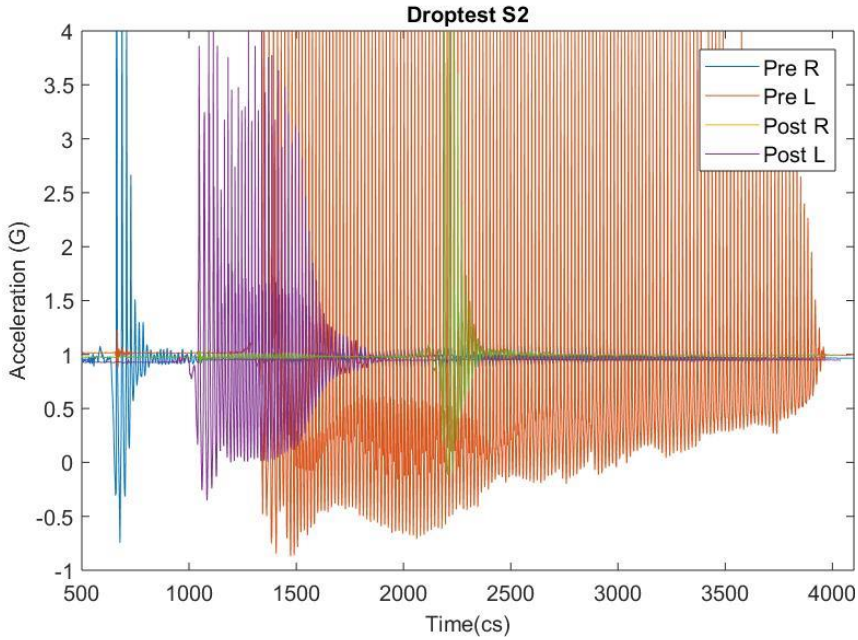

Figure 5-9: Observation of the drop-test on the left and right legs, before and after the experiment. Raw vertical acceleration data from the leg Chimera boards plotted in Gs over time.

5.4 Results

5.4.1 Over-ground Results

The over-ground study was conducted on four subjects over five sessions (repeated S2 after 10 days), each session with multiple trials that tested the efficacy of the anti-clonus intervention on various terrains. A total of eleven trials were evaluated. Data from each trial was parsed using Matlab and video footage was evaluated by a human evaluator using Youtube Creator Studio stabilization and slow-motion. Each trial consisted of two sub-trials where the subject traversed a course for approximately 5 minutes while acquiring inertial and video data. During the first sub-trial the stimulator was turned off while the sensors collected data; during the second sub-trial the stimulator was activated allowing the controller to administer anti-clonus stimulation.

Data from video was analyzed for the following metrics: percentage of clonus, percentage of foot off, and instances of clonus normalized by trail time (clonus rate). Key metrics per trial and experimental medians are shown in Table 5-4. Video data validates the FES controller substantially reduced the foot from slipping off the foot rest with median of 28.6±18% without FES and 3.0±3.4% with the FES controller on. Furthermore, the FES reduced the presence of clonus by nearly a factor of seven, from 20±6% (mean and std, normal dataset) to 2.9±2.1%. The pathologies of clonus, foot-off, and clonus rate were significantly reduced with the intervention to a within a 95% confidence interval using the Wilcoxon signed rank test. The data further indicates the FES controller retained 71±7.6% of the trials in the prevent state

and reduced the clonus rate from 1.2±0.45 episodes per minute to 0.4±0.18 episodes per minute. Median plus and minus half of the interquartile range were used as the data fails the Lilliefors test for normality.

The percent pathology difference is the percent difference of the sums of clonus and foot-off (pathologies) of the control and intervention sub-trials. This metric summarizes the efficacy of the anti-clonus intervention for treating pathological clonus during wheelchair mobility over rough terrain. Ten of the eleven trials saw a decrease in spasticity as a result of activating the FES controller. The median percent pathology difference is 86%, suggesting the treatment has meaningful benefits for wheelchair users with clonus.

Parsed controller data also provides stimulations metrics and state prevalence. The mean clonus and preventative stimulation amplitudes were normalized to the maximum set at the beginning of the experimental session. The prevent and clonus prevalence (%) are the percentage of the sub-trial spent in the corresponding state.

Table 5-4: Over-ground clonus evaluation results showing the average of both legs for the control and intervention sub-trials. Metrics reported include: rater evaluated prevalence of clonus and foot off (*% Video Cl* and *% Video FO*), the SmartDrive measure of speed, the clonus rate in instances (n) per minute. Additionally mean FES metrics for both legs are reported for the intervention sub-trial: mean active stimulation amplitude during the clonus and rough terrain states (*AC amplitude* and *Preventative Amp.*) and the prevalence of the rough terrain and clonus states. Median and interquartile range (IQR) for the eleven trials is reported below. Lastly the percent pathology is the difference in video evaluated prevalence of foot off and clonus between the control and intervention sub-trials.

Sub-trial:			Control Sub-trial				FES Intervention Sub-trial								
TRAIL	Subject	Terrain	% Video Cl	% Video FO	Speed (mph)	Clonus rate (n/min)	% Video Cl	%Video FO	Speed(mph)	Clonus rate (n/min)	Preventative Amp. (mA)	AC amplitude (mA)	Rough-terrain detected %	Clonus detected %	% Pathology Difference
1	1	B	44.6	47.4	2.5	1.65	0.6	0.0	2.5	0.40	47.2	49.4	74.0	1.3	99%
2	1	A	35.9	59.8	3.1	1.41	4.3	0.0	3.5	0.47	72.3	62.3	87.4	5.0	96%
3	2	A	12.0	28.6	1.5	1.30	32.2	13.3	1.6	1.08	64.6	85.1	45.2	37.1	-12%
4	2	A	18.5	42.7	1.1	2.15	5.4	0.0	1.7	0.64	55.5	77.5	78.2	8.4	91%
5	3	B	22.4	29.3	3.1	1.86	2.9	0.2	3.4	0.45	82.3	79.8	67.9	13.5	94%
6	3	B	25.4	40.4	3.7	0.64	5.9	3.0	3.3	0.87	69.5	65.4	68.2	11.9	86%
7	2	B	16.5	1.6	1.7	0.35	5.3	6.7	1.3	0.36	43.8	34.5	64.7	3.5	33%
8	2	A	28.2	7.1	1.7	0.87	1.8	11.2	1.9	0.28	44.5	25.0	81.4	0.1	63%
9	2	A	20.0	10.0	1.9	1.02	2.2	0.0	2.1	0.22	44.8	NA	91.5	0.0	93%
10	4	C	15.0	3.2	0.9	1.23	1.0	6.8	1.3	0.21	72.0	86.8	23.5	45.5	57%
11	4	B	1.7	5.3	2.4	0.10	0.0	4.4	2.3	0.00	66.3	72.3	71.1	11.6	37%
Median			20.0	28.6	1.9	1.2	2.9	3.0	2.1	0.4	64.6	68.8	71.1	8.4	86%
IQR			12.1	36.4	1.4	0.89	4.2	6.8	1.5	0.36	25.9	66.9	15.1	10.7	51.8

The prevalence of foot-off and clonus of each foot for each sub-trial is displayed in the Fig. 5-10 bar plot below. The data shows correlation between video evaluated clonus prevalence and controller clonus state prevalence, however, large discrepancies suggest the controller is limited in detecting clonus accurately. For example, Trial 10 is likely to have numerous false positives as the gravel terrain likely causes sufficient interference to resulting in the controller to remain in the clonus state; such may arise due to insufficient tuning of the clonus threshold for the rougher terrain. Other sub-trials, such as the control for 6 and 7, had substantial video detected clonus, however the subthreshold nature of the clonus did not result in the controller detecting the clonus.

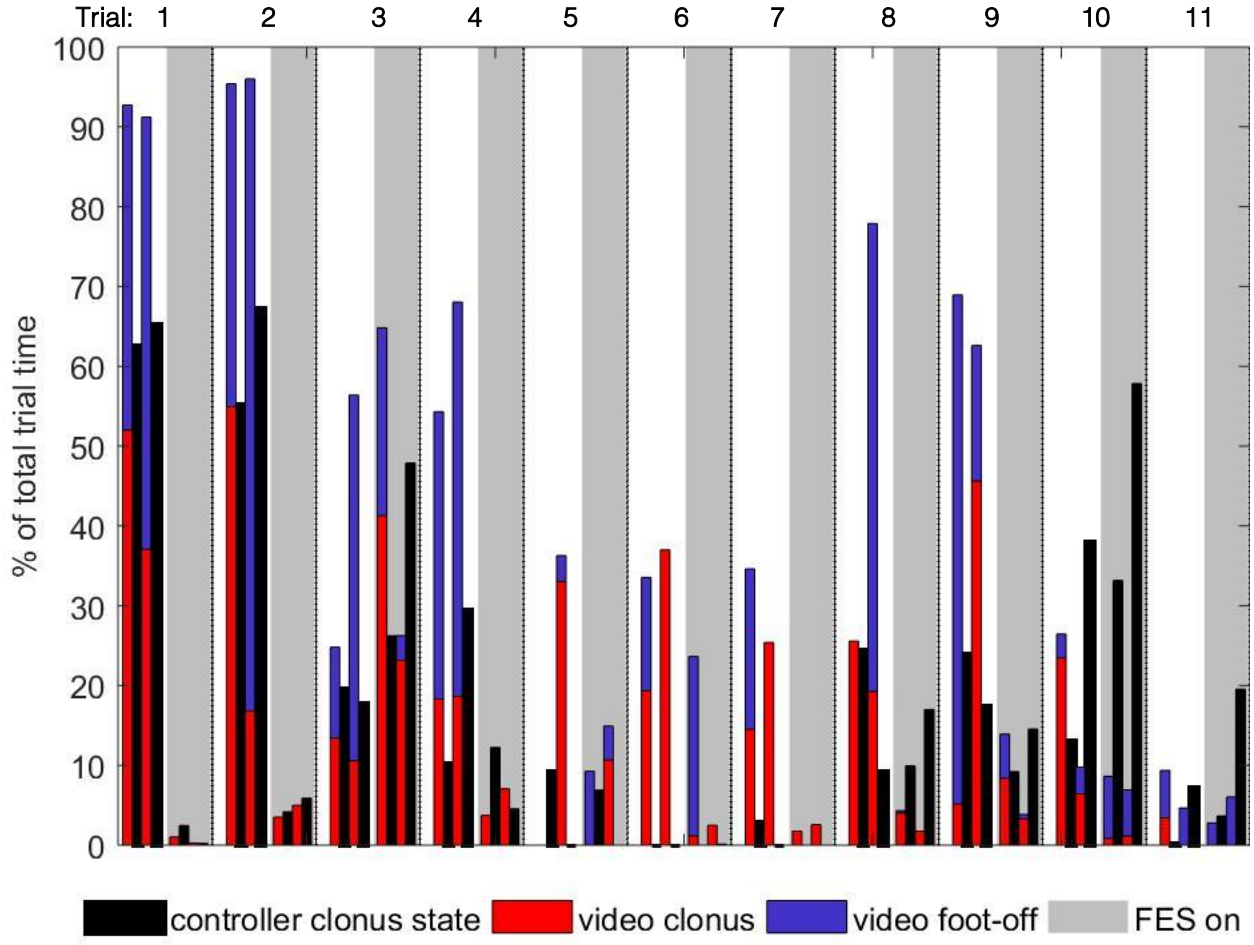

Figure 5-10: Detailed evaluation metrics for each leg during each sub-trial. White bands are control sub-trials and grey bands are intervention sub-trials.

Below exemplary data from Trial 6 is plotted in Fig. 5-11 and 5-12; first with FES off, then with FES on. These exemplary sessions show the anti-clonus stimulation adapts to prevent and suppress clonus. The preventative stimulation was incremented as clonus state was triggered within six seconds of the preceding clonus state indicating the terrain is triggering clonus. Longer clonus episodes influenced the

controller to increment the clonus stimulation amplitude until the clonus is suppressed within the prescribed time (i.e., 3 s). After the FES stimulation is incremented the value is stored to rapidly reduce future instances of clonus rather than restarting from the minimum amplitude. The stimulation amplitude represented in the plots are normalized to the predetermined maximum amplitude.

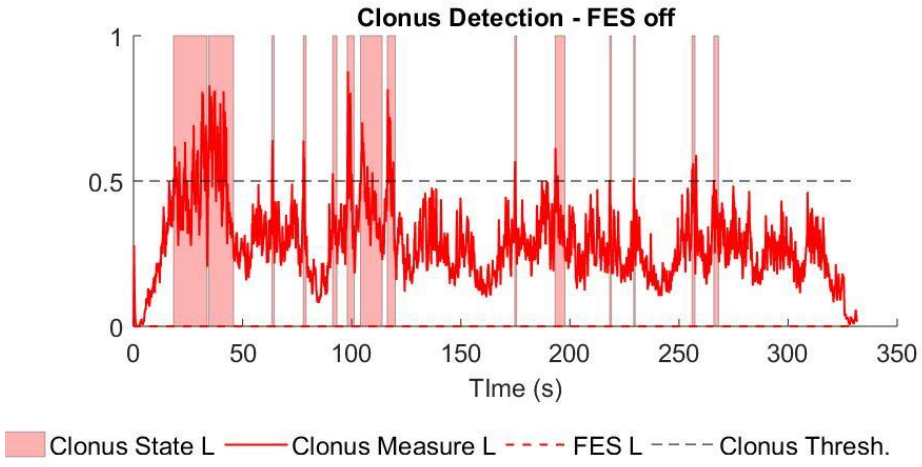

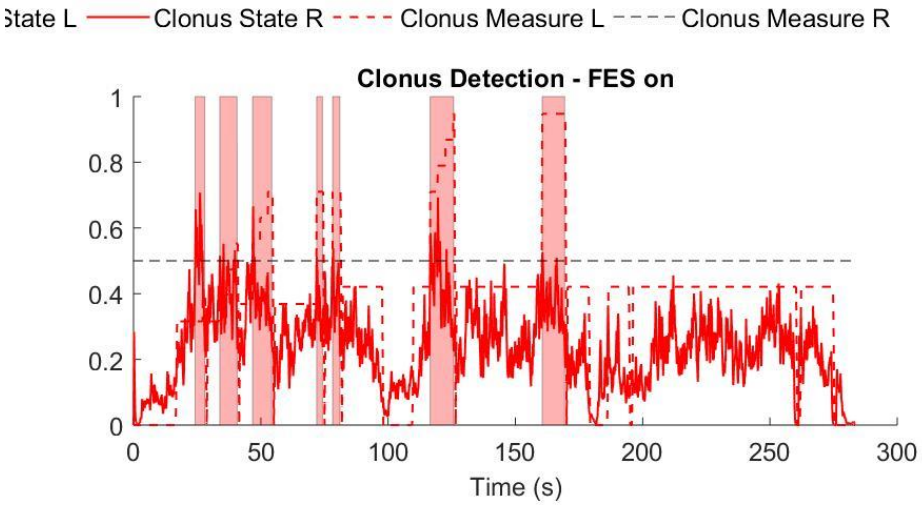

Figure 5-11: Exemplary clonus signal data from the left leg during Trial 6.

The terrain measurement is tasked to identify traversing of rough terrain that is likely to evoke clonus. The measure gates transitions T1 and T2 of the state machine (Fig. 5-3 above) whereby the controller transitions to or from *rest state* to the *rough terrain state*. Within the *rough terrain* state the anti-clonus stimulation ramps up to a preventative stimulation if the terrain measurement exceeds a threshold (e.g., 0.28). The preventative stimulation begins at the prescribed minimum stimulation amplitude. Each leg has a separate IMU, hence a unique terrain measurement and unique stimulation amplitude. Figure 5-12 shows rough terrain is detected for majority of the sub-trials.

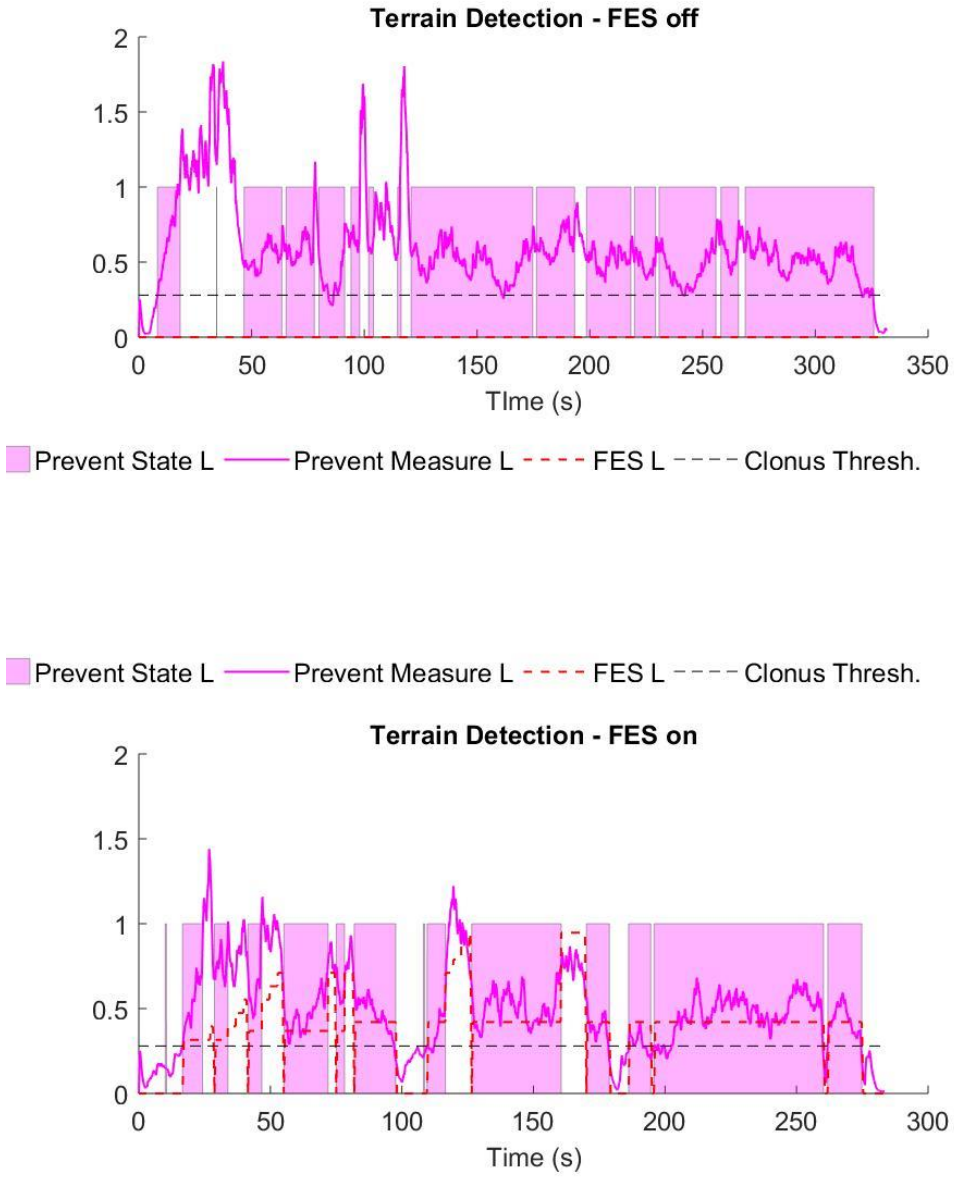

Figure 5-12: Exemplary terrain signal data from the left leg of Trial 6.

5.4.2 Subject Evaluation Results

Results from the subject evaluations, shown in Table 5-5, describe some physiological changes that may be a result of the intervention or over-ground propulsion. Subjects' clonus evaluations were mixed. There is no clear indication that the intervention affects the general clonus spasticity level, although on average the measures of clonus (drop test and SCATS clonus test) showed a slight decline in excitability after the experimental protocol. The pre- and post-intervention physiological measures each fail the Wilcoxon signed rank test for significance; a greater sample size is needed to determine the effect of the intervention on responsiveness to stimulation and excitability with confidence.

The data shows the maximum FES amplitudes, or withdrawal threshold, consistently increased after the intervention except for Session 1. Some subjects did not reach an uncomfortable level or elicit the flexion withdrawal reflex by the device maximum of 80 mA. Increased tolerance of the withdrawal reflex may be due to accommodation or habituation (see discussion). The minimum threshold, muscle twitch threshold, also increase after the experiment, indicative of fatigue.

Table 5-5: Summary of subject physiological evaluations pre and post experimental protocol.

	Drop Test (s)		SCATS		Min (mA)		Max (mA)	
Session	Pre	Post	Pre	Post	Pre	Post	Pre	Post
1	31.6	39.4	2.8	2.5	8	8	18	14
2	14.3	6.6	2.7	2.7	20	24	32	56
3	3.1	1.3	2.7	1	18	24	40	60
4	1.2	2.1	0.7	1.2	12	16	32	38
5	2.8	1	2	1.5	12	16	16	28
Mean % Increase		-14		-5		24		39

5.5 Discussion

Fatigue, Accommodation and Habituation

The minimum twitch stimulation threshold evaluated before and after the experimental session increased by an average of 24% for each subject. This measure is likely due to fatigue of the muscle. Motor axons of the underlying nerve have a larger cross-sectional diameter than sensory neurons and are recruited first by electrical stimulation. Furthermore, the artificial stimulation activates motor fibers synchronously, as opposed to the natural asynchronous recruitment, causing fatigue more quickly than normal. FES conditioning of muscles improves resistance to fatigue.

The mean increase of 39% of the maximum stimulation threshold that activates the flexor withdrawal reflex at is an indication of habituation or accommodation. Accommodation is a short-term loss of responsiveness that occurs when a constant stimulus, such as the preventative stimulus, acts on the

sensory system. One subject, S2, a single leg accommodate the stimulator maximum of 80 mA after each session had. One possibility is the withdrawal reflex is had been stimulated significantly to undergo habituation whereby synapses undergo physiological change to become less sensitive to a stimulus. Short-term and long term habituation are dependent on the interval of the stimuli application and likely act on interneurons involved in the flexion reflex ([9] p. 1250).

Habituation may limit the feasibility of long term use of the device and motivates maintaining the saturation levels further below the maximum stimulation threshold. Addition of the SCATS withdrawal test in a larger study is recommended to further explore plasticity in reflex related electrophysiology and eliminate changes intrinsic to the Chimera (e.g., low-battery, worn electrodes). Extended trials and regular-use experiments will further inform the physiological changes observed.

Terrain Detection

The SmartDrive enabled real-time velocity measurements from the encoder to be synchronously parsed with the Chimera sensors. The terrain signal data from the chair mounted Chimera has minimal clonus interference and was found to correlate greatest with a Pearson correlation coefficient of 0.85 while the terrain signal and clonus signal from an exemplary leg (right) had a correlation coefficient of 0.5 and 0.43 respectively. see Fig. 5-13. P-values of zero indicates there is positive correlation between the filtered vertical acceleration from both legs and the chair. The significance of this finding is that the vertical accelerometer signal feasibly indicates movement over a rough terrain. It is evident that the legs absorb vibrations from the ground damping the terrain signals measured from the footrest. While the terrain signal from a chair mounted IMU provides the greatest correlation to velocity, any of IMUs correlate sufficiently to detect binary motion (moving or not moving).

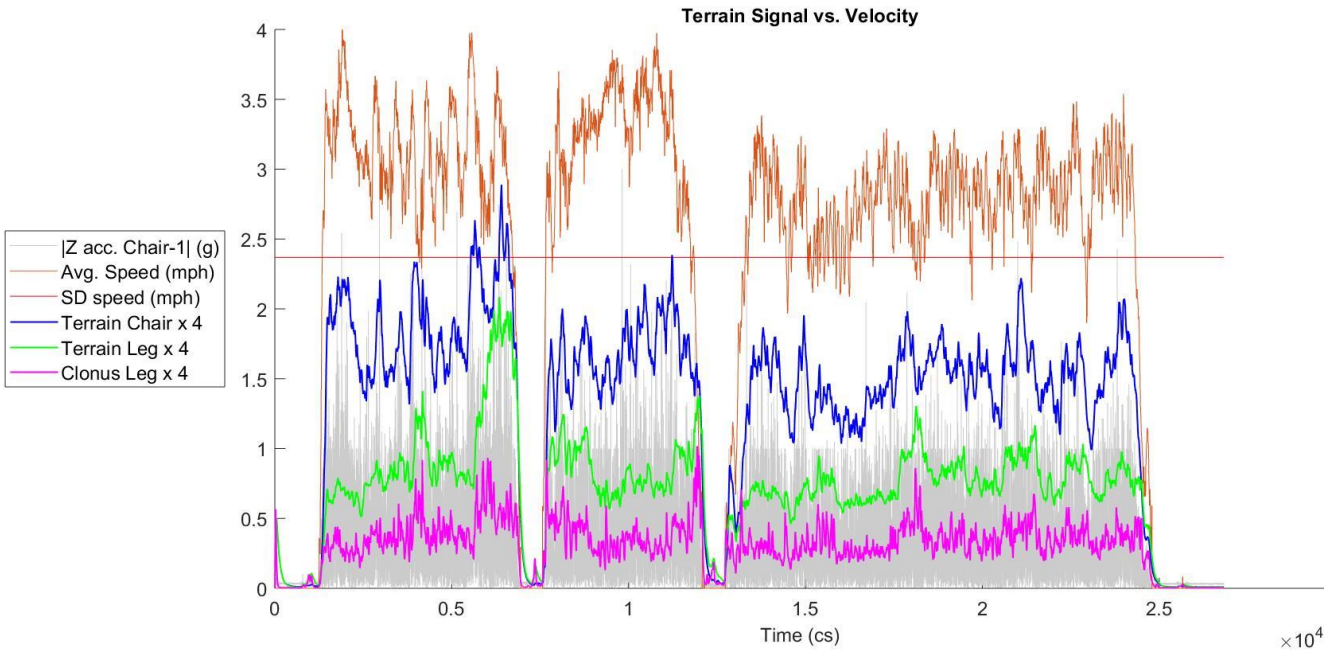

Figure 5-13: Velocity measure from the SmartDrive correlates to processed Chimera data from the leg and chair.

The terrain measurement is prone to interference from clonus. In a practical sense this is a nonissue for this application, since if clonus is present, it is desirable the state machine to advance from the rough terrain state to clonus. Alternatively, clonus of one leg causes mild interference with terrain measurement of the contralateral leg and chair since these units are physically interfaced through the chair frame which is vertically bound by the ground. A notch filter could potentially remove the interference caused by the clonus signal, although this would simultaneously eliminate terrain signals that resonate in the clonus bandwidth.

Bandpass Filter Improves Signal to Noise Ratio of Clonus Signal

Similar acceleration amplitudes caused by movements other than clonus are unusual but may include high frequency impulses such as when traversing door jams or curb ramp lips. The clonus signal filters the raw vertical acceleration between 3-8 Hz, then rectifies the signal and envelopes the resulting signal with a 0.5 Hz lowpass filter. This narrow bandpass substantially attenuates the amplitude of the signals caused by traversing bumpy terrain; the chair clonus signal (shown in Fig. 5-11 and 5-12) remains well within the clonus threshold while traversing a bumpy terrain. The clonus and terrain signals can be compared using signal to noise ratio (SNR), where the signal is the root mean square of the signal value during the clonus state, while the noise is the root-mean-square of signal value in the rough-terrain state. The clonus signal had a median SNR of 2.3 while the terrain signal had a median SNR of 2.0. These results validate the value of the bandpass filter for processing the clonus signal, from leg data from all the trials.

Raw Signal Spectral Analysis

The anti-clonus controller successfully determined instances of clonus that exceeded the threshold set empirically above the noise in the measurement caused by terrain A. The controller is limited to identifying clonus that exceeds the threshold. Sub-threshold clonus activity is shown in Fig. 5-14 in the "Not Detected" column; hence the activity in the clonus frequency of 5 Hz, however this disturbance has much less significant power, approximately one-fifth the power of the clonus-detected spectral analysis. Other techniques such as spike feature extraction, principle component analysis, or wavelet extraction may be employed for more rapid clonus detection without sacrificing specificity [141].

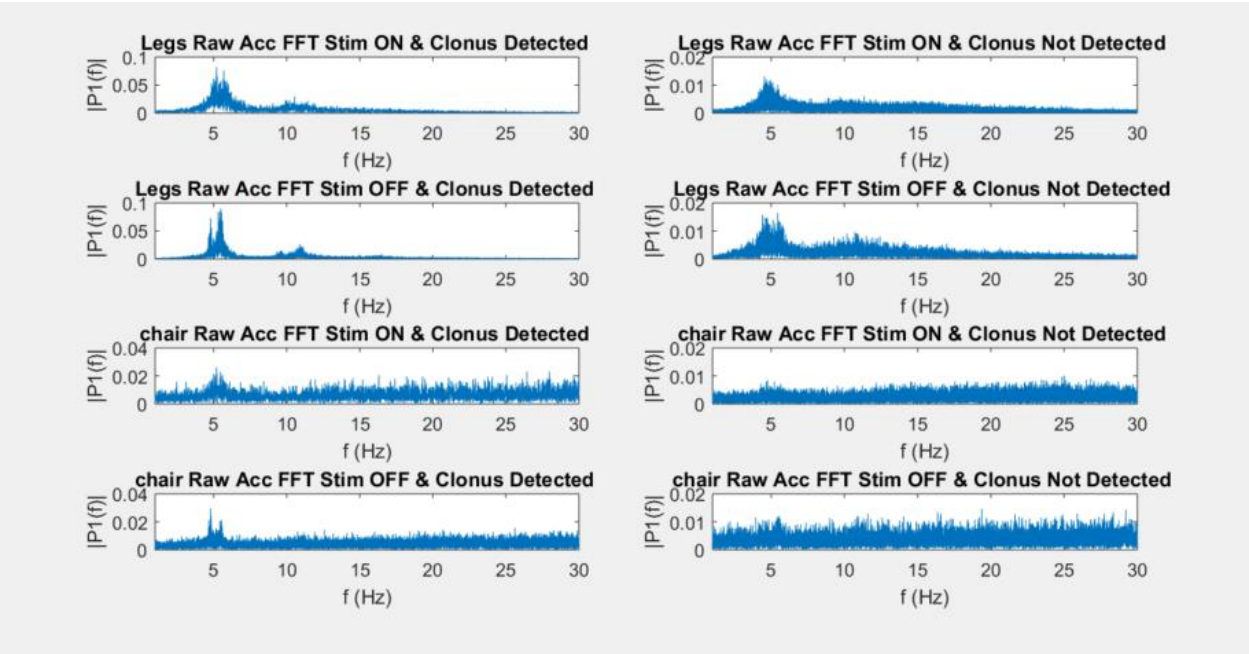

Figure 5-14: FFT analysis shows clonus presents prominently in the 5 Hz frequency range on the legs. Clonus from the wheelchair inertia is about a fourth the power of clonus inertia at the legs. Old-asphalt has no significant peak frequency within the bandwidth sampled.

Subjects evaluated had a range of clonus intensity. Fast-Fourier transform (FFT) of the legs' raw IMU data during the controller-detected clonus state reveals the power of the characteristic clonus frequency in acceleration data from the legs, see Fig. 5-15 below. S1 and S2 had pronounced clonus with power greater than 0.1, however S2 had very mild clonus upon returning for another experimental session ten days after the first. This particular reduction in clonus intensity is not believed to be caused by the intervention; a urinary tract infection that was reported a few days post-session, in addition to other uncontrolled variables such as caffeine ingestion the morning of the second session, and extra stretching the night before. S3 and S4 have mild to moderate levels of pathological clonus.

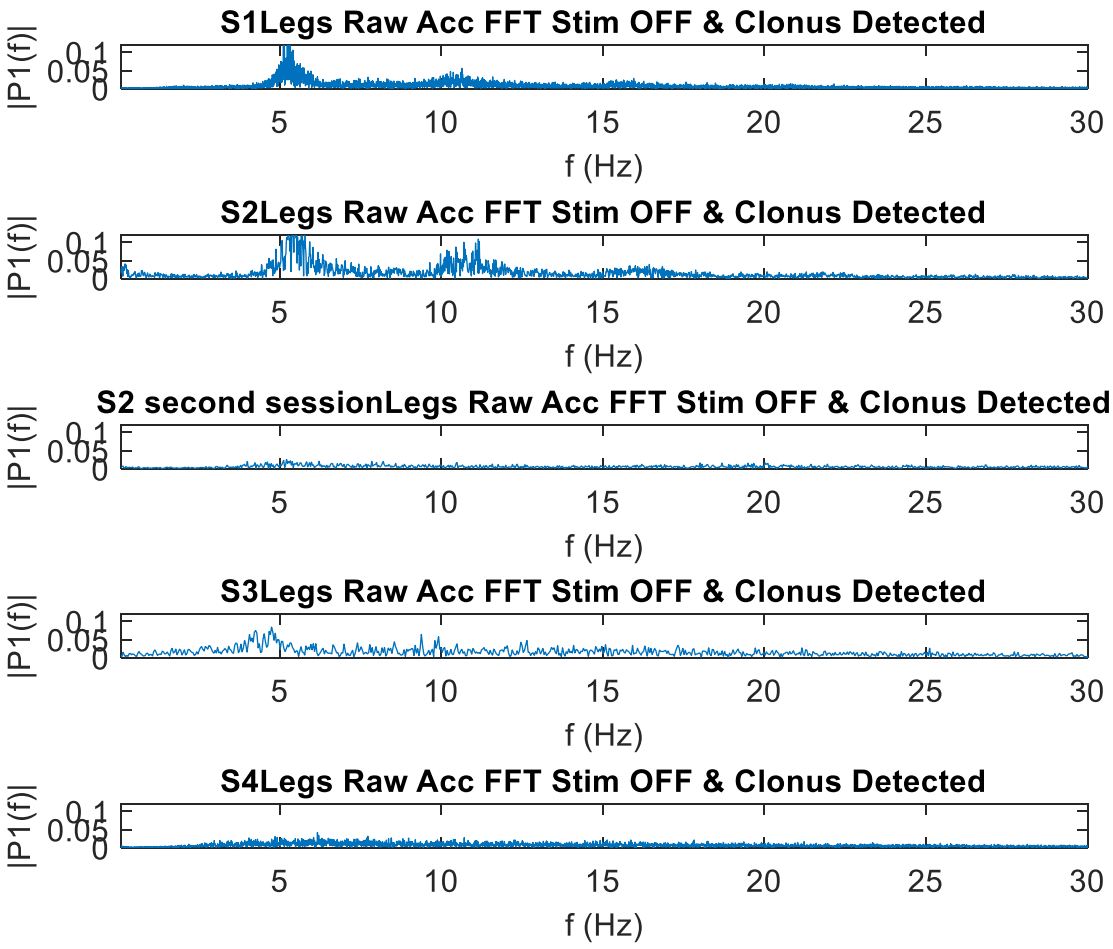

Figure 5-15: Varying degrees of clonus activity were observed between and within subjects.

5.6 Conclusion

Analysis of video data enabled validation that the developed anti-clonus method reduced pathological spasticity during wheelchair propulsion of rough-terrain. The median reduction of pathological symptoms, including clonus and foot-off, was found to be 86% for the eleven trials conducted. The evaluated technology has potential to provide a non-invasive solution for an industry dependent on pharmaceuticals or surgical procedures. Further testing should be done to assess how the anti-clonus FES method endures habituation, fatigue, and accommodation.

CONCLUDING STATEMENTS

Novel rehabilitation techniques were explored with the state-of-the-art mechatronic devices. The controllers presented are all intended to enhance the condition of lower limb paralysis and each have been validated on a few persons with spinal cord injury (SCI). SCI is an underrepresented population (<1% of the US population), however, the severe level of impairment and the long-term prognosis warrant advancing the technology for restoring function whenever possible. The exoskeleton, functional electrical stimulation, and applications with both have proven capable of enabling people to exceed limitations imposed by neurological impairment. The application of assistive technology is expansive as neurological impairment leads to a broad heterogenous scope of pathological symptoms. The controllers described successfully demonstrated means for assisting paraplegic individuals with climbing stairs, walking despite extensor tone and treating clonus when traversing rough terrain in a wheelchair.

The devices described in Chapter 2 include the Indego exoskeleton and the Chimera multi-functional electrical stimulation device. Simulink provided means for real-time control of the devices which expedited exploration of numerous interventions. Clinical testing with a variety of subjects with spinal cord injury enabled evaluation of the prototyped interventions. The Indego commercial venture is in the process of incorporating FES into the FDA-approved device. The controllers described in Chapters 3 and 4 are well suited for integration with the commercial hardware. Expanded validation studies should be conducted to ensure optimal control strategies and rigorous failure analysis promotes user safety. Chapter 3 details the contributions towards the expansion of the Indego exoskeleton controller for stair ascent and descent and the successful demonstration of robust accommodation of variable stair height for three users with SCI. Chapter 4 quantifies the kinematic improvement awarded by supplemental stimulation of the common peroneal nerve during exoskeleton assisted gait for two individuals with sever extensor spasticity as a result of SCI.

Chapter 5 details a novel method developed for evaluating clonus evoked by natural means during wheelchair propulsion for four individuals with SCI. Further studies should evaluate the long-term implications of an anti-clonus FES device. Provided the method's acute efficacy is prolonged, the method could be a significant enhancement to conventional spasticity treatments; with potential to reduce both financial burden and risks of adverse effects.

The Appendices contain additional information on exploratory case studies and technical documentation resulting from the doctoral program tenure. Together these efforts have demonstrated promising restoration of function after SCI and establish a foundation for translating the novel functions to the intended population.

REFERENCES

[1] R. Riener, M. Rabuffetti, and C. Frigo, "Stair ascent and descent at different inclinations," *Gait Posture*, vol. 15, no. 1, pp. 32–44, 2002.

[2] R. Bohannon and M. Smith, "Interrater reliability of a modified Ashworth Scale of muscle spasticity," *Phys. Ther.*, vol. 67, pp. 206–207, 1987.

[3] E. N. Benz, T. G. Hornby, R. K. Bode, R. A. Scheidt, and B. D. Schmit, "A physiologically based clinical measure for spastic reflexes in spinal cord injury," *Arch. Phys. Med. Rehabil.*, vol. 86, no. 1, pp. 52–59, Jan. 2005.

[4] B. S. Armour, E. A. Courtney-Long, M. H. Fox, H. Fredine, and A. Cahill, "Prevalence and Causes of Paralysis—United States, 2013," *Am. J. Public Health*, vol. 106, no. 10, pp. 1855–1857, Oct. 2016.

[5] S. Herculano-Houzel, "The Human Brain in Numbers: A Linearly Scaled-up Primate Brain," *Front. Hum. Neurosci.*, vol. 3, Nov. 2009.

[6] T. Nguyen, "Total Number of Synapses in the Adult Human Neocortex," *Undergrad. J. Math. Model. One Two*, vol. 3, no. 1, May 2013.

[7] X. Duan, E. Kang, C. Y. Liu, G. Ming, and H. Song, "Development of neural stem cell in the adult brain," *Curr. Opin. Neurobiol.*, vol. 18, no. 1, pp. 108–115, Feb. 2008.

[8] R. Adami *et al.*, "Reduction of Movement in Neurological Diseases: Effects on Neural Stem Cells Characteristics," *Front. Neurosci.*, vol. 12, May 2018.

[9] E. Kandel, J. Schwartz, and T. Jessell, *Principles of Neural Science*, Fourth. McGraw-Hill, 2000.

[10] M. W. O'Dell *et al.*, "Response and Prediction of Improvement in Gait Speed From Functional Electrical Stimulation in Persons With Poststroke Drop Foot," *PM&R*, vol. 6, no. 7, pp. 587–601, Jul. 2014.

[11] R. Lindenberg, V. Renga, L. L. Zhu, F. Betzler, D. Alsop, and G. Schlaug, "Structural integrity of corticospinal motor fibers predicts motor impairment in chronic stroke," *Neurology*, vol. 74, no. 4, p. 280, Jan. 2010.

[12] T. J. Kimberley, S. Samargia, L. G. . Moore, J. K. Shakya, and C. E. Lang, "Comparison of amounts and types of practice during rehabilitation for traumatic brain injury and stroke," *J. Rehabil. Res. Dev.*, vol. 47, no. 9, p. 851, 2010.

[13] "Spinal Reflexes and Descending Motor Pathways (Section 3, Chapter 2) Neuroscience Online: An Electronic Textbook for the Neurosciences | Department of Neurobiology and Anatomy - The University of Texas Medical School at Houston." [Online]. Available: https://nba.uth.tmc.edu/neuroscience/s3/chapter02.html. [Accessed: 11-Jul-2018].

[14] L. M. Mendell, "The size principle: a rule describing the recruitment of motoneurons," *J. Neurophysiol.*, vol. 93, no. 6, pp. 3024–3026, Jun. 2005.

[15] H. J. Freund, "Motor unit and muscle activity in voluntary motor control.," *Physiol. Rev.*, vol. 63, no. 2, pp. 387–436, Apr. 1983.

[16] A. Faroni, S. A. Mobasseri, P. J. Kingham, and A. J. Reid, "Peripheral nerve regeneration: Experimental strategies and future perspectives," *Adv. Drug Deliv. Rev.*, vol. 82–83, pp. 160–167, Mar. 2015.

[17] K. R. Jessen and R. Mirsky, "The repair Schwann cell and its function in regenerating nerves," *J. Physiol.*, pp. 3521–3531.

[18] E. A. Huebner and S. M. Strittmatter, "Axon Regeneration in the Peripheral and Central Nervous Systems," in *Cell Biology of the Axon*, Springer, Berlin, Heidelberg, 2009, pp. 305–360.

[19] R. Descartes, "Descartes, Treatise on Man Reading," in *Selection translated from De l'homme et de la formation du foetus, edited by Claude Clerselier (Paris, 1664). Translated by P. R. Sloan*, p. 7.

[20] P. I. Pavlov (1927), "Conditioned reflexes: An investigation of the physiological activity of the cerebral cortex," *Ann. Neurosci.*, vol. 17, no. 3, pp. 136–141, Jul. 2010.

[21] C. S. Sherrington, "Flexion-reflex of the limb, crossed extension-reflex, and reflex stepping and standing," *J. Physiol.*, vol. 40, no. 1–2, pp. 28–121, 1910.

[22] *Sports-Specific Rehabilitation*. Elsevier, 2007.

[23] W. M. Oo, “Efficacy of Addition of Transcutaneous Electrical Nerve Stimulation to Standardized Physical Therapy in Subacute Spinal Spasticity: A Randomized Controlled Trial,” *Arch. Phys. Med. Rehabil.*, vol. 95, no. 11, pp. 2013–2020, Nov. 2014.

[24] K. Minassian *et al.*, “Spinal Rhythm Generation by Step-Induced Feedback and Transcutaneous Posterior Root Stimulation in Complete Spinal Cord–Injured Individuals , Spinal Rhythm Generation by Step-Induced Feedback and Transcutaneous Posterior Root Stimulation in Complete Spinal Cord–Injured Individuals,” *Neurorehabil. Neural Repair*, vol. 30, no. 3, pp. 233–243, Mar. 2016.

[25] J. A. Beres-Jones, T. D. Johnson, and S. J. Harkema, “Clonus after human spinal cord injury cannot be attributed solely to recurrent muscle-tendon stretch,” *Exp. Brain Res.*, vol. 149, no. 2, pp. 222–236, Mar. 2003.

[26] K. Fouad and C. Hurd, “Repairing the injured spinal cord: sprouting versus regeneration. Is this a realistic match?,” *Neural Regen. Res.*, vol. 9, no. 5, p. 462, Mar. 2014.

[27] C. C. Maguire, J. M. Sieben, and R. A. de Bie, “The influence of walking-aids on the plasticity of spinal interneuronal networks, central-pattern-generators and the recovery of gait post-stroke. A literature review and scholarly discussion,” *J. Bodyw. Mov. Ther.*, vol. 21, no. 2, pp. 422–434, Apr. 2017.

[28] National Spinal Cord Injury Statistical Center, “Spinal Cord Injury (SCI) Facts and Figures at a Glance,” Birmingham, AL: University of Alabama at Birmingham, 2016.

[29] R. J. Marino *et al.*, “International Standards For Neurological Classification Of Spinal Cord Injury,” *J. Spinal Cord Med.*, vol. 26, no. sup1, pp. S50–S56, Jan. 2003.

[30] M. M. Adams and A. Hicks, “Spasticity after spinal cord injury,” *Spinal Cord*, vol. 43, pp. 577–586, 2005.

[31] P. Decq, “[Pathophysiology of spasticity],” *Neurochirurgie.*, vol. 49, no. 2-3 Pt 2, p. 163—184, May 2003.

[32] F. Biering-Sørensen, J. B. Nielsen, and K. Klinge, “Spasticity-assessment: a review,” *Spinal Cord*, vol. 44, no. 12, pp. 708–722, 2006.

[33] P. Akpinar, A. Atici, F. U. Ozkan, I. Aktas, D. G. Kulcu, and K. N. Kurt, “Reliability of the Spinal Cord Assessment Tool for Spastic Reflexes,” *Arch. Phys. Med. Rehabil.*, vol. 98, no. 6, pp. 1113–1118, Jun. 2017.

[34] K. J. Manella, K. E. Roach, and E. C. Field-Fote, “Temporal Indices of Ankle Clonus and Relationship to Electrophysiologic and Clinical Measures in Persons With Spinal Cord Injury:,” *J. Neurol. Phys. Ther.*, vol. 41, no. 4, pp. 229–238, Oct. 2017.

[35] R. W. Angel and W. W. Hofmann, “The H Reflex in Normal, Spastic, and Rigid Subjects: Studies,” *Arch. Neurol.*, vol. 8, no. 6, pp. 591–596, Jun. 1963.

[36] G. Demirel, H. Yilmaz, N. Paker, and S. Önel, “Osteoporosis after spinal cord injury,” *Spinal Cord*, vol. 36, no. 12, pp. 822–826, Dec. 1998.

[37] G. D. Bazo HAC, “Thoracic Level Complete Paraplegiaâ□“Walking Performance, Training and Medical Benefits with the PARASTEP FES System,” *Int. J. Phys. Med. Rehabil.*, vol. 03, no. 05, 2015.

[38] F. Bethoux *et al.*, “The Effects of Peroneal Nerve Functional Electrical Stimulation Versus Ankle-Foot Orthosis in Patients With Chronic Stroke , The Effects of Peroneal Nerve Functional Electrical Stimulation Versus Ankle-Foot Orthosis in Patients With Chronic Stroke: A Randomized Controlled Trial , A Randomized Controlled Trial,” *Neurorehabil. Neural Repair*, vol. 28, no. 7, pp. 688–697, Sep. 2014.

[39] R. Betz, B. Boden, R. Triolo, M. Mesgarzadeh, E. Gardner, and R. Fife, “Effects of functional electrical stimulation on the joints of adolescents with spinal cord injury,” *Paraplegia*, vol. 34, no. 3, pp. 127–136, Mar. 1996.

[40] K. Dunning, M. W. O’Dell, P. Kluding, and K. McBride, “Peroneal Stimulation for Foot Drop After Stroke: A Systematic Review,” *Am. J. Phys. Med. Rehabil.*, vol. 94, no. 8, pp. 649–664, Aug. 2015.

[41] S. Hamid and R. Hayek, “Role of electrical stimulation for rehabilitation and regeneration after spinal cord injury: an overview,” *Eur. Spine J.*, vol. 17, no. 9, pp. 1256–1269, Sep. 2008.

[42] G. Demirel, H. Yilmaz, N. Paker, and S. Önel, “Osteoporosis after spinal cord injury,” *Spinal Cord*, vol. 36, no. 12, pp. 822–825, Dec. 1998.

[43] K. K. BeDell, A. M. E. Scremin, K. L. Perell, and C. F. Kunkel, “EFFECTS OF FUNCTIONAL ELECTRICAL STIMULATION-INDUCED LOWER EXTREMITY CYCLING ON BONE DENSITY OF SPINAL CORD-INJURED PATIENTS1,” *Am. J. Phys. Med. Rehabil.*, vol. 75, no. 1, p. 29, Feb. 1996.
[44] P. Eser, E. D. D. Bruin, I. Telley, H. E. Lechner, H. Knecht, and E. Stüssi, “Effect of electrical stimulation-induced cycling on bone mineral density in spinal cord-injured patients,” *Eur. J. Clin. Invest.*, vol. 33, no. 5, pp. 412–419.
[45] T. Mohr, J. Pødenphant, F. Biering–Sørensen, H. Galbo, G. Thamsborg, and M. Kjær, “Increased Bone Mineral Density after Prolonged Electrically Induced Cycle Training of Paralyzed Limbs in Spinal Cord Injured Man,” *Calcif. Tissue Int.*, vol. 61, no. 1, pp. 22–25, Jul. 1997.
[46] L. Giangregorio and N. McCartney, “Bone loss and muscle atrophy in spinal cord injury: epidemiology, fracture prediction, and rehabilitation strategies,” *J. Spinal Cord Med.*, vol. 29, no. 5, pp. 489–500, 2006.
[47] S.-C. Chen, C.-H. Lai, W. P. Chan, M.-H. Huang, H.-W. Tsai, and J.-J. J. Chen, “Increases in bone mineral density after functional electrical stimulation cycling exercises in spinal cord injured patients,” *Disabil. Rehabil.*, vol. 27, no. 22, pp. 1337–1341, Jan. 2005.
[48] P. J. Pacy, R. Hesp, D. A. Halliday, D. Katz, G. Cameron, and J. Reeve, “Muscle and bone in paraplegic patients, and the effect of functional electrical stimulation,” *Clin. Sci.*, vol. 75, no. 5, pp. 481–487, Nov. 1988.
[49] L. R. Sheffler and J. Chae, “Neuromuscular electrical stimulation in neurorehabilitation,” *Muscle Nerve*, vol. 35, no. 5, pp. 562–590, May 2007.
[50] L. M. Rohde, B. R. Bonder, and R. J. Triolo, “Exploratory study of perceived quality of life with implanted standing neuroprostheses,” *J. Rehabil. Res. Dev.*, vol. 49, no. 2, pp. 265–278, 2012.
[51] M. A. Regan, R. W. Teasell, D. L. Wolfe, D. Keast, W. B. Mortenson, and J.-A. L. Aubut, “A Systematic Review of Therapeutic Interventions for Pressure Ulcers After Spinal Cord Injury,” *Arch. Phys. Med. Rehabil.*, vol. 90, no. 2, pp. 213–231, Feb. 2009.
[52] L. R. Solis, D. P. Hallihan, R. R. E. Uwiera, R. B. Thompson, E. D. Pehowich, and V. K. Mushahwar, “Prevention of pressure-induced deep tissue injury using intermittent electrical stimulation,” *J. Appl. Physiol.*, vol. 102, no. 5, pp. 1992–2001, May 2007.
[53] P. L. Jacobs, B. Johnson, and E. T. Mahoney, “Physiologic responses to electrically assisted and frame-supported standing in persons with paraplegia,” *J. Spinal Cord Med.*, vol. 26, no. 4, pp. 384–389, 2003.
[54] D. Hobbs, “Electrical Stimulation and Neuroplasticity.”
[55] G. R. Cybulski, R. D. Penn, and R. J. Jaeger, “Lower extremity functional neuromuscular stimulation in cases of spinal cord injury,” *Neurosurgery*, vol. 15, no. 1, pp. 132–146, Jul. 1984.
[56] C. L. LYNCH and M. R. POPOVIC, “Functional Electrical Stimulation,” *IEEE Control Syst.*, vol. 28, no. 2, pp. 40–50, Apr. 2008.
[57] T. Yan, C. W. Y. Hui-Chan, and L. S. W. Li, “Functional Electrical Stimulation Improves Motor Recovery of the Lower Extremity and Walking Ability of Subjects With First Acute Stroke: A Randomized Placebo-Controlled Trial,” *Stroke*, vol. 36, no. 1, pp. 80–85, Jan. 2005.
[58] L. Kawasaki, V. K. Mushahwar, C. Ho, S. P. Dukelow, L. L. H. Chan, and K. M. Chan, “The mechanisms and evidence of efficacy of electrical stimulation for healing of pressure ulcer: A systematic review,” *Wound Repair Regen.*, vol. 22, no. 2, pp. 161–173.
[59] D. Lala, S. J. Spaulding, S. M. Burke, and P. E. Houghton, “Electrical stimulation therapy for the treatment of pressure ulcers in individuals with spinal cord injury: a systematic review and meta-analysis,” *Int. Wound J.*, vol. 13, no. 6, pp. 1214–1226.
[60] M. Goldfarb, “A control-brake orthosis for FES-aided gait,” Thesis, Massachusetts Institute of Technology, 1994.
[61] F. F. Offner and W. T. Liberson, “Method of muscular stimulation in human beings to aid in walking,” US3344792A, 03-Oct-1967.
[62] R. B. Stein, “Assembly for functional electrical stimulation during movement,” US5814093A, 29-Sep-1998.
[63] “Freedom to Walk Foundation | Servicing Children & Adults with Foot Drop,” *Freedom To Walk Foundation*. .
[64] M. Durand, “Consumer Alert: Two new devices for foot drop,” *Momentum*, no. Fall, p. 46, 2008.

[65] F. Bethoux *et al.*, "Long-Term Follow-up to a Randomized Controlled Trial Comparing Peroneal Nerve Functional Electrical Stimulation to an Ankle Foot Orthosis for Patients With Chronic Stroke," *Neurorehabil. Neural Repair*, vol. 29, no. 10, pp. 911–922, Dec. 2015.
[66] P. H. Peckham and J. S. Knutson, "Functional Electrical Stimulation for Neuromuscular Applications," *Annu. Rev. Biomed. Eng.*, vol. 7, no. 1, pp. 327–360, 2005.
[67] T. Bajd, A. Kralj, R. Turk, H. Benko, and J. Šega, "The Use of a Four-Channel Electrical Stimulator as an Ambulatory Aid for Paraplegic Patients," *Phys. Ther.*, vol. 63, no. 7, pp. 1116–1120, Jul. 1983.
[68] "Non-invasive neuromuscular electrical stimulation in patients with central nervous system lesions: An educational review." [Online]. Available: http://www.medicaljournals.se/jrm/content/abstract/10.2340/16501977-0941. [Accessed: 27-Jun-2018].
[69] "Announcements | Sigmedics Inc." [Online]. Available: http://www.sigmedics.com/announcements. [Accessed: 27-Jun-2018].
[70] R. Brissot *et al.*, "Clinical experience with functional electrical stimulation-assisted gait with Parastep in spinal cord-injured patients," *Spine*, vol. 25, no. 4, pp. 501–508, Feb. 2000.
[71] J. L. Contreras-Vidal *et al.*, "Powered exoskeletons for bipedal locomotion after spinal cord injury," *J. Neural Eng.*, vol. 13, no. 3, p. 031001, Jun. 2016.
[72] T. Yan, M. Cempini, C. M. Oddo, and N. Vitiello, "Review of assistive strategies in powered lower-limb orthoses and exoskeletons," *Robot. Auton. Syst.*, vol. 64, pp. 120–136, Feb. 2015.
[73] H. Quintero, R. Farris, C. Hartigan, I. Clesson, and M. Goldfarb, "A Powered Lower Limb Orthosis for Providing Legged Mobility in Paraplegic Individuals," *Top. Spinal Cord Inj. Rehabil.*, vol. 17, no. 1, pp. 25–33, Jul. 2011.
[74] "suitX announces 'world's most affordable' powered exoskeleton – the Phoenix." [Online]. Available: https://newatlas.com/suitx-phoenix-exoskeleton/41678/. [Accessed: 08-Jul-2018].
[75] A. J. Young and D. P. Ferris, "State of the Art and Future Directions for Lower Limb Robotic Exoskeletons," *IEEE Trans. Neural Syst. Rehabil. Eng.*, vol. 25, no. 2, pp. 171–182, Feb. 2017.
[76] "Bionic Suit, Bionic Exsoskeleton Legs, EksoGT, Mobility Device," *Ekso Bionics*. [Online]. Available: https://eksobionics.com/eksohealth/products/. [Accessed: 08-Jul-2018].
[77] A. Rossi, R. Mazzocchio, and C. Scarpini, "Clonus in Man: a rythmic oscillation maintained by a reflex mechanism," *Electroencephalogr. Clin. Neurophsiology*, vol. 75, no. 1–2, pp. 56–63, Feb. 1990.
[78] J. A. Beres-Jones, T. D. Johnson, and S. J. Harkema, "Clonus after human spinal cord injury cannot be attributed solely to recurrent muscle-tendon stretch," *Exp. Brain Res.*, vol. 149, no. 2, pp. 222–236, Mar. 2003.
[79] D. Harel, "Statecharts: a visual formalism for complex systems," *Sci. Comput. Program.*, vol. 8, no. 3, pp. 231–274, Jun. 1987.
[80] H. A. Quintero, R. J. Farris, and M. Goldfarb, "A method for the autonomous control of lower limb exoskeletons for persons with paraplegia," *J. Med. Devices*, vol. 6, no. 4, p. 041003, 2012.
[81] R. J. Farris, H. A. Quintero, and M. Goldfarb, "Performance evaluation of a lower limb exoskeleton for stair ascent and descent with paraplegia," in *Engineering in medicine and biology society (EMBC), 2012 annual international conference of the IEEE*, 2012, pp. 1908–1911.
[82] K. H. Ha, S. A. Murray, and M. Goldfarb, "An Approach for the Cooperative Control of FES With a Powered Exoskeleton During Level Walking for Persons With Paraplegia," *IEEE Trans. Neural Syst. Rehabil. Eng.*, vol. 24, no. 4, pp. 455–466, Apr. 2016.
[83] E. Merson, "Electrical safety of equipment for functional electrical stimulation," presented at the IFESS, 2017, p. 1.
[84] R. J. Farris, H. A. Quintero, and M. Goldfarb, "Performance evaluation of a lower limb exoskeleton for stair ascent and descent with paraplegia," in *2012 Annual International Conference of the IEEE Engineering in Medicine and Biology Society*, 2012, pp. 1908–1911.
[85] A. Ekelem, S. Murray, and M. Goldfarb, "Preliminary assessment of variable geometry stair ascent and descent with a powered lower limb orthosis for individuals with paraplegia," in *2015 37th Annual International Conference of the IEEE Engineering in Medicine and Biology Society (EMBC)*, 2015, pp. 4671–4674.
[86] J. L. Contreras-Vidal *et al.*, "Powered exoskeletons for bipedal locomotion after spinal cord injury," *J. Neural Eng.*, vol. 13, no. 3, p. 031001, Jun. 2016.

[87] S. Wang *et al.*, “Design and Control of the MINDWALKER Exoskeleton,” *IEEE Trans. Neural Syst. Rehabil. Eng.*, vol. 23, no. 2, pp. 277–286, Mar. 2015.
[88] A. Tsukahara, Y. Hasegawa, K. Eguchi, and Y. Sankai, “Restoration of Gait for Spinal Cord Injury Patients Using HAL With Intention Estimator for Preferable Swing Speed,” *IEEE Trans. Neural Syst. Rehabil. Eng.*, vol. 23, no. 2, pp. 308–318, Mar. 2015.
[89] M. R. Tucker *et al.*, “This is an open-access article distributed under the terms of the Cre...,” *J. NeuroEngineering Rehabil.*, no. 12:1, 2015.
[90] A. Ekelem, S. Murray, and M. Goldfarb, “Preliminary assessment of variable geometry stair ascent and descent with a powered lower limb orthosis for individuals with paraplegia,” in *Engineering in Medicine and Biology Society (EMBC), 2015 37th Annual International Conference of the IEEE*, 2015, pp. 4671–4674.
[91] M. B. Yandell, B. T. Quinlivan, D. Popov, C. Walsh, and K. E. Zelik, “Physical interface dynamics alter how robotic exosuits augment human movement: implications for optimizing wearable assistive devices,” *J. NeuroEngineering Rehabil.*, vol. 14, no. 1, p. 40, May 2017.
[92] A. Schiele, “Ergonomics of exoskeletons: Subjective performance metrics,” in *2009 IEEE/RSJ International Conference on Intelligent Robots and Systems*, St. Louis, MO, USA, 2009, pp. 480–485.
[93] S. Chen *et al.*, “Cascade force control of lower limb hydraulic exoskeleton for human performance augmentation,” in *IECON 2016 - 42nd Annual Conference of the IEEE Industrial Electronics Society*, 2016, pp. 512–517.
[94] M. Aach *et al.*, “Exoskeletal Neuro-Rehabilitation in Chronic Paraplegic Patients – Initial Results,” in *Converging Clinical and Engineering Research on Neurorehabilitation*, vol. 1, J. L. Pons, D. Torricelli, and M. Pajaro, Eds. Berlin, Heidelberg: Springer Berlin Heidelberg, 2013, pp. 233–236.
[95] S. A. Kolakowsky-Hayner, “Safety and Feasibility of using the EksoTM Bionic Exoskeleton to Aid Ambulation after Spinal Cord Injury,” *J. Spine*, 2013.
[96] A. Esquenazi, M. Talaty, A. Packel, and M. Saulino, “The ReWalk Powered Exoskeleton to Restore Ambulatory Function to Individuals with Thoracic-Level Motor-Complete Spinal Cord Injury:,” *Am. J. Phys. Med. Rehabil.*, vol. 91, no. 11, pp. 911–921, Nov. 2012.
[97] E. Isakov, R. Douglas, and P. Berns, “Ambulation using the reciprocating gait orthosis and functional electrical stimulation,” *Spinal Cord*, vol. 30, no. 4, pp. 239–245, 1992.
[98] M. Goldfarb, K. Korkowski, B. Harrold, and W. Durfee, “Preliminary evaluation of a controlled-brake orthosis for FES-aided gait,” *IEEE Trans. Neural Syst. Rehabil. Eng.*, vol. 11, no. 3, pp. 241–248, 2003.
[99] T. C. Bulea, R. Kobetic, M. L. Audu, J. R. Schnellenberger, and R. J. Triolo, “Finite State Control of a Variable Impedance Hybrid Neuroprosthesis for Locomotion After Paralysis,” *IEEE Trans. Neural Syst. Rehabil. Eng.*, vol. 21, no. 1, pp. 141–151, Jan. 2013.
[100] S. R. Chang, R. Kobetic, and R. J. Triolo, “Effect of exoskeletal joint constraint and passive resistance on metabolic energy expenditure: Implications for walking in paraplegia,” *PloS One*, vol. 12, no. 8, p. e0183125, 2017.
[101] K. H. Ha, S. A. Murray, and M. Goldfarb, “An Approach for the Cooperative Control of FES With a Powered Exoskeleton During Level Walking for Persons With Paraplegia,” *IEEE Trans. Neural Syst. Rehabil. Eng.*, vol. 24, no. 4, pp. 455–466, Apr. 2016.
[102] E. P. Zehr, T. Komiyama, and R. B. Stein, “Cutaneous reflexes during human gait: electromyographic and kinematic responses to electrical stimulation,” *J. Neurophysiol.*, vol. 77, no. 6, pp. 3311–3325, 1997.
[103] T. Bajd, A. Kralj, M. Štefančič, and N. Lavrač, “Use of functional electrical stimulation in the lower extremities of incomplete spinal cord injured patients,” *Artif. Organs*, vol. 23, no. 5, pp. 403–409, 1999.
[104] T. Street and C. Singleton, “A clinically meaningful training effect in walking speed using functional electrical stimulation for motor-incomplete spinal cord injury.,” *J. Spinal Cord Med.*, pp. 1–6, Nov. 2017.
[105] M. R. Dimitrijevic, F. Gracanin, and Prevec TS, “An anti-clonus model,” *Proc. Seventh Int. Conf. Med. Biol. Eng.*, p. Stockholm, SWE, 1967.
[106] C. Sköld, R. Levi, and Å. Seiger, “Spasticity after traumatic spinal cord injury: Nature, severity, and location,” *Arch. Phys. Med. Rehabil.*, vol. 80, no. 12, pp. 1548–1557, Dec. 1999.

[107] J. A. Strommen, “Management of Spasticity from Spinal Cord Dysfunction,” *Neurol. Clin.*, vol. 31, no. 1, pp. 269–286, Feb. 2013.
[108] K. A. Holtz, R. Lipson, V. K. Noonan, B. K. Kwon, and P. B. Mills, “Prevalence and Effect of Problematic Spasticity After Traumatic Spinal Cord Injury,” *Arch. Phys. Med. Rehabil.*, vol. 98, no. 6, pp. 1132–1138, Jun. 2017.
[109] J. M. Hidler and W. Z. Rymer, “Limit cycle behavior in spasticity: analysis and evaluation,” *IEEE Trans. Biomed. Eng.*, vol. 47, no. 12, pp. 1565–1575, Dec. 2000.
[110] R. Iansek, “The effects of reflex path length on clonus frequency in spastic muscles.,” *J. Neurol. Neurosurg. Psychiatry*, vol. 47, no. 10, pp. 1122–1124, Oct. 1984.
[111] D. M. Wallace, B. H. Ross, and C. K. Thomas, “Motor unit behavior during clonus,” *J. Appl. Physiol.*, vol. 99, no. 6, pp. 2166–2172, Dec. 2005.
[112] H. Uysal, İ. Boyraz, S. Yağcıoğlu, F. Oktay, P. Kafalı, and E. Tönük, “Ankle clonus and its relationship with the medium-latency reflex response of the soleus by peroneal nerve stimulation,” *J. Electromyogr. Kinesiol.*, vol. 21, no. 3, pp. 438–444, Jun. 2011.
[113] P. Brown, J. C. Rothwell, P. D. Thompson, and C. D. Marsden, “Propriospinal myoclonus: Evidence for spinal ‘pattern’ generators in humans,” *Mov. Disord.*, vol. 9, no. 5, pp. 571–576.
[114] D. M. Wallace, B. H. Ross, and C. K. Thomas, “Characteristics of Lower Extremity Clonus after Human Cervical Spinal Cord Injury,” *J. Neurotrauma*, vol. 29, no. 5, pp. 915–924, Mar. 2012.
[115] M. R. Dimitrijevic, P. W. Nathan, and A. M. Sherwood, “Clonus: the role of central mechanisms.,” *J. Neurol. Neurosurg. Psychiatry*, vol. 43, no. 4, pp. 321–332, Apr. 1980.
[116] A. Ward, “Long-term modification of spasticity,” *J. Rehabil. Med.*, vol. 35, no. 0, pp. 60–65, Oct. 2003.
[117] S. Kirshblum, “Treatment Alternatives for Spinal Cord Injury Related Spasticity,” *J. Spinal Cord Med.*, vol. 22, no. 3, pp. 199–217, Jan. 1999.
[118] M. Sadeghi, J. McIvor, H. Finlayson, and B. Sawatzky, “Static standing, dynamic standing and spasticity in individuals with spinal cord injury,” *Spinal Cord*, vol. 54, no. 5, pp. 376–382, May 2016.
[119] K.-H. TSAI, C.-Y. YEH, H.-Y. CHANG, and J.-J. CHEN, “Effects of a Single Session of Prolonged Muscle Stretch on Spastic Muscle of Stroke Patients,” p. 6.
[120] I. G. Milanov, “Mechanisms of baclofen action on spasticity,” *Acta Neurol. Scand.*, vol. 85, no. 5, pp. 305–310, May 1992.
[121] R. F. Jones, D. Burke, J. E. Marosszeky, and J. D. Gillies, “A new agent for the control of spasticity,” *J. Neurol. Neurosurg. Psychiatry*, vol. 33, no. 4, pp. 464–468, Aug. 1970.
[122] “Baclofen (Baclofen Tablets): Side Effects, Interactions, Warning, Dosage & Uses,” *RxList*. [Online]. Available: https://www.rxlist.com/baclofen-drug.htm. [Accessed: 13-Aug-2018].
[123] P. Nance, O. Schryvers, B. Schmidt, H. Dubo, B. Loveridge, and D. Fewer, “Intrathecal Baclofen Therapy for Adults with Spinal Spasticity: Therapeutic Efficacy and Effect on Hospital Admissions,” *Can. J. Neurol. Sci.*, vol. 22, no. 1, pp. 22–29, Feb. 1995.
[124] T. Bajd, M. Gregoric, L. Vodovnik, and H. Benko, “Electrical stimulation in treating spasticity resulting from spinal cord injury,” *Arch. Phys. Med. Rehabil.*, vol. 66, no. 8, pp. 515–517, Aug. 1985.
[125] L. Vodovnik, A. Stefanovska, and T. Bajd, “Effects of stimulation parameters on modification of spinal spasticity,” *Med. Biol. Eng. Comput.*, vol. 25, no. 4, pp. 439–442, Jul. 1987.
[126] M. F. Levin and C. W. Y. Hui-Chan, “Relief of hemiparetic spasticity by TENS is associated with improvement in reflex and voluntary motor functions,” *Electroencephalogr. Clin. Neurophysiol. Potentials Sect.*, vol. 85, no. 2, pp. 131–142, Apr. 1992.
[127] A. Stefanovska, L. Vodovnik, N. Gros, S. Rebersek, and R. Acimovic-Janezic, “FES and spasticity,” *IEEE Trans. Biomed. Eng.*, vol. 36, no. 7, pp. 738–745, Jul. 1989.
[128] A. Karakoyun, İ. Boyraz, R. Gunduz, A. Karamercan, and N. Ozgirgin, “Electrophysiological and clinical evaluation of the effects of transcutaneous electrical nerve stimulation on the spasticity in the hemiplegic stroke patients,” *J. Phys. Ther. Sci.*, vol. 27, no. 11, pp. 3407–3411, 2015.
[129] A. van der Salm, P. H. Veltink, M. J. IJzerman, K. C. Groothuis-Oudshoorn, A. V. Nene, and H. J. Hermens, “Comparison of Electric Stimulation Methods for Reduction of Triceps Surae Spasticity in Spinal Cord Injury,” *Arch. Phys. Med. Rehabil.*, vol. 87, no. 2, pp. 222–228, Feb. 2006.
[130] J. A. Dewald, J. D. Given, and W. Z. Rymer, “Long-lasting reductions of spasticity induced by skin electrical stimulation,” *IEEE Trans. Rehabil. Eng.*, vol. 4, no. 4, pp. 231–242, Dec. 1996.

[131] U. S. Hofstoetter, W. B. McKay, K. E. Tansey, W. Mayr, H. Kern, and K. Minassian, “Modification of spasticity by transcutaneous spinal cord stimulation in individuals with incomplete spinal cord injury,” *J. Spinal Cord Med.*, vol. 37, no. 2, pp. 202–211, Mar. 2014.
[132] R. Nardone *et al.*, “Noninvasive Spinal Cord Stimulation: Technical Aspects and Therapeutic Applications,” *Neuromodulation Technol. Neural Interface*, vol. 18, no. 7, pp. 580–591.
[133] H. K. Guðfinnsdóttir 1989, “Evaluation of tSCS treatment for the alleviation of lower limb spasticity,” Thesis, 2016.
[134] Y. P. Gerasimenko *et al.*, “Noninvasive Reactivation of Motor Descending Control after Paralysis,” *J. Neurotrauma*, vol. 32, no. 24, pp. 1968–1980, Jun. 2015.
[135] S. Harkema *et al.*, “Effect of epidural stimulation of the lumbosacral spinal cord on voluntary movement, standing, and assisted stepping after motor complete paraplegia: a case study,” *The Lancet*, vol. 377, no. 9781, pp. 1938–1947, Jun. 2011.
[136] A. Naro *et al.*, “Breakthroughs in the spasticity management: Are non-pharmacological treatments the future?,” *J. Clin. Neurosci.*, vol. 39, pp. 16–27, May 2017.
[137] P. B. Mills and F. Dossa, “Transcutaneous Electrical Nerve Stimulation for Management of Limb Spasticity: A Systematic Review,” *Am. J. Phys. Med. Rehabil.*, vol. 95, no. 4, p. 309, Apr. 2016.
[138] W. Mayr *et al.*, “Modulation of stimulation frequency of spinal cord afferents with unchanged intensity and electrode site can induce a variety of movements,” in *World Congress on Medical Physics and Biomedical Engineering, September 7 - 12, 2009, Munich, Germany*, Springer, Berlin, Heidelberg, 2009, pp. 543–545.
[139] J. E. Arle and J. L. Shils, *Innovative Neuromodulation*. Academic Press, 2017.
[140] E. N. Benz, T. G. Hornby, R. K. Bode, R. A. Scheidt, and B. D. Schmit, “A physiologically based clinical measure for spastic reflexes in spinal cord injury,” *Arch. Phys. Med. Rehabil.*, vol. 86, no. 1, pp. 52–59, Jan. 2005.
[141] A. Pavlov, V. A. Makarov, I. Makarova, and F. Panetsos, “Separation of Extracellular Spikes: When Wavelet Based Methods Outperform the Principle Component Analysis,” in *Mechanisms, Symbols, and Models Underlying Cognition*, 2005, pp. 123–132.

APPENDIX A – MOTOR INCOMPLETE GAIT PHASE DETECTION CASE STUDY

Abstract

Functional electrical stimulation (FES) devices recognize gait-phase intent and stimulate weakened muscle groups to treat gait abnormalities. A unique controller mechanism and a multi-channel stimulator were developed to improve upon the gait-phase intent detection ability and overall applicability of FES devices. The controller was evaluated on a single subject with a motor incomplete spinal cord injury (C5 ASIA-C) by comparing the onset of swing as estimated by the controller to swing initiation by means of a push-button FES system. The controller was found to predict swing intention 0.212±0.xxx s prior to the push-button which is 20-100% more accurate than other controllers modeled after industry standards. The novel stimulator was then used and evaluated by comparing walking with and without FES stimulation. During FES intervention, gait distance and cadence increased from an average of 19.1±0.3 m and 15.3 steps/min to 42.9±0.3 m and 22.0 steps/min and several kinematic aspects of gait also improved. Although the results of the present study are encouraging, the single-subject experimental design prevents generalization. Further testing with a larger sample size is required to validate this study and the efficacy of the FES system.

APPENDIX B – MOTOR COMPLETE GAIT PHASE DETECTION CASE STUDY

Introduction

Spinal cord injury (SCI) often inhibits the ability to voluntarily initiate gait due to lower limb paralysis. Technology, including motorized exoskeletons and functional electrical stimulation (FES), can return movement to paralyzed limbs. Such systems, however, require a means by which a user can indicate intent to step. This study explores the use of electromyography (EMG) from muscles above the paretic injury level to indicate user's intention to initiate steps.

Other efforts towards intuitive robot interaction have explored using electroencephalography (EEG) to interface robotic gait. EEG relies on similar differential amplifier technology as EMG, however, EEG targets signals on the surface of the brain, through the skull. This method has been repeatedly demonstrated ineffective for feasibility of functional gait that resembles normal walking recruitment. Other invasive brain computer interface techniques such as cortical probes, neural dust and electrocorticography (ECoG) have promise, but will not be feasible nor affordable in the near future. However, percutaneous EMG is minimally invasive (needle electrodes) and may be explored to examine the feasibility of implantable EMG sensors for targeting muscles inaccessible to surface EMG.

EMG results in a signal to noise ratio over two orders of magnitude better than EEG because the electrical activity of muscles is inherently more pronounced and the target sites for surface EMG are typically closer to the noninvasive electrodes on the surface of the skin.

An intuitive controller was prototyped to infer step intent via compensatory muscle activation; the controller monitors trunk muscle activity with EMG from muscles above the paretic injury level to identify patterns that indicate the user's intention to initiate steps. The controller was further developed to utilize the EMG signals to proportionally modulate the stimulation amplitude during each step, enabling the user to intuitively appropriate assistance.

Materials and Methods

An exploratory study was conducted using a single subject with a T11 ASIA B SCI. The subject was tested for EMG trunk muscle sites that coincided with swing intention. Once promising sites were located, initial experiments were conducted using push buttons to indicate step intent, while recorded EMG from the external oblique muscles. EMG features were then correlated with step intent, and subsequently used in place of the push buttons to initiate stepping. Validation experiments were then conducted, still using both EMG and push button inputs, but using EMG to command steps and push buttons as an indication of volitional intent.

The results for the EMG identifier that targeted the external obliques for the subject had strong correlation, so the controller was further developed to enable an open loop proportional modulation of the stimulation amplitude. Hence a separate preliminary experiment was designed to evaluate if effort can successfully be mapped to from the oblique compensatory activation to peroneal stimulation. To evaluate the efficacy a random color was illuminated on a screen indicating the user take a small, medium or large step. The root-mean-square of the EMG and proportional FES were reviewed to evaluate the user's ability to control FES amplitude during each step.

Results

For the T11 subject, the EMG activity from the external obliques strongly correlated with step intention, as measured by the push button input. A sensitivity of 100% was found for both right (n=96) and left (n=93) steps. The specificity of 100% was found for the right and 96.9% for the left.

The integrated EMG over the swing state had significantly different means when commanding a small, medium, or large step with greater than 95% confidence. Hence, the controller was successful in enabling users to control step effort within three tiers (small, medium and large).

Discussion

Although healthy walking does not have a strong correlation between oblique activity and swing initiation, the oblique activity may be a form of compensation in SCI individuals, or may result from use of a stability aid, enabling an intuitive input for swing initiation.

Implementation with an exoskeleton will maximize the potential suitable subjects. Expanding the controls for exoskeleton can be done in numerous ways. A flow controller may be used to accommodate a breath of users with varying gait capabilities. A phase plane controller would enable forward and backwards control, possibly taking advantage of the variability of the EMG signal. These control topologies will exceed the limited movement patterns dictated by trajectory-based impedance controllers. Such controllers would thus allow real-time use more fluid movements where the user may alter intra-step characteristics in real-time using the EMG interface.

Conclusion

An intuitive and reliable swing intent indicator was developed from external oblique EMG signals, enabling a SCI subject to voluntarily control step commands during FES-aided ambulation.

APPENDIX C – CHIMERA TECHNICAL SHEETS

PCB Component Layout:

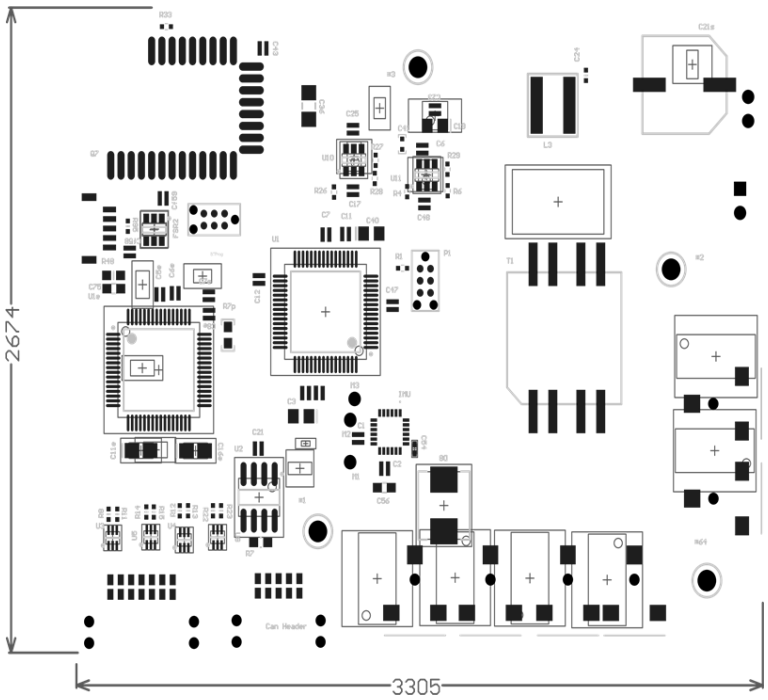

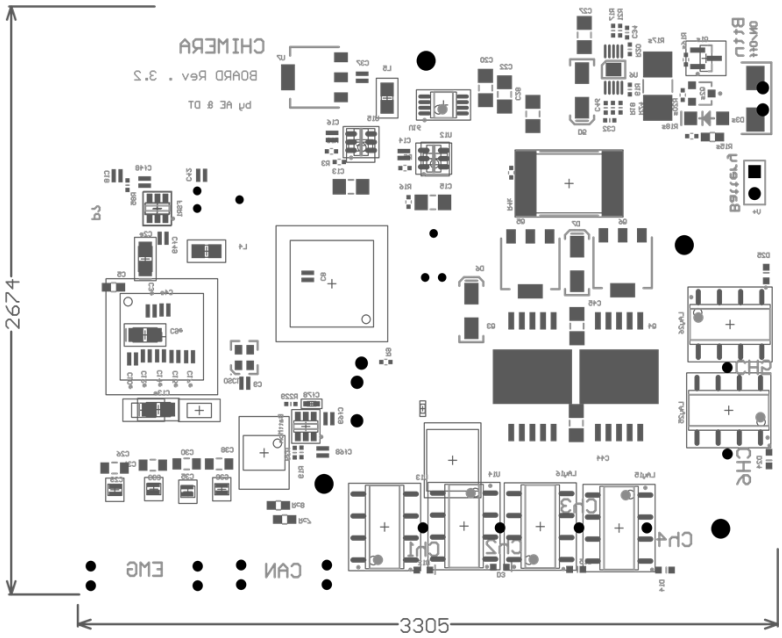

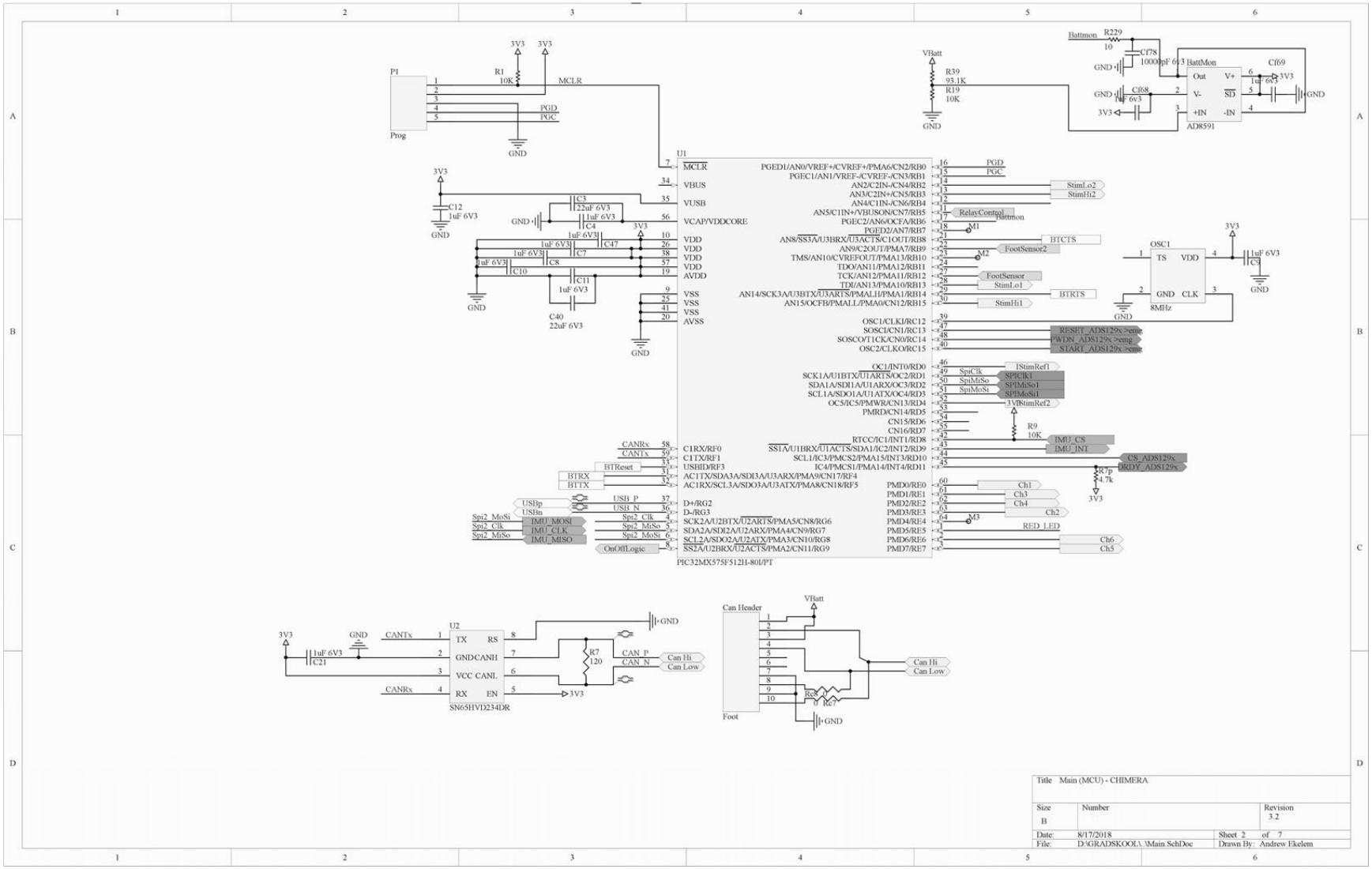
P1
Prog
R1
10K
MCLR
PGD
PGC
U1
PIC32MX575F512H-80I/PT
VBUS
VUSB
VCAP/VDDCORE
VDD
VSS
AVDD
AVSS
C3
22uF 6V3
C4
1uF 6V3
C12
C40
C47
C7
C8
C10
C11
R39
93.1K
R19
10K
VBatt
Battmon
R229
Cf78
10000pF 6V3
Cf68
Cf69
BattMon
AD8591
Out
V+
V-
SD
+IN
-IN
OSC1
8MHz
C5
RelayControl
M1
M2
M3
BTCTS
FootSensor2
FootSensor
StimLo1
StimHi1
BTRTS
StimLo2
StimHi2
RESET_ADS129x
PWDN_ADS129x
START_ADS129x
SpiClk
SpiMiSo
SpiMoSi
IStimRef1
SPIClk1
SPIMiSo1
SPIMoSi1
3VIStimRef2
R9
10K
IMU_CS
IMU_INT
CS_ADS129x
DRDY_ADS129x
R7p
4.7k
Ch1
Ch3
Ch4
Ch2
Ch6
Ch5
RED_LED
CANRx
CANTx
BTReset
BTRX
BTTX
USBp
USBn
USB_P
USB_N
Spi2_MoSi
Spi2_Clk
Spi2_MiSo
IMU_MOSI
IMU_CLK
IMU_MISO
OnOffLogic
U2
SN65HVD234DR
TX
RS
GND
CANH
VCC
CANL
RX
EN
C21
R7
120
CAN_P
CAN_N
Can Hi
Can Low
Can Header
Foot
Res
Title Main (MCU) - CHIMERA
Size B
Number
Revision 3.2
Date: 8/17/2018
Sheet 2 of 7
File: D:\GRADSKOOL\..\Main.SchDoc
Drawn By: Andrew Ekelem

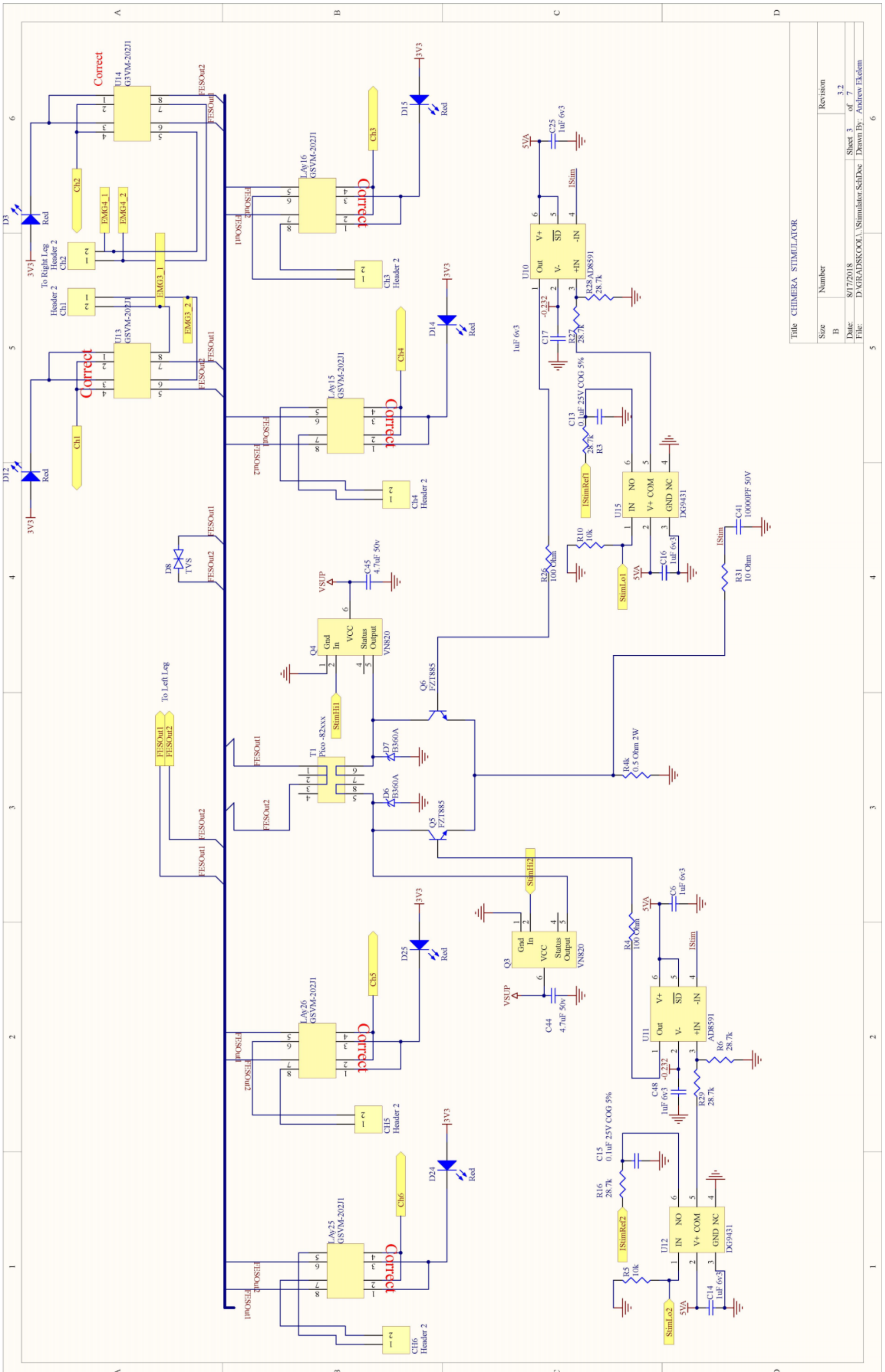
Title CHIMERA STIMULATOR
Size B
Number
Revision 3.2
Date: 8/17/2018
Sheet 3 of 7
File: D:\GRADSKOOL\...\Stimulator.SchDoc
Drawn By: Andrew Ekelem

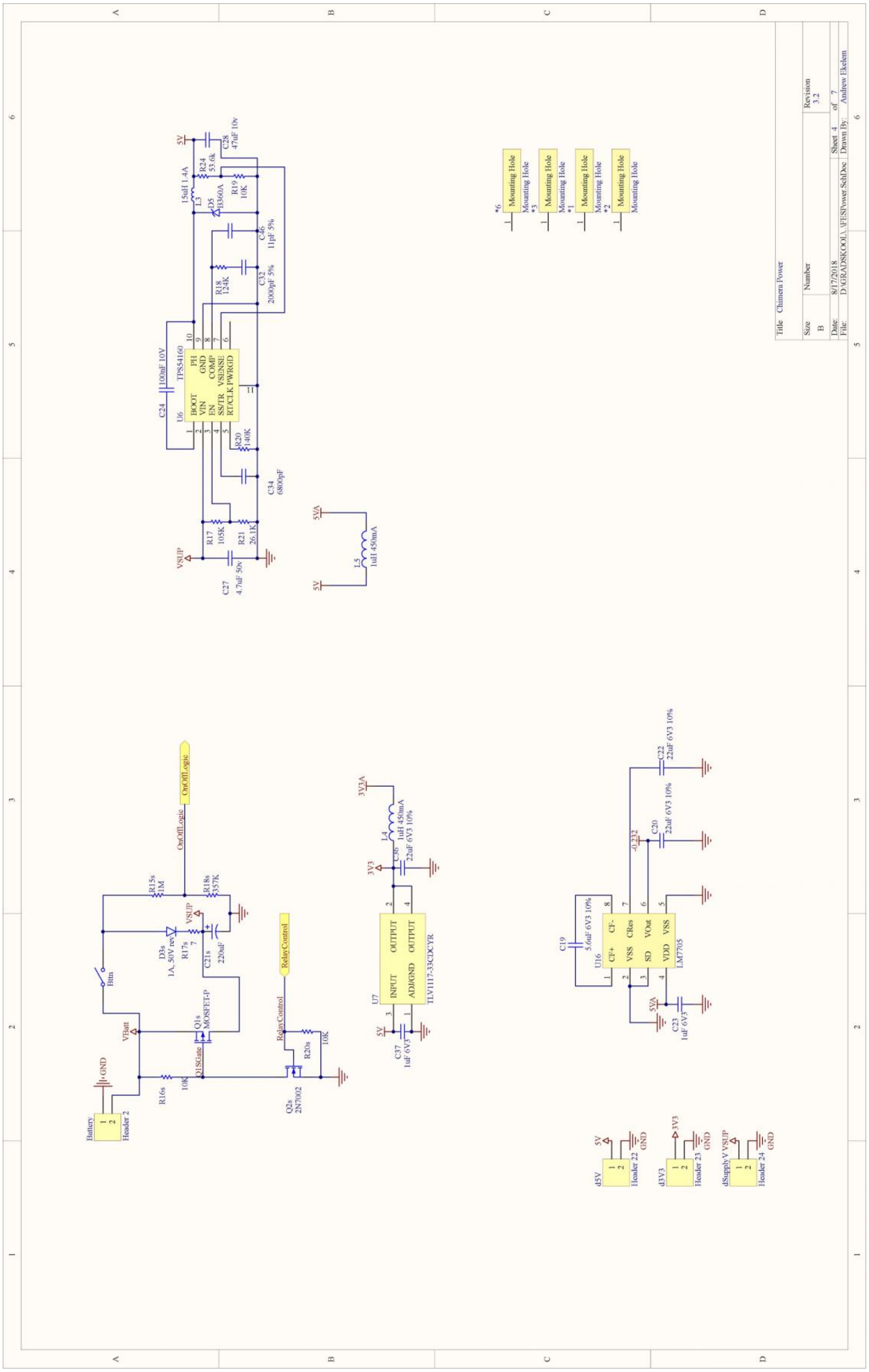
Title Chimera Power
Size B
Number
Revision 3.2
Date 8/17/2018
Sheet 4 of 7
File D:\GRADSKOOL\...\FESPower.SchDoc
Drawn By: Andrew Ekelem
TPS54160
U6
BOOT
VIN
EN
SS/TR
RT/CLK
PH
GND
COMP
VSENSE
PWRGD
C24 100nF 10V
L3 15uH 1.4A
D5 B360A
R24 53.6k
C28 47uF 10v
R19 10K
C46 11pF 5%
R18 124K
C32 2000pF 5%
R20 140K
C34 6800pF
R17 105K
R21 26.1K
C27 4.7uF 50v
VSUP
5V
5VA
L5 1uH 450mA
Mounting Hole
Battery
Header 2
GND
VBatt
Bttn
R15s 1M
R18s 357K
OnOffLogic
D3s 1A, 50V rev
R17s 7
C21s 220uF
Q1s MOSFET-P
Q1SGate
R16s 10K
Q2s 2N7002
R20s 10K
RelayControl
U7
INPUT
ADJ/GND
OUTPUT
TLV1117-33CDCYR
C37 1uF 6V3
3V3
C36 22uF 6V3 10%
L4 1uH 450mA
3V3A
U16
CF+
VSS
SD
VDD
CF-
CRes
VOut
LM7705
C19 5.6uF 6V3 10%
C20 22uF 6V3 10%
C22 22uF 6V3 10%
C23 1uF 6V3
-0.232
d5V
Header 22
d3V3
Header 23
dSupplyV
Header 24

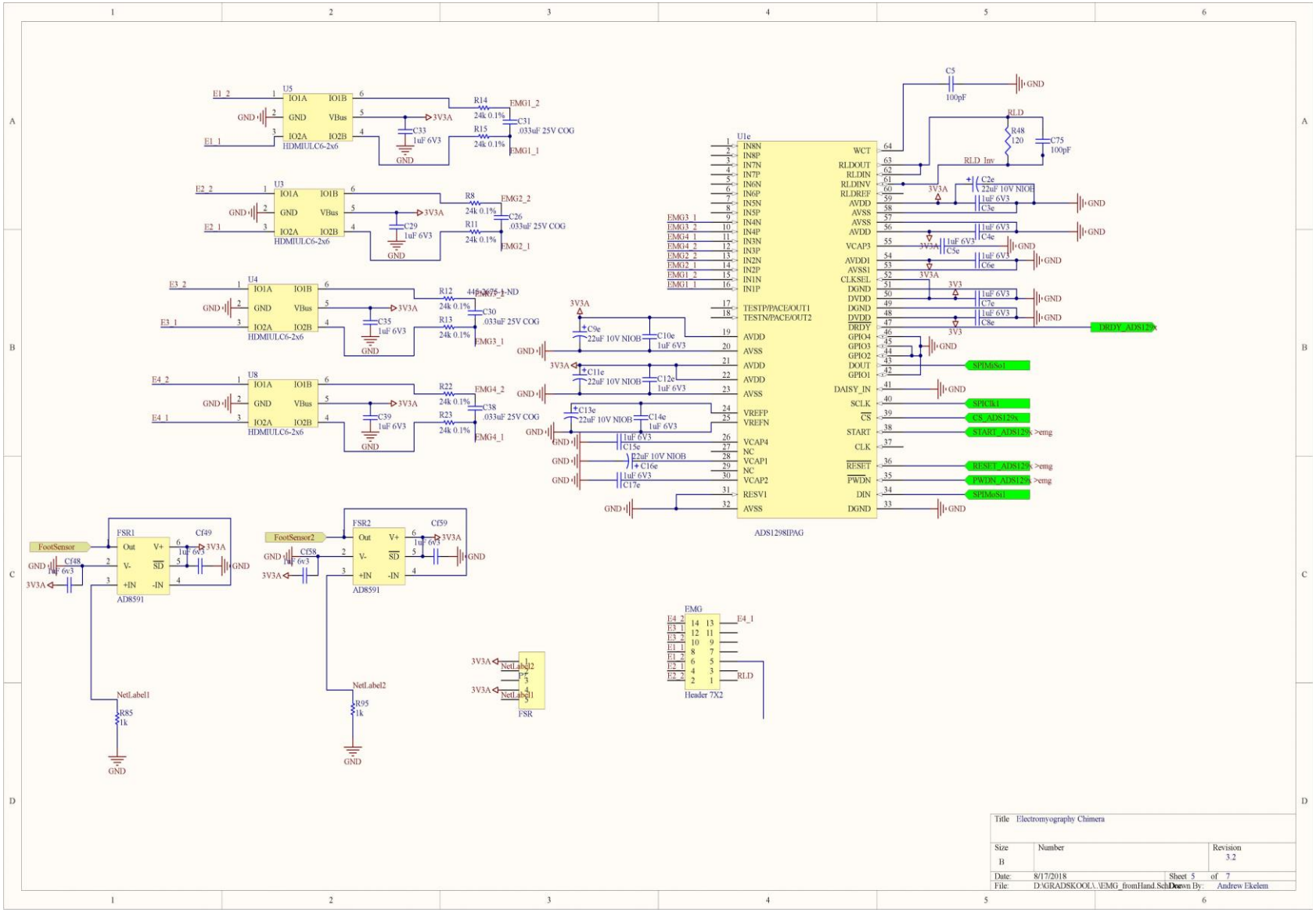
U5
IO1A
IO1B
GND
VBus
IO2A
IO2B
HDMIULC6-2x6
E1_2
E1_1
R14
24k 0.1%
EMG1_2
C31
.033uF 25V COG
R15
EMG1_1
C33
1uF 6V3
3V3A
U3
E2_2
E2_1
R8
EMG2_2
C26
R11
EMG2_1
C29
U4
E3_2
E3_1
R12
EMG3_2
C30
R13
EMG3_1
C35
U8
E4_2
E4_1
R22
EMG4_2
C38
R23
EMG4_1
C39
U1e
IN8N
IN8P
IN7N
IN7P
IN6N
IN6P
IN5N
IN5P
IN4N
IN4P
IN3N
IN3P
IN2N
IN2P
IN1N
IN1P
TESTP/PACE/OUT1
TESTN/PACE/OUT2
AVDD
AVSS
VREFP
VREFN
VCAP4
NC
VCAP1
VCAP2
RESV1
WCT
RLDOUT
RLDIN
RLDINV
RLDREF
AVSS1
CLKSEL
DGND
DVDD
DRDY
GPIO4
GPIO3
GPIO2
DOUT
GPIO1
DAISY_IN
SCLK
CS
START
CLK
RESET
PWDN
DIN
ADS1298IPAG
C5
100pF
RLD
R48
120
C75
100pF
RLD_Inv
C2e
22uF 10V NIOB
C3e
C4e
C5e
C6e
C7e
C8e
C9e
C10e
C11e
C12e
C13e
C14e
C15e
C16e
C17e
DRDY_ADS129x
SPIMiSo1
SPIClk1
CS_ADS129x
START_ADS129x
RESET_ADS129x
PWDN_ADS129x
SPIMoSi1
>emg
FSR1
FSR2
AD8591
FootSensor
FootSensor2
Cf48
Cf49
Cf58
Cf59
NetLabel1
NetLabel2
R85
1k
R95
1k
FSR
EMG
Header 7X2
Title Electromyography Chimera
Size B
Number
Revision 3.2
Date: 8/17/2018
Sheet 5 of 7
File: D:\GRADSKOOL\...\EMG_fromHand.SchDoc
Drawn By: Andrew Ekelem

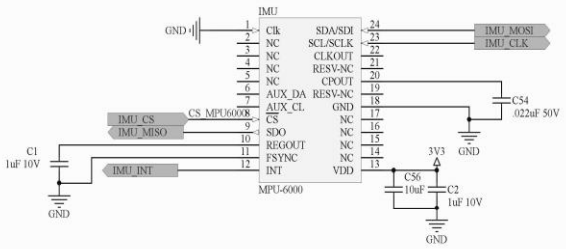

Title	Inertial Measurement Unit - Chimera		
Size	Number		Revision
B			3.2
Date:	8/17/2018	Sheet 6 of 7	
File:	D:\GRADSKOOL\..\IMU.SchDoc	Drawn By:	Andrew Ekelem

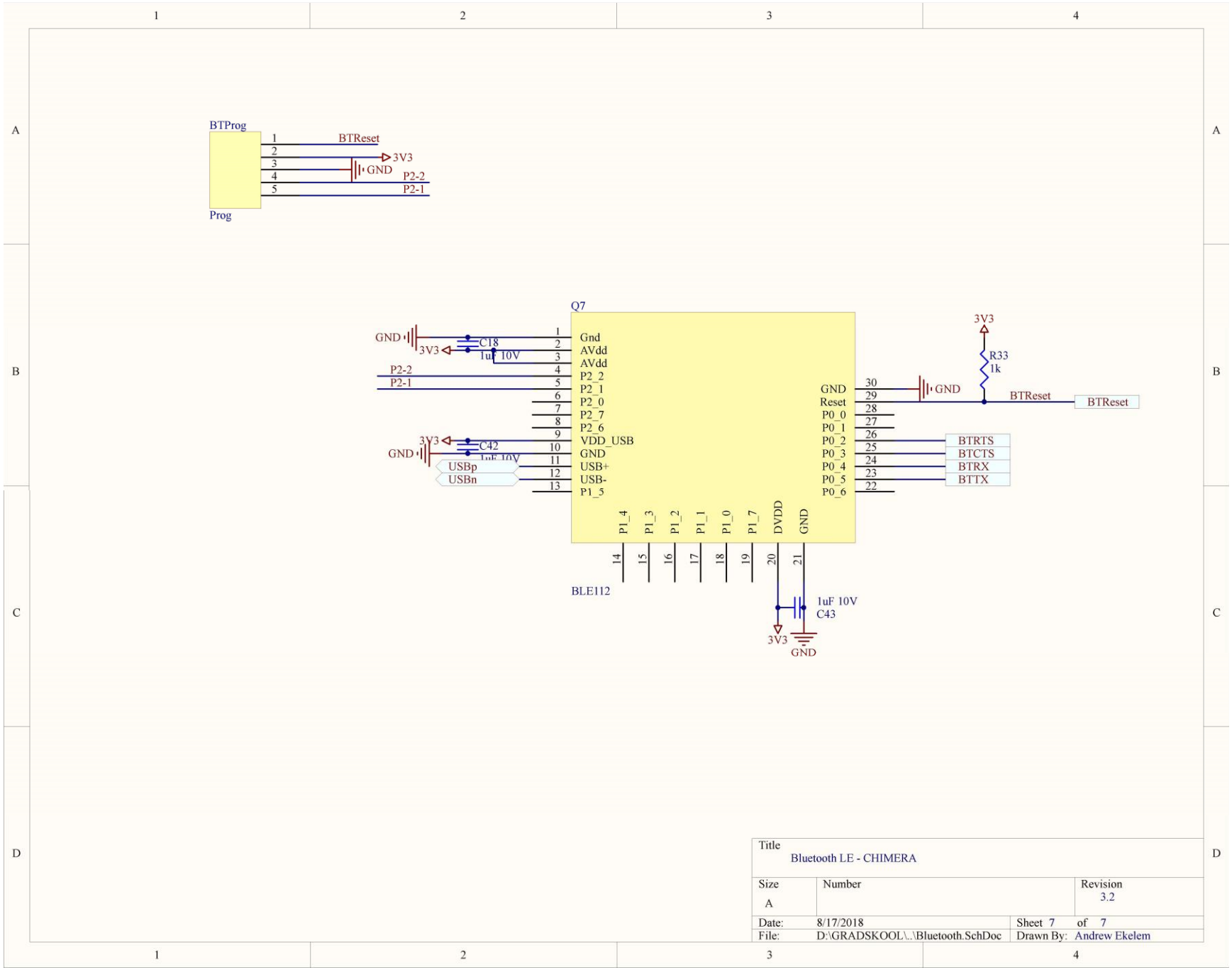
BTProg
1
2
3
4
5
BTReset
3V3
GND
P2-2
P2-1
Prog
Q7
GND
C18
3V3
1uF 10V
P2-2
P2-1
3V3
C42
GND
USBp
USBn
Gnd
AVdd
AVdd
P2_2
P2_1
P2_0
P2_7
P2_6
VDD_USB
GND
USB+
USB-
P1_5
P1_4
P1_3
P1_2
P1_1
P1_0
P1_7
DVDD
GND
BLE112
3V3
R33
1k
GND
Reset
P0_0
P0_1
P0_2
P0_3
P0_4
P0_5
P0_6
BTReset
BTRTS
BTCTS
BTRX
BTTX
1uF 10V
C43
3V3
GND
Title
Bluetooth LE - CHIMERA
Size
A
Number
Revision
3.2
Date:
8/17/2018
Sheet 7 of 7
File:
D:\GRADSKOOL\..\Bluetooth.SchDoc
Drawn By:
Andrew Ekelem

Sample Code:

```
void task_control(void)
{
/* task control runs every main loop
 control determines function depending on mode selected*/
   switch (gCON.mode) {
      case 99: //sleep
         asm volatile( "wait" );// put device in selected Power-Saving mode (did not work)
         break;
      case 5: //EMG stand and walk
         emg_walk_control();
         break;
      case 1: //Clonus Attenuator
         ch = 0;
         //Bang-Bang Controller
         if (gDSS.clonus_x > gCON.thresholdlltimers[FES3]>0) { //Clonus detected
            for (ch = 0; ch <= 1; ch++) {
               amp[ch] = max[ch];}
            if (poststim==5){
               timers[FES3]=1500;}
            if (gDSS.clonus_x < gCON.threshold) poststim=0; //turn off poststim flag when clonus
stops
            timers[FES2]=1500; //set this timer to "x"/500 (seconds) to
            //see if clonus reappears instantly
         }
         else { //no clonus detected
            for (ch = 0; ch <= 1; ch++) {
               amp[ch] = 0;}
            if (timers[FES2]>0){//address clonus reappearing quickly
               poststim=5;}
           if(timers[FES2]==0) {
               poststim=0;}
         }
            /*Proportional Controller*/
            //amp[ch] = gDSS.clonus_x/12; //12 is an arbitrary number that works well AE, should be
replaced with a PID controller

         for (ch = 0; ch <= chMAX; ch++) {
            if (amp[ch] > max[ch]) //SATURATION
            {
               amp[ch] = max[ch];}
         }
         UpdateFES();
         break;
      case 3 : //individual board simple button control
         ///////// FES BUTTON CONTROLLER
         if (ON_SIGNAL==1){
            for (ch = 0; ch <= 1; ch++) {
               amp[ch] = max[ch];}
         }
         else{
            for (ch = 0; ch <= 1; ch++) {
               amp[ch] = 0; }
         }
```

```
        break;

    case 4: //CAN Simulink control

        UpdateFES();
        break;

    case 2: //BLE INTERMITTENT

        if (timers[FES1] ==0){// 0&&timers[FES1] < offperiod-501) {
            for (ch=0;ch<=chMAX;ch++)
            {
                amp[ch]=gCON.threshold2*1000;
                state[ch]=1;
                tics[ch]=1;}
            //UpdateFES and set on timer
            UpdateFES();
            timers[FES2] = onperiod;
            timers[FES1] = onperiod +500;}
        if (timers[FES2] == 0){//> 0&&timers[FES2] < onperiod-501) {
            for (ch=0;ch<=chMAX;ch++)
            {   amp[ch]=0;
                state[ch]=0;
                tics[ch]=1;}
            //UpdateFES and set on timer
            UpdateFES();
            timers[FES1] = offperiod;
            timers[FES2] = offperiod + 500;}
        break;
    default:
        break;}
}
```

APPENDIX D -CLONUS BENCHTOP PILOT STUDY DATA

Benchtop Study Results

Clonus was artificially stimulated in two of the four subjects, S1 and S2; albeit, S2 only responded to the disturbance stimulus on during the first session, and not on the session 10 days later when substantially less clonus was present. The data on subject one (S1) is shown here as an exemplary data set for repetitive FES activation and suppression.

Four six-minute sessions were taken sequentially on one subject, data shown in Fig. 6.2. This data shows two trends, an inverse relationship between anti-clonus stimulation amplitude and settling time, and the self-excitatory behavior of clonus. The first seventeen disturbances did not elicit continuous clonus, then clonus occurred until an anti-clonus stimulus of 15 mA suppressed it, the next five disturbances required 20 mA, and the last four required 25 mA to suppress the clonus within five seconds.

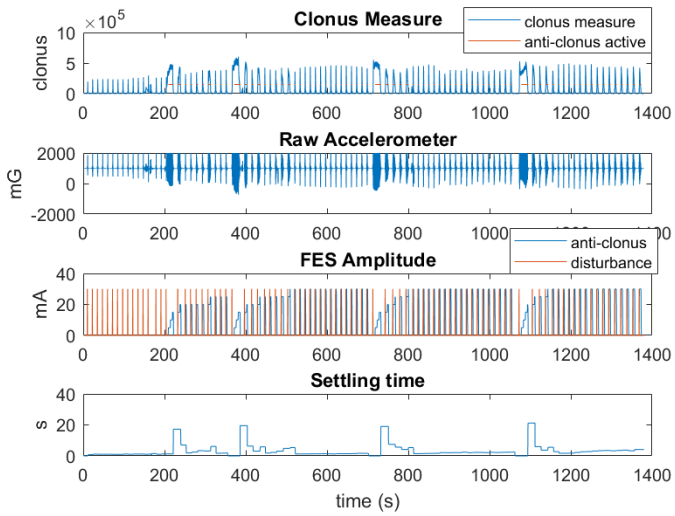

Fig. 6.1 Four six-minute data sessions of clonus compiled

The second six-minute session continuous clonus happened after the first disturbance to which 15 mA quelled. The next two disturbances were suppressed with 20 mA, then 5 disturbances at 25 mA, and the remaining fifteen disturbances required 30 mA. The third six-minute session had one disturbance at 15 mA, one at 20 mA, two at 25 mA, then nineteen at 30 mA. The fourth six-minute session had one 20 mA, two 25 mA, and fourteen at 30 mA.

One off the disturbance response that did not result in continuous clonus can be seen in Fig. 6.3. A pulse like this may be used to set the clonus threshold, although during this set up this was above the threshold, but due to it being in the beginning of the session the FES amplitude was set to zero, allowing the leg to calm without anti-clonus stimulation.

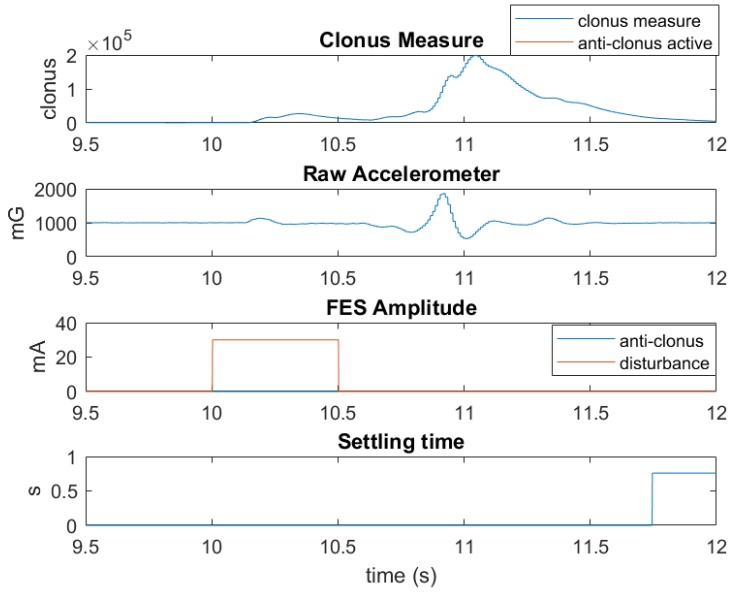

Figure 6.2 Disturbance response without clonus

The instance that clonus becomes continuous, the oscillatory amplitude ramps up, as seen in Fig. 6.4 at 205 s. The clonus continues for greater than 15 seconds as the anti-clonus stimulation is ramped up to 15 mA.

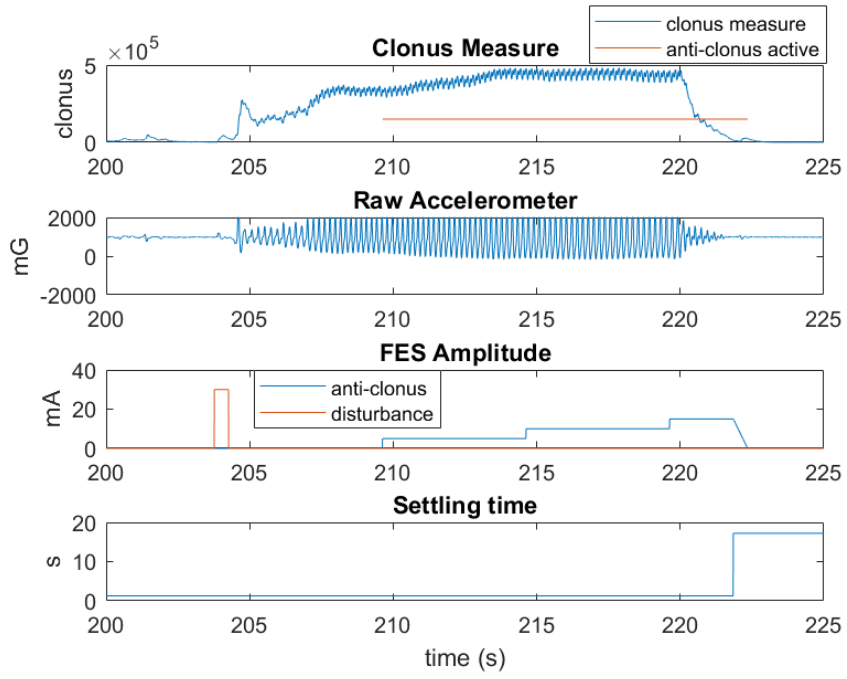

Fig. 6.3 Continuous clonus is self-exciting and continued until the anti-clonus stimulation reached 15 mA

The anti-clonus evaluation shows the accelerometer successfully identifies clonus and anti-clonus stimulation successfully quells the ankle. Figure 6.5 shows the raw accelerometer data, specifically that the disturbance stimulus initiates the oscillatory behavior. When the clonus signal exceeds a threshold, the anti-clonus stimulation is activated until the clonus signal is below one-tenth the threshold.

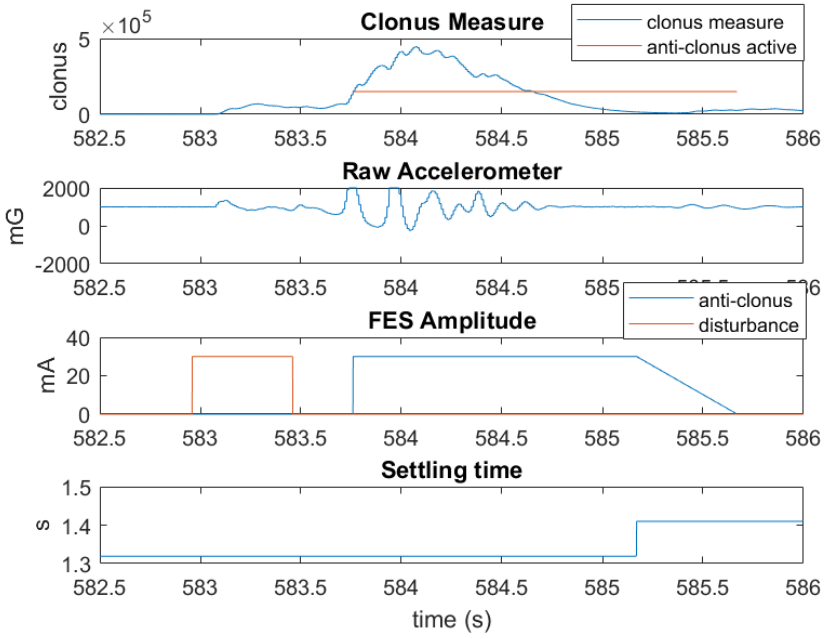

Figure 6.4 Clonus was detected and suppressed with 30 mA within 1.5s

An anti-clonus stimulation of 30 mA suppressed clonus in 2.1±0.7 s. Figure 6.6 shows 46 disturbances suppressed by 30 mA. Note a clear upward trend shows the self-exciting nature of clonus.

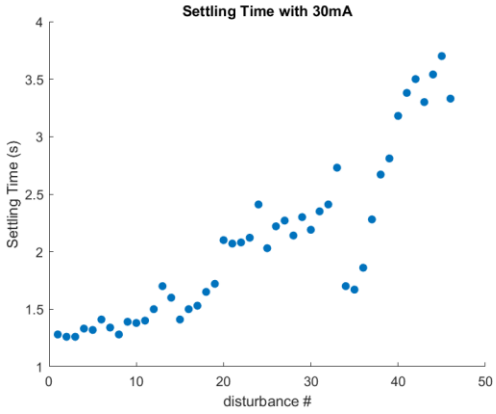

Fig. 6.5: Self-excitatory behavior of clonus shows clonus becomes more resistant to suppression with increase disturbances

A method for evaluating means of clonus suppression was evaluated on a single subject. A total of 92 disturbances were observed in 24 minutes of four successive trials. The amplitude was self-incrementing to maintain the settling time of the clonus within five seconds. Two trends were observed: settling time was inversely affected by suppression stimulation amplitude, and the clonus response became excited as more disturbances had occurred.

The controller autonomously identifies a suitable stimulation amplitude to reduce clonus. A disturbance stimulus to the ankle plantar flexors enables clonus to be repeatedly initiated. Stimulation of the common peroneal nerve with a stimulation amplitude of 30 mA settled clonus in 2.1±0.7 s.